STIMULI-TAILORED DISPERSION STATE OF AQUEOUS CARBON NANOTUBE SUSPENSIONS AND SOLID POLYMER NANOCOMPOSITES

A Dissertation

by

KRISHNA CHAITANYA ETIKA

Submitted to the Office of Graduate Studies of
Texas A&M University
in partial fulfillment of the requirements for the degree of

DOCTOR OF PHILOSOPHY

December 2010

Major Subject: Materials Science and Engineering

Stimuli-Tailored Dispersion State of Aqueous Carbon Nanotube Suspensions and Solid Polymer Nanocomposites

STIMULI-TAILORED DISPERSION STATE OF AQUEOUS CARBON NANOTUBE SUSPENSIONS AND SOLID POLYMER NANOCOMPOSITES

A Dissertation

by

KRISHNA CHAITANYA ETIKA

Submitted to the Office of Graduate Studies of
Texas A&M University
in partial fulfillment of the requirements for the degree of

DOCTOR OF PHILOSOPHY

Approved by:

Chair of Committee,	Jaime C. Grunlan
Committee Members,	Dimitris C. Lagoudas
	Hae-Kwon Jeong
	Bing Guo
Intercollegiate Faculty Chair,	Ibrahim Karaman

December 2010

Major Subject: Materials Science and Engineering

ABSTRACT

Stimuli-Tailored Dispersion State of Aqueous Carbon Nanotube Suspensions and Solid Polymer Nanocomposites. (December 2010)

Krishna Chaitanya Etika, B.Tech, Sri Venkateswara University;

M.Tech, Indian Institute of Technology Kharagpur

Chair of Advisory Committee: Dr. Jaime C. Grunlan

Nanoparticles (such as, carbon nanotubes, carbon black, clay etc.) have one or more dimensions of the order of 100 nm or less. Owing to very high van der Waals force of attraction, these nanoparticles exist in a highly aggregated state. It is often required to break these aggregates to truly experience the "nanosize" effect for any required end use. There are several strategies proposed for dispersing/exfoliating nanoparticles but limited progress has been made towards controlling their dispersion state. The ability to tailor nanoparticle dispersion state in liquid and solid media can ultimately provide a powerful method for tailoring the properties of solution processed nanoparticle-filled polymer composites.

This dissertation reports the use of a variety of stimuli-responsive polymers to control the dispersion state of single-walled carbon nanotubes. Stimuli-responsive polymers exhibit conformational transitions as a function of applied stimulus (like pH, temp, chemical etc.). These variations in conformations of the polymer can be used tailor nanotube dispersion state in water and solid composites.The use of pH and temperature

responsive polymers to stabilize/disperse single walled carbon nanotubes (SWNTs) in water is presented. Non-covalent functionalization of SWNTs using pH and temperature responsive polymer show tailored dispersion state as a function of pH and temperature, respectively. Carbon nanotube microstructure in these aqueous suspensions was characterized using several techniques (cryo-TEM, viscosity measurements, uv-vis spectroscopy, zeta potential measurements and settling behavior). Furthermore, nanotube dispersion state in aqueous suspensions is preserved to a large extent in the composites formed by drying these suspensions as evidenced by SEM images and electrical conductivity measurements. Based on the results obtained a mechanism is proposed to explain the tailored dispersion of SWNTs as a functions of applied external stimulus (i.e., pH, temperature). Such stimuli-controlled dispersion of carbon nanotubes could have a variety of applications in nanoelectronics, sensing, and drug and gene delivery systems. Furthermore, this dissertation also contains a published study focused on controlling the dispersion state of carbon black (CB) in epoxy composites using clay.

To,
My mom, dad,
My wife, Kiran, and
My Advisor, Dr. Jaime Grunlan.

ACKNOWLEDGEMENTS

Firstly, I would like to express my sincere gratitude to my advisor, Dr. Jaime Grunlan, for his constant motivation, advice, and availability. Without his support and encouragement, I could never have achieved this goal. His passion for research, problem solving ability and leadership qualities have deeply impacted me. I hope that one day I will be just as good as him.

I would also like to thank my committee members, Dr. Dimitris C. Lagoudas, Dr. Hae-Kwon Jeong and Dr. Bing Guo for taking time out of their busy schedule for serving on my Ph.D. committee. I am grateful to Dr. Patrick Theato and Dr. Florian Jochum for providing me with the thermoresponsive polymers. I had the opportunity to work with one of the brightest undergraduate students of Texas A&M - Michael Cox, Lance Hess, Andrew Stephenson and Majemite Dafionne. Without their support, this research could never have been possible. I would also like to thank Dr. Christos Savva and Dr. Tom Stephenson for helping me with the cryo-TEM and SEM. The support and cooperation from my research group members is also deeply acknowledged.

Finally, I would like to thank my parents, brother, sister and my wife, Kiran for blindly supporting my ambition of getting a Ph.D. Their candid trust in me and their belief that I will achieve my goal kept me motivated during testing times. I am indebted to Kiran for bearing up with my strenuous schedule that often required working long hours, especially, on the weekends. I hope that I can reciprocate her favors during her medical residency in the USA.

NOMENCLATURE

SWNT	Single-walled Carbon Nanotubes
MWNT	Multi-walled Carbon Nanotubes
UV-Vis	Ultraviolet- Visible
PAA	Poly(acrylic acid)
PMAA	Poly(methacrylic acid)
PEI	Poly(ethyleneimine)
PAAm	Poly(allylamine)
p-PNCPA	Pyrene Functionalized Poly(*N*-cyclopropylacrylamide)
p-PNIPAM	Pyrene Functionalized Poly(*N*-isopropylacrylamide)
SEM	Scanning Electron Microscopy
LCST	Lower Critical Solution Temperature
NMR	Nuclear Magnetic Resonance
FTIR	Fourier Transform Infrared Spectroscopy

TABLE OF CONTENTS

CHAPTER Page

LIST OF FIGURES

FIGURE Page

FIGURE Page

FIGURE Page

LIST OF TABLES

LIST OF SCHEMES

CHAPTER I

INTRODUCTION

1.1 Background and Objectives

Carbon nanotubes are one-dimensional forms of carbon, which can be visualized as rolled hexagonal carbon networks that are capped by pentagonal carbon rings. Owing to their high aspect ratio and conjugated chemical structure, nanotubes possess unique properties that provide a wide range of applications.[1] For example, nanotube-filled polymer composites offer tremendous potential for mechanical and transport property improvements, even at very small concentrations.[2] Carbon nanotube suspensions are being studied for variety of applications, such as biocompatible transportation of proteins,[3] drug delivery systems[4-5] and optical sensors.[6] Despite their utility, as produced carbon nanotubes are aggregated into bundles because of strong van der Waals force of attractions, which not only reduces their aspect ratio, but also create processing and handling difficulties.[7-8] It is desirable to debundle nanotubes to truly realize the *"nano-size"* effect and harness their full potential. There are several strategies reported for dispersion/exfoliation of nanotubes,[9-18] but very limited progress has been made towards controlling their dispersion state. The ability to control nanotube dispersion state in liquid and solid media can ultimately provide a powerful method for tailoring the properties of solution-processed nanotube-filled polymer composites.

This dissertation follows the style of *Journal of the American Chemical Society*.

A variety of covalent and non-covalent methods are reported in the literature to disperse single-walled carbon nanotubes(SWNTs) in solvents.[9-18] Covalent functionalization of nanotubes is realized by chemically attaching moieties to the nanotubes surface. A major drawback of covalent functionalization is the disruption of the extended π conjugation in nanotubes, which results in inferior electrical properties because each functionalization site scatters electrons.[19] On the other hand, non-covalent stabilization involves physical adsorption of polymers or surfactants on the surface of the nanotubes.[20] This method of functionalization does not involve breaking bonds in the nanotube sidewalls and thereby better preserves electrical properties. When these adsorbed molecules are stimuli-responsive, there is an opportunity to tailor nanotube dispersion upon exposure to a given stimulus (e.g., pH, temperature, and/or light).[21-26]

Stimuli-responsive polymers exhibit conformational changes with an applied external stimulus like pH, temperature or light.[27-28] For example, weak polyelectrolytes are one class of stimuli-responsive polymers that contain a large number of ionizable groups and exhibit pKa values between 3 and 10, which makes them pH-responsive.[29] These polymers undergo reversible changes in conformation as a function of pH due to changes in charge density of ionizable groups.[21-22] The use of stimuli-responsive polymers for non-covalent functionalization of nanotubes in water will not only facilitate their dispersion, but also provides a mean for controlling their dispersion state as a function of applied stimulus. In many potential applications, such as SWNT based switching devices, sensors, and drug delivery systems, it may be necessary to control the dispersion or aggregation of SWNTs in solvent with external stimuli.[30] In spite of these

merits, only a few studies in this direction, mostly with pH-responsive polymers, are reported in the literature.[21-22,25] Furthermore, the underlying mechanism of SWNT dispersion and stabilization using pH-responsive polymers is not well understood. Studies with other types of stimuli-responsive polymers are extremely rare and would benefit from this research. Furthermore, this technique of manipulating the dispersion state with stimuli-responsive polymers could be useful for other types of nanoparticles (e.g., inorganic nanowires, fullerenes, graphene, etc).

This dissertation is primarily focused on non-covalent stabilization, and tailoring of carbon nanotubes dispersions in aqueous suspensions, using pH and thermoresponsive polymers. The dispersion characteristics of nanotubes in solid composites are also examined. An overview of this research is shown in Figure 1.1. The key objectives are:

1. To gain a fundamental understanding of the influence of pH on nanotubes dispersion state, in aqueous single-walled carbon nanotubes (SWNTs) suspensions, stabilized with pH responsive polymers.
2. To stabilize SWNTs in water using thermoresponsive pyrene-functionalized poly(*N*-cyclopropylacrylamide) (p-PNCPA), and poly(*N*-isopropylacrylamide) (p-PNIPAM) polymers, and to investigate the effect of temperature on nanotube dispersion state.
3. To understand the influence of pyrene concentration in p-PNCPA on strength of polymer-nanotube interaction and the ability to tailor aqueous SWNT dispersions and nanocomposites.

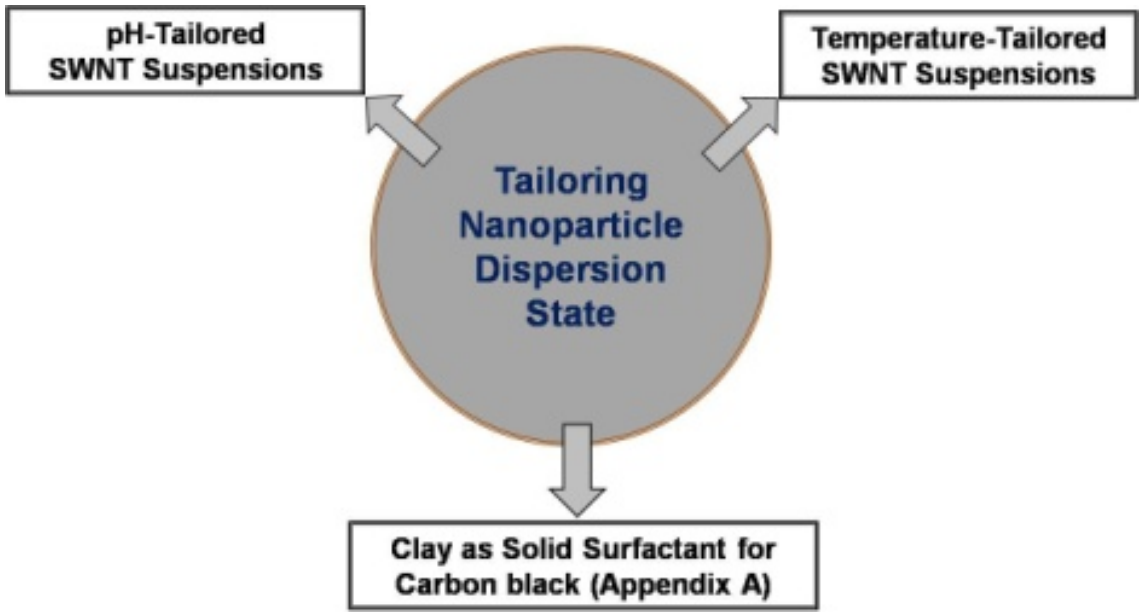

Figure 1.1. Overview of the research work presented in this dissertation.

1.2. Dissertation Outline

Chapter II is a literature review that contains comprehensive information regarding carbon nanotubes, especially SWNTs, including their synthesis, chemical structure and properties. A detailed description of covalent and non-covalent functionalization strategies is also provided. Finally, a brief review of stimuli-responsive polymers, with a special emphasis on pH and temperature response, is also presented.

Chapter III reports on the studies performed on aqueous SWNT dispersions stabilized with pH-responsive poly(acrylic acid) (PAA), poly(methacrylic acid) (PMAA), poly(allyl amine) (PAAm) and branched poly ethylenimine (PEI). Nanotube dispersion state as a function of pH in these suspensions is investigated using cryo-TEM, viscosity shifts, UV-Vis spectroscopy and zeta potential measurements. SWNT

microstructure in solid composites, obtained by drying the aqueous suspensions, is characterized using scanning electron microscopy and electrical conductivity measurements. This chapter also includes a stabilization mechanism to explain the altered nanotubes dispersion state as a function of pH.

Chapter IV presents SWNT stabilization in water using 1,3 and 5 mol% pyrene functionalized poly(*N*-cyclopropylacrylamide) (p-PNCPA)and poly(*N*-isopropylacryl-amide) (p-PNIPAM), respectively. It includes the procedure to synthesize p-PNCPA and p-PNIPAM with varying amounts of pyrene, along with characterization of the synthesized polymer using ^{1}H-NMR, UV and fluroscence emission spectroscopy. Nanotube dispersion state as function of temperature is characterized using cryo-TEM, settling behavior of suspensions and viscosity. Lower critical solution temperature (LCST) of the polymers was determined with turbidity measurements. Composites prepared by drying the suspensions at temperatures below and about the LCST of polymer were studied using SEM images and electrical conductivity measurements. A stabilization mechanism is hypothesized to explain the observed nanotube microstructure as a function of temperature.

Chapter V offers some concluding remarks to summarize the findings of this work and future research plan that could involve other stimuli-responsive polymers and nanoparticles. Preliminary results obtained on aqueous fullerenes suspensions stabilized with a temperature-responsive polymer, poly(2-ethylene-2-oxozaline) (PEtOx), and the use of azobenzene containing polymer to realize light tailoring of carbon nanotube dispersion state is presented.

Apendix A is a published study focused on controlling the dispersion state of carbon black (CB) in epoxy composites. The relative stability of acetone-based suspensions containing CB and clay are shown and the microstructure is characterized using a cryo-TEM and zeta potential measurements. Electrical and mechanical properties of epoxy composites containing different weight ratios of CB and clay are presented to highlight the synergy between these two nanoparticles. A network forming mechanism for CB in the presence of clay (in epoxy composites) explains these results.

CHAPTER II

LITERATURE REVIEW

2.1. Carbon Nanotubes

The discovery of carbon nanotubes can be traced back to as early as 1952 when Russian scientists Radushkevich and Lukyanovich published micrographs of carbon nanofibers that were about 50nm in diameter.[31-32] Nanotubes are effectively tubular fullerenes which are cage like spherical molecules composed entirely of sp2 hybridized carbon atoms (Fig. 2.1(a)).[33] Endo later observed nanotubes in 1976, but the rediscovery was still unable to grab the attention of scientific community.[34] More than a decade later, a tube like structure with diameter ~ 1nm was hypothesized by Richard Smalley, and theoretically verified by Dresselhaus with a model of carbon nanotube end caped by fullerene hemispheres in 1991.[35] That same year, distinctive physical evidence of carbon nanotubes were presented in TEM images of multiwalled carbon nanotubes (MWNTs) by Iijima.[36] Two years later, single-walled carbon nanotubes (SWNTs) were discovered simultaneously, yet independently by Iijima and Bethune (Fig. 2.1).[37-38] Following this seminal work, the study of carbon nanotubes has established itself as one of the nanotechnology's leading research areas. Much of this nanotube research is focused on using the nanotubes for various applications.

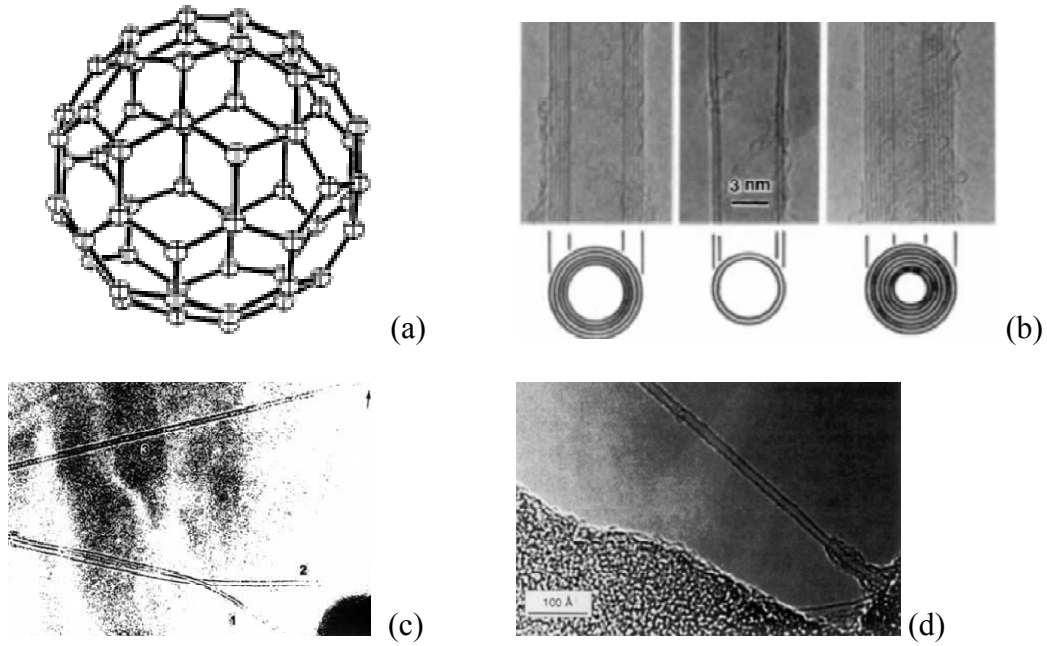

Figure 2.1. Ball and stick model of fullerene (C_{60}) molecule (a),[39] first TEM image of MWNTs published by Iijima (b)[36] and first TEM images of SWNTs published simultaneously by Iijima (c)[37] and Bethune (d)[38].

Carbon nanotubes have been evaluated for various applications due to their attractive combination of electrical,[40] thermal,[41] and mechanical[42] properties. Structurally, carbon nanotubes can be classified into two main categories: SWNTs and MWNTs. SWNTs have a structure resembling a graphite sheet rolled to from a cylinder capped with hemispheres of a fullerene molecule.[43-45] Within this basic SWNT structure, many variations exist, based on the orientation of hexagons with respect to nanotubes axis. This orientation, called chirality, is often used to classify SWNTs into three groups: armchair, zigzag and chiral, as shown in Figure 2.2 (a)-(c). Electronic properties and van der Waals interaction between the SWNTs depend on this chirality. Another parameter used to structurally classify SWNTs is the circumferencial vector which is defined as

$C_h = na_1 + ma_2$, where a1 and a2 are the hexagonal lattice unit vectors and n and m are integers.[40] These integers are used to identify nanotubes configuration with notation (n,m). The nanotubes in Fig 2.2(a)-(c) are (5,5), (9,0) and (10,5), respectively. If the difference between n and m is zero, or a multiple of 3, then the nanotube is metallic, but semiconducting otherwise. Based on this, it can be seen that armchair nanotubes (n=m) are always metallic in nature, but zigzag and chiral nanotubes may be metallic or semiconducting. MWNTs, shown in Figure 2.2 (d), consist of coaxial graphite cylinders arranged around a central hollow core with an interlayer spacing of ~0.34 nm, which is close to the interlayer distance of graphite.[46]

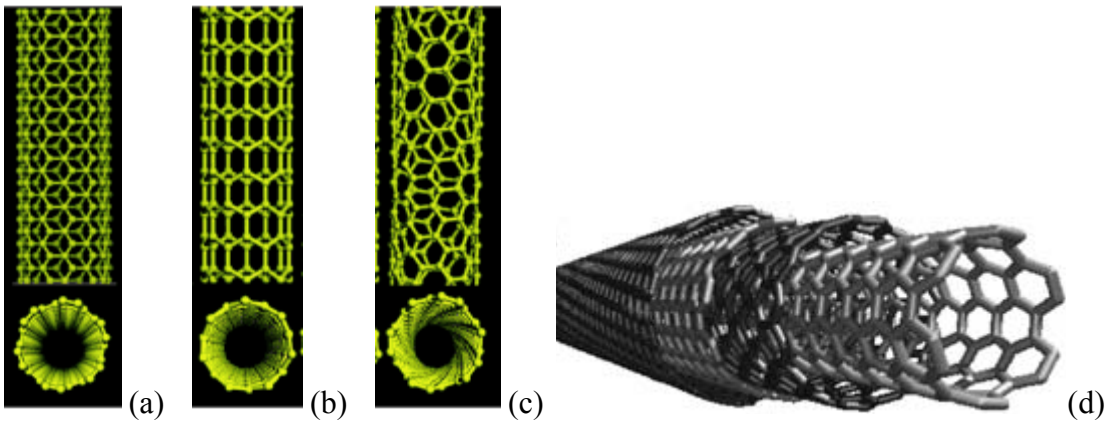

Figure 2.2. Types of SWNTs based on chiral angle[45]: armchair (a), zigzag(b), chiral(c), MWNT (d)[47] and chiral vector indices plotted on the graphene sheet (e).[40]

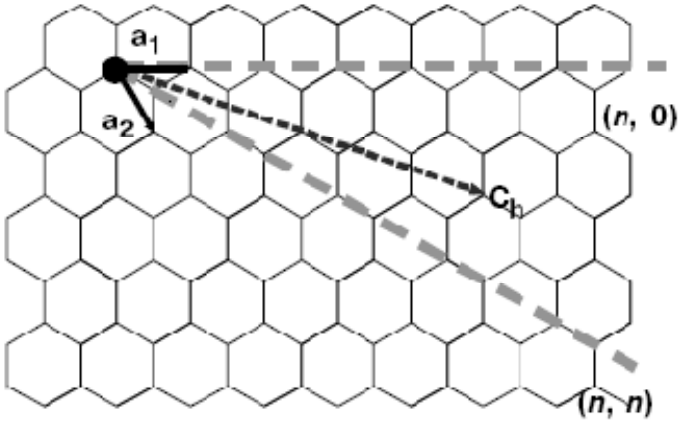

(e)

Figure 2.2. Continued.

2.1.1. SWNT Production

There are three major methods for producing large quantities of SWNTs: arc-discharge,[37-38,48] pulsed laser vaporization,[49-50] and high pressure carbon monoxide (HiPco).[51-52] In the arc-discharge method, current and voltage are applied across electrodes to vaporize carbon from graphite rods in the chamber. SWNTs are deposited on the cathode by plasma, as shown in Figure 2.3(a) with an average process yield of 80% and average diameter of 1.4 nm. The most common catalysts used are transition metal species, such as cobalt, nickel or iron.[53] In pulsed laser vaporization ,a laser is used to vaporize the carbon from a graphite target containing nickel and cobalt catalysts.[54] Nanotubes are deposited on a collector at the opposite end of the reactor. Figure 2.3(b) shows a typical reactor used for nanotube production. The average diameter of the tubes produced by this method is `1.4 nm and the reported yield is between 70-90%.[49] This method can produce better quality nanotubes than arc-discharge method, but it is also more expensive.

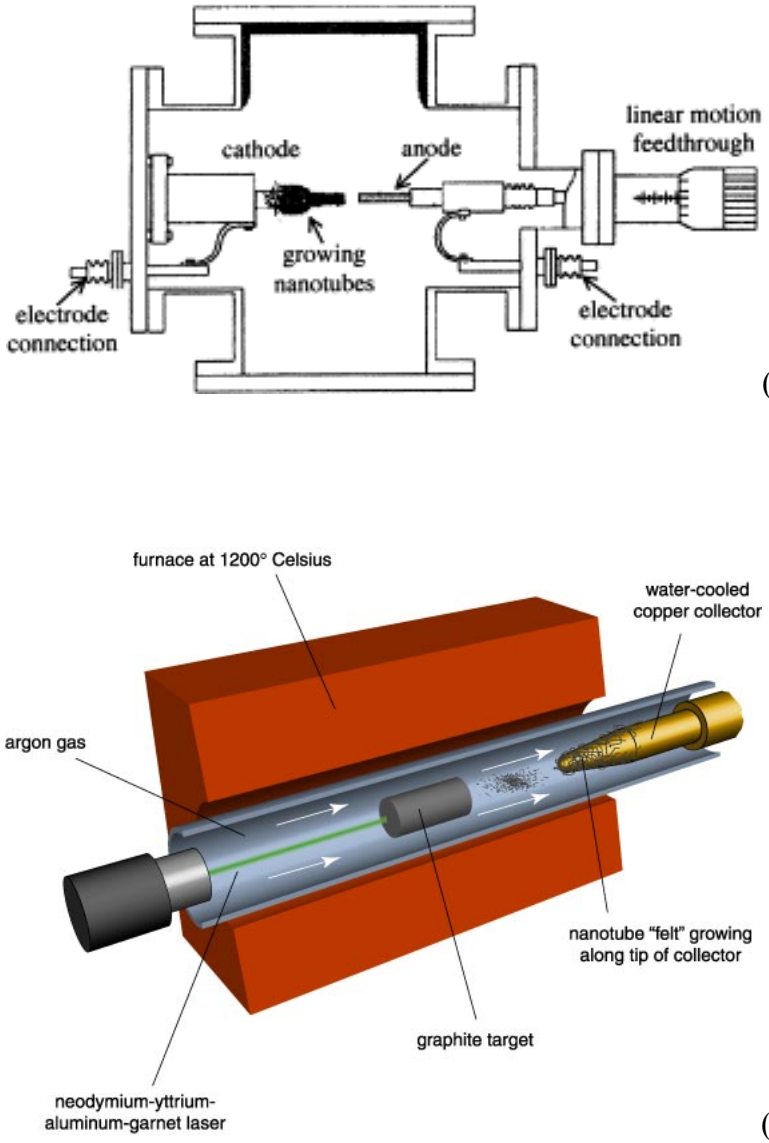

Figure 2.3. Schematic of an arc-discharge apparatus (a)[53]and a pulsed laser-ablation apparatus for nanotubes production (b).[54]

In the case of the HiPco process, carbon monoxide gas is used as a precursor material, which distinguishes it from the previous two techniques that use solid carbon as a source. Figure 2.4 shows the general schematic of this process. An iron

pentacarbonyl catalyst is added to flowing carbon monoxide. The catalyst decomposes when exposed to the high temperature and pressure, and SWNTs grown onto the newly formed iron clusters. The reported yield of this process is 97% and the product is high purity nanotubes.[55] All the methods described so far to produces a mixture of nanotubes with different chiralities, diameters, lengths with different amount of impurities and structural defects. HiPco is the method used to make the SWNTs used in this dissertation.

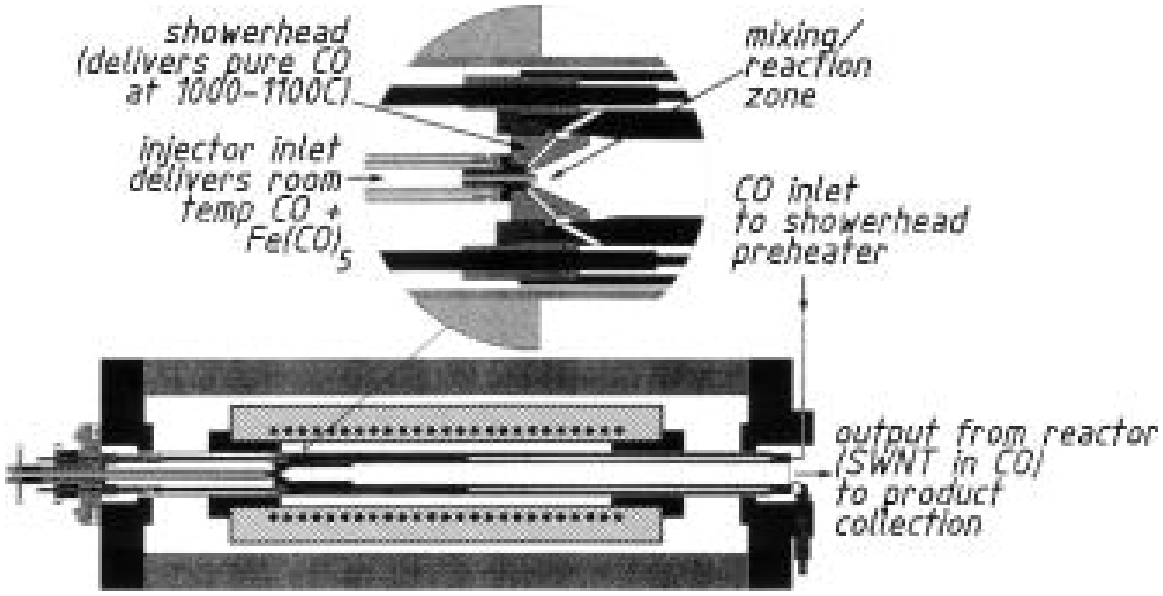

Figure 2.4. Schematic of the HiPco process for producing carbon nanotubes.[51]

2.1.2 SWNT Properties

The unique atomic structure of SWNT imparts many attractive multifunctional properties that make them suitable for a variety of applications. Experimentally measured values for tensile strength and modulus for SWNTs ropes are 13-53 GPa and 1

TPa, respectively, making them superior to steel.[42,56-57] Individual SWNTs are expected to have even better properties as failure in nanotube ropes occur due to slipping of nanotubes, which is easier than breaking of carbon-carbon bonds in individualized SWNT.[2] Furthermore, SWNTs have low density (~1.3 g/cm3) with exceptional flexibility.[58] Electrical conductivity measured along the length of a SWNT rope is approximately 100-200 S/m and the thermal conductivity of individualized SWNTs can be greater than 3500 W/(m.K).[49,59]

2.2. Carbon Nanotube Functionalization

The inert nanotube surface comprised of sp^2 carbon and strong inter-tube van der Waals attractions, makes them insoluble in most organic solvents, especially water.[20,60] The van der Waals interaction between two SWNTs is estimated to be as high as 5 eV/nm, which makes them indispersible in common solvents without the aid of a solublizing/stabilizing agent.[61] Difficulty associated with dispersion of nanotubes is a significant hurdle for their widespread use, as nanotubes bundles have inferior properties than individual tubes.[62] There has been extensive research on the development of both covalent and non-covalent fucntionalization methods that results in better dispersion of nanotubes, as described below.

2.2.1 Covalent Functionalization of SWNTs

Covalent (or chemical) functionalization of nanotubes is often the result of intense mixing due to the presence of local strain in carbon nanotubes arising from

pyramidalization and misalignment of the π-orbitals of the sp^2-hybridized carbon atoms.[63] The presence of local strain in SWNTs makes them more reactive than a flat graphene sheet, which makes it relatively easy for the chemical moieties to attach to the surface.[64] This chemical reaction is more feasible at the SWNT ends than at sidewalls because of the dimentional curvature. On the contrary, the inner surface of nanotubes exhibit very low reactivity which makes the core of nanotubes suitable for chemical storage.[65] Sidewall, defect and end site functionalization are most commonly used techniques for chemical modification of SWNTs.[66] The chemical functionalization of SWNTs significantly improves their dispersion in solvents, which eases their processability but at the same time degrades electrical and optical properties of nanotubes.[19] Despite this drawback, covalently functionalized nanotubes can undergo chemical reactions with the polymer matrix so that the interfacial interaction, between the polymer and nanotubes, is dramatically enhanced resulting in improved mechanical performance of composites.[67-69]

Defect functionalization of nanotubes is achieved by attaching chemical molecules at the defect sites. Defects in SWNTs are important because they act as anchor points for further functionalization or are created during functionalization. Figure 2.5 illustrates the typical defects in SWNTs: stone-wales defect (i.e., pentagon-heptagon pairs), sp^3-hybridized carbon, and vacancies in the nanotubes lattice.[66,70-71] Another common defect induced during purification of nanotubes is the incorporation of carboxy groups at the nanotube ends and sidewalls.[9,72] Purification is often performed prior to nanotube functionalization to remove amorphous carbon and catalyst particles.

Purification of SWNTs is generally done by using oxidizing acids, microfiltration or chromatographic procedures.[50,73-74] Various chemical moieties and nanoparticles have been attached to these defects sites to increase the dispersability of SWNTs and/or to impart added functionality, as described below.

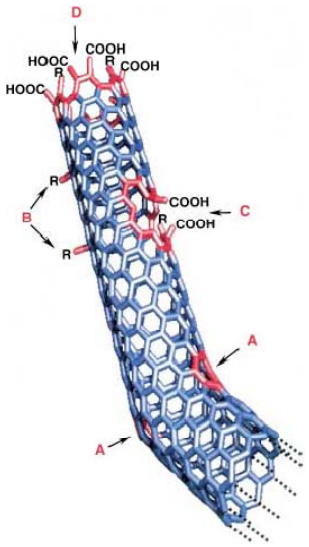

Figure 2.5. Typical defects in a SWNT: (A) Stone-wales defect, (B) sp^3 hybridized defects, (C) carboxy groups at side wall, (D) open end of SWNT with carboxy group.[66]

SWNTs have been functionalized with various small molecules (such as esters, acid chloride and pyrene derivatives) at the defect sites to make them soluble in organic solvents.[9,75-76] For aqueous solubilization, functionalization of defect sites with glucosamine and 2-aminoethanesulfonic acid are known to be effective.[77-78] Figure 2.6 illustrates the most common functionalization strategies at SWNT ends and defect sites. Furthermore, several inorganic nanoparticles, such as CdSe, Ag and Au, have also been attached to SWNT surfaces, through their ends and defect sites, to impart additional functionality to the nanotubes.[79-80] Biocompatibility of SWNTs can also be enhanced by defect and end site functionalization. For example, boving serum albumin (BSA) was shown to strongly associate with poly(ethylene glycol) modified SWNTs.[81] Metal coordination compounds have also been attached at the oxidized functional groups on SWNT sidewalls and end sites, for potential applications as reusable catalyst supports and for varying solublization and bundling characteristics of SWNTs.[82-83] For example, Wilkinson's compound [RhCl(PPh3)2] was attached to the ends and sidewalls of SWNTs, to be used for recyclable catalytic hydrogenation of cyclohexane.[84]

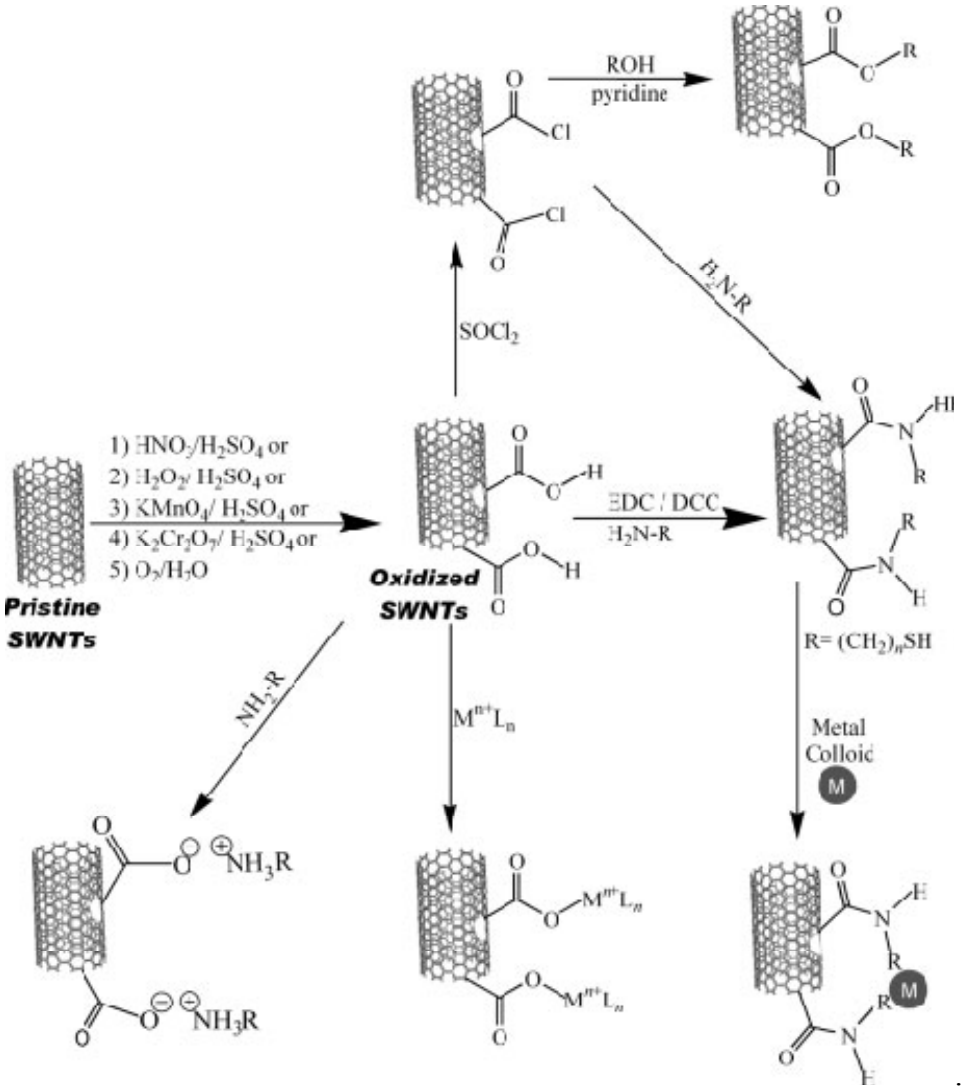

Figure 2.6. Schematic of common covalent functionalization methods used to derivatize SWNTs at ends and defect sites.[85]

Sidewalls in SWNTs have relatively low reactivity, so they need more intense reactive conditions.[86] This is attributed to the one dimensional curvature (cyclic) in nanotubes sidewalls.[87] Figure 2.7 illustrates the most common reaction schemes for sidewall functionalization reactions of SWNTs. One advantage of sidewall functionalization is the high degree of derivatization by this method.[88] Initial attempts in this direction were focused towards attaching fluorine moieties to nanotube sidewalls. Fluorination was chosen for these initial studies as it was used for the chemical transformation of graphite.[89] These fluorinated SWNTs were soluble in alcohols and were shown to be useful for transformation using wet chemistry techniques.[90-91] For example, fluorine atoms were substituted by alkyl groups by treatment with alkyl lithium or Grignard compounds and alkylated SWNTs were soluble in chloroform.[92] In contrast to this indirect method, direct sidewall functionalization of SWNTs with organic moieties is also shown to improve their solubility in organic solvents.[9] For example, necleophilic carbenes attached to SWNTs leads to a very stable suspension in DMSO.[93] In yet another example, SWNTs were functionalized by reaction with azomethinylide, which resulted in a very high degree of derviatization.[94]

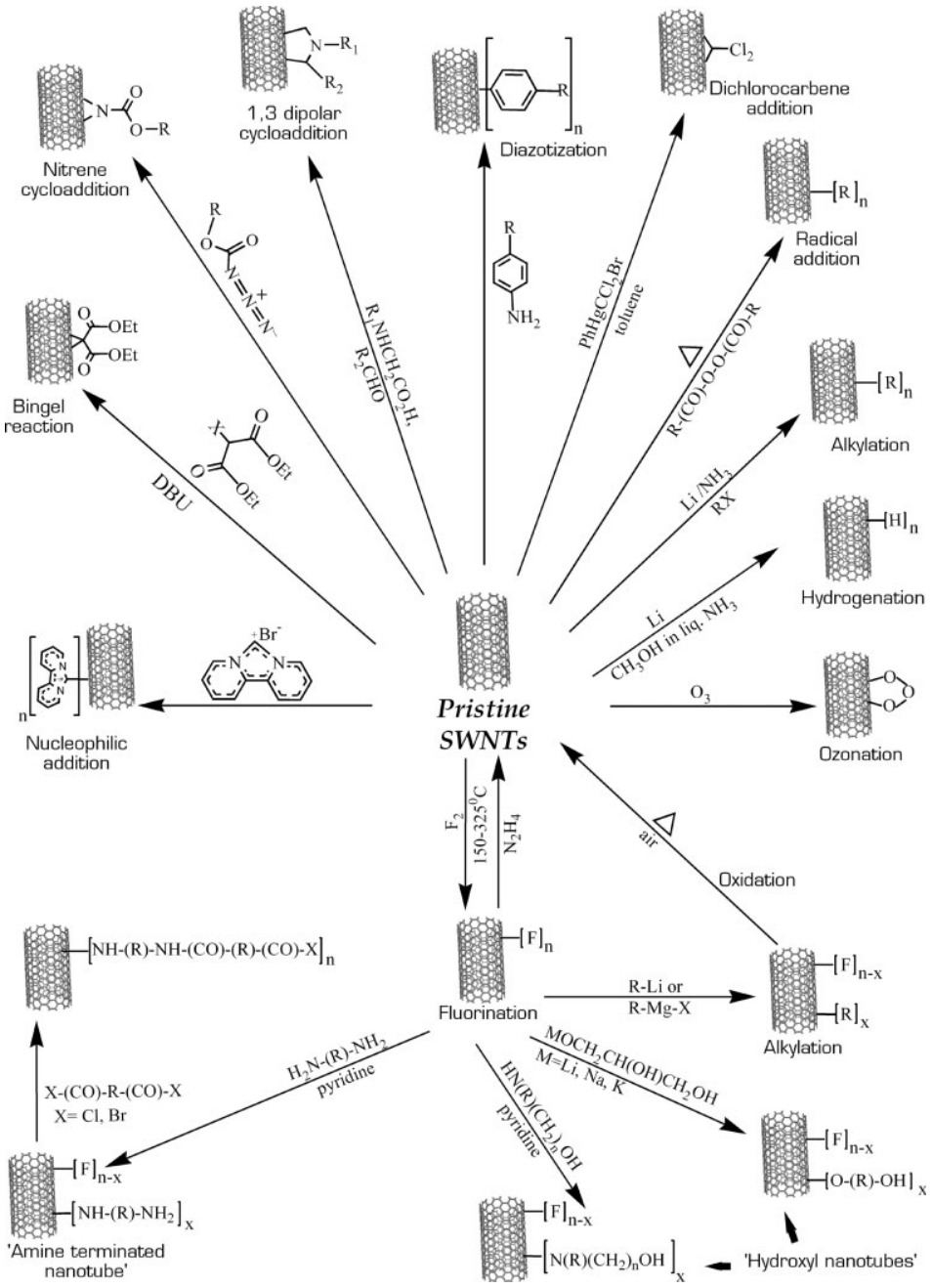

Figure 2.7. Sidewall-functionalization routes for covalent modification of SWNTs.[85]

In a similar manner to small molecules, polymers have also been chemically grafted to SWNT sidewalls to facilitate their dispersion and ease processing of polymer composites.[95] There are two general strategies for attaching polymer chains to nanotubes sidewalls: "*grafting to*" and "*grafting from*" methods.[96] In the *grafting to* method, end-functionalized polymer molecules are made to react with functional groups of chemically-functionalized SWNTs.[97-99] The reaction between these functional groups results in bonding of polymer chains. In the *grafting from* method, initiators are attached to a nanotube's surface and followed by in-situ polymerization of appropriate monomers.[100-102] The former method offers better control over polymer molecular weight, while the latter yields a higher degree of grafting.

2.2.2 Non-Covalent SWNT Functionalization

With non-covalent functionalization, the stabilizing species noncovalently interacts with the SWNT sidewalls, typically through adsorption. Unlike covalent functionalization, no chemical bond formation/breakage is required to functionalize SWNTs, therefore it better preserves their structure and electrical properties, while at the same time improving their solubility in common solvents.[103-105] Typical noncovalent functionalization of SWNTs (Fig. 2.8) includes the wrapping by polymers, adsorption of surfactants or small molecules, and π-π stacking by rigid, conjugated macromolecules or polymers.[66]

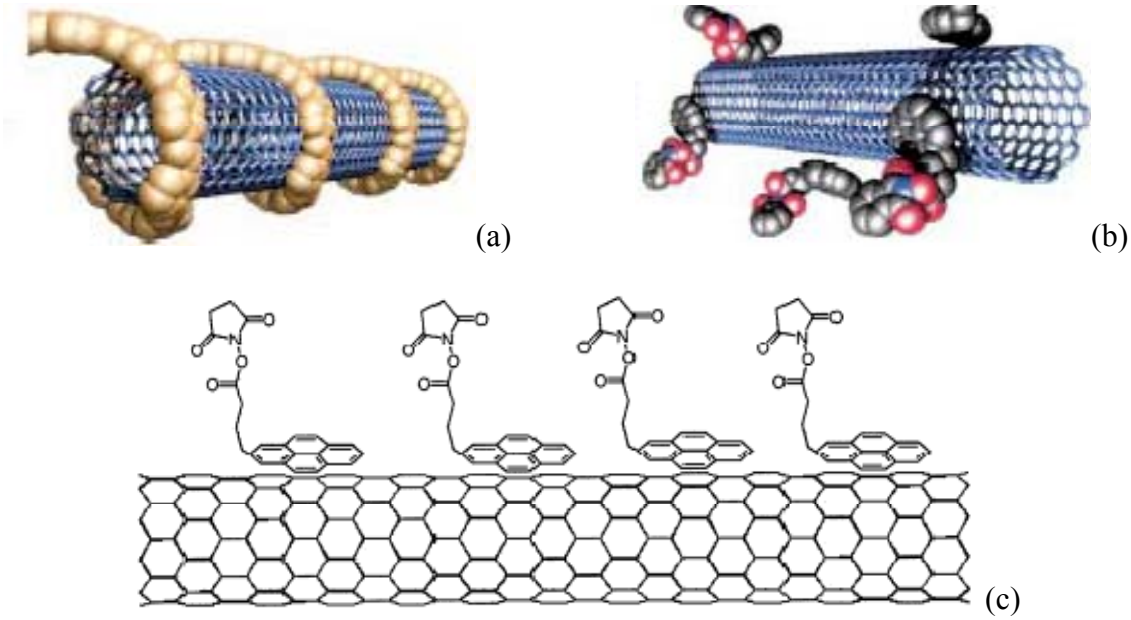

Figure 2.8. Typical non-covalent funtionalization strategies for SWNTs: wrapping with polymers (a), surfactant adsorption on the sidewall (b) [66] and π-π stacking by conjugated macromolecules (c).[15]

Water-soluble polymers can wrap around SWNT sidewalls to solubilize them in water, which is important because of potential the biomedical applications of nanotubes.[60,104,106] Wrapping of nanotubes by these polymers was proposed to be a result of the thermodynamic drive to reduce hydrophobic interfaces between nanotubes and the aqueous medium.[104] For example, poly(vinyl pyrrolidone) (PVP) and poly(stryrene sulfonate) (PSS) were shown to helically wrap around nanotube surfaces and to stabilize high concentrations (g/l) in water.[104] Other polymers and biomacromolecules, such as porphyrin-based polymers,[107] amylase,[108] startch-iodides,[109] peptides,[110] and single stranded DNA (ssDNA),[111] have also been shown to non-covalently stabilize carbon nanotubes in water. DNA is especially effective in dispersing nanotubes in water and the resulting DNA-nanotube suspensions are stable for months at room temperature.[112]

Furthermore, DNA-stabilized SWNTs can be separated on the basis of diameter using ion-exchange chromatography or by ultracentrifugation through an aqueous density gradient.[111]

Significant effort has been made towards solubilizing SWNTs in water using surfactants.[14,113-115] The most commonly used surfactants for noncovalent functionalization of SWNTs are sodium dodecyl sulfate (SDS),[116-118] sodium dodecylbenzene sulfate (SDBS),[8,119-121] gum arabic,[122-124] and sodium deoxycholic acid (DOC).[125-127] It is believed that nanotubes occupy the hydrophobic interiors of surfactant micelles, which results in a stable dispersion. Surfactant molecules containing aromatic groups are capable of more strongly adsorbing to SWNTs due to π-π stacking interactions. For example, sodium dodecylbenzene sulfate (SDBS) is more effective in stabilizing SWNTs than SDS due to the presence of an aromatic benzene ring in its structure that can stack on the nanotubes sidewalls.[8] Bile salt detergents, such as sodium salts of deoxycholic acid (DOC) and tarodeoxycholic acid (TDOC) are also excellent stabilizers of SWNTs in water.[125] These surfactants form stable micelles around nanotubes, which provide a homogeneous environment. Furthermore, the surfactants can be tailored to fit specific needs. For example, the hydrophobic tails of the surfactants can be modified with aromatic molecules, such as pyrene, porphyrin and their derivatives, to increase their interaction with SWNTs, where as the hydrophilic ends can be functionalized for other purposes.[66] This effect was demonstrated by functionalizing nanotubes with *N*-succinimidyl-1-pyrenebutanoate, where the pyrene groups anchor to

SWNT sidewalls and succinimidyl groups could be substituted with amino groups from proteins, such as ferritin or streptavidin, for potential application in biosensors.[15]

Aromatic and hetrocyclic polyaromatic molecules, such as anthracenes, benzenes, pyrenes, porphyrins, phtalocyanines and sapphyrins, have also been shown to interact strongly with SWNT sidewalls through π-π stacking.[128] Pyrene groups have an especially high affinity for the carbon nanotube surface. For example, ammonium amphiphiles carrying a pyrenyl group act as excellent stabilizers for SWNTs in water.[129-130] Similarly, SWNTs are also shown to strongly interact with pthalocyanines, porphirines, and zinc porphirins.[131] The nature of the interaction between SWNTs and polyaromatic compounds is believed to be van der Waals attraction. Conjugated polymers and dendrimers, such as poly(m-phenylenevinylene)-co-(2,5-dicotoxy-p-phenylene) vinylene (PmPV),[16] poly-(5-alkoxy-*m*-phenylenevinylene)-co-(2,5-dioctoxy-*p*-phenylene)vinylene(PAmPV),[132] poly(phenyl -eneethynylene)s (PPE)[133] and stilbine-like dendrimers[134] can also solubilize SWNTs in organic solvents. These conjugated polymers form supramolecular complexes with carbon nanotubes. Molecular dynamics studies suggest the interaction between conjugated polymers and SWNTs is dependent on polymer structure.[135] The polymers with aromatic rings in their backbone were found to be better in solubilizing nanotubes because of stronger interactions arising from π-π stacking.

2.3 Stimuli-Responsive Polymers

The polymers that are capable of conformational and chemical changes on exposure to external stimulus are called stimuli-responsive polymers.[136] The conformational changes of the polymer manifests as changes in its physical properties that can be triggered by environmental factors such as temperature, chemical composition, ionic strength, light or mechanical force.[137] These changes in polymer conformation usually involve ionic interactions, hydrogen bonding or hydrophobic effects. Responsive polymers can be made in different forms and used in a variety of applications (e.g., smart drug delivery, sensors and coatings etc, as shown in Figure 2.9.[137]

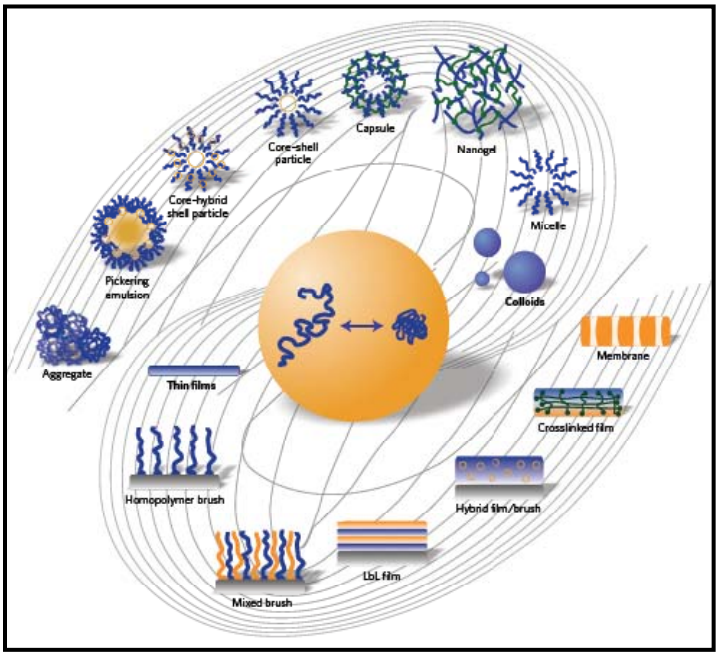

Figure 2.9. Schematic of nanostructured forms of stimuli-responsive polymeric materials.These polymers undergo conformational transitions as a function of applied stimulus which results in altered physical properties.[137]

2.3.1. pH- Responsive Polymers

pH-responsive polymers exhibit reversible solubility, volume and conformational changes as a function of pH.[138] These polymers usually have pKa values between 3 and 10 and can be used for fabrication of responsive materials with tailorable properties.[29] Many of these so-called weak polyelectrolytes contain pendant acid and base groups, such as carboxylic acids, phosphoric acid and amines, which can change their ionization state upon variation of the pH (Fig 2.10).[139] The presence of these ionizable groups in pH-responsive polymers drives backbone conformational changes and a swelling change in hydrogels. Most anionic pH-responsive polymers are based on polyacrylic acid (PAA) or its derivatives.[138] Apart from PAA, polymethacrylic acid (PMAA), polyethyleneimine poly(L-lysine), and poly(*N*,*N*-dimethyl aminoethyl methacrylamide) are also well studied pH-responsive polymers.[140-141] These homo-polymers are often co-polymerized with other monomers to yield a multi-functional material. For example, copolymer networks of poly (methacrylic acid) grafted with poly(ethylene glycol) with reversible pH-dependent swelling behavior.[142] In another example, pH-sensitive PAA was co-polymerized with temperature responsive poly(*N*-isopropylacrylamide) to yield both pH and temperature response.[143]

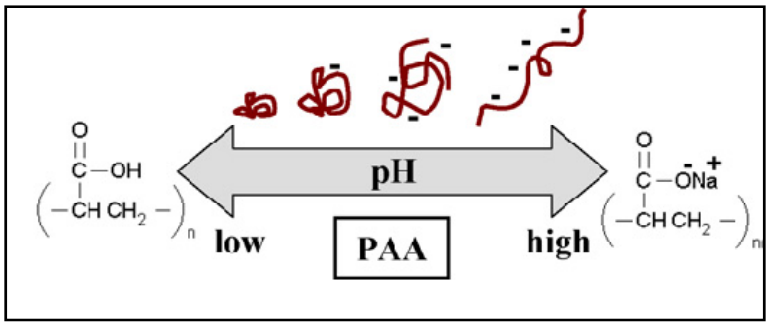

Figure 2.10. pH induced conformational transitions in PAA. At high pH, the carboxylic acid groups are de-protonated which causes extensive intra-chain repulsion and leads to an more extended conformation.[21]

2.3.2 Thermoresponsive Polymers

Most thermoresponsive polymers undergo a phase transition at a particular temperature, which results in changes in their conformation, solubility and hydrophobic-hydrophilic interactions.[136] Most of the synthetic polymers with temperature sensitive phase transformations belong to three families: poly(acrylamides), poly(*N*-vinylamides) and poly(ethylene oxide)-based polymers.[144] Some natural polymers used in pharmacy also exhibit thermoresponsive behavior, like gelatin, cellulose derivatives and chitosan.[145-146] Elastin-like polypeptides (ELP's) also have a thermally-sensitive phase transition that has been utilized in targeting a drug to hyperthermic tumor cells or in thermogelling-injections.[147-148] Thermoresponsive polymers that dissolve upon heating demonstrate upper critical solution temperature (UCST) and polymers that exhibit the reverse behavior have a lower critical solution temperature (LCST). These polymers contain both hydrophilic and hydrophobic groups. For polymers that show LCST, at low temperatures hydrogen-bonding between the hydrophilic groups of the polymer and

water molecules is dominant and leads to enhanced dissolution in water.[139] With increasing temperature, partial displacement of water from the polymer coil results in weakening of the hydrogen bonds and interactions between hydrophobic segments of the polymer increases.[149] As a result, the polymer collapses. Aggregation and phase separation occurs due to increased affinity for intra- and inter-molecular association between the hydrophobic parts of the polymer molecule over the hydrogen-bonding with water molecules (at lower temperatures). This phenomenon is reversible, as depicted in Figure 2.11. At temperatures below LCST, the polymer chain is more extended and, as result, the polymer swells and is dissolved in water. At temperatures above the LCST, the polymer chain collapses and associates with neighboring chains that often leads to precipitation.[150]

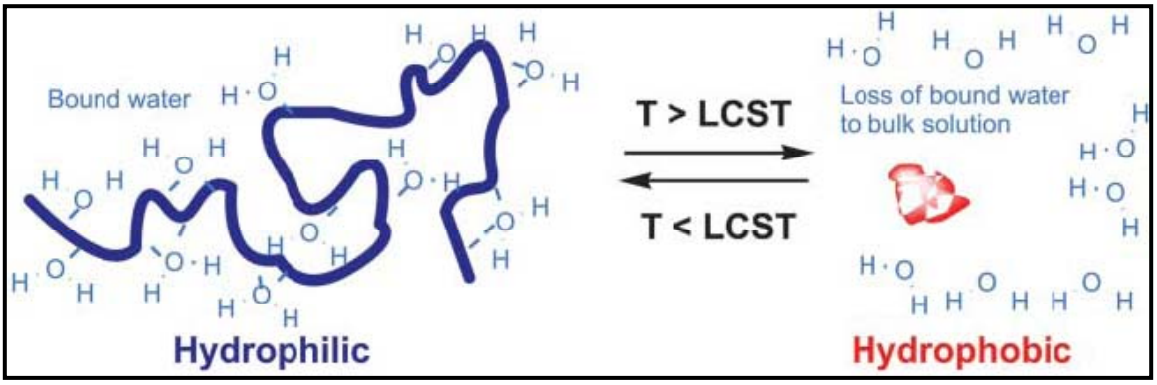

Figure 2.11. Effect of temperature on a thermoresponsive polymer that shows LCST behavior.[150]

2.3.3 Other Responsive Polymers

Light (or photo) responsive polymers exhibit conformational changes as a function of exposure. Typical mechanisms responsible for photo responsive behavior include: photoisomerization,[151] photoreactivity[152] and photo-induced ionic dissociation.[153] Azobenzene molecules undergo cis-trans isomerization upon exposure to UV light. When these groups are attached to polymer chains, the inter-conversion between the two photoisomers can induce macroscopic changes in the polymeric material. For instance, azobenzene based liquid crystalline elastomers have been shown to exhibit lower degrees of alignment due to photoisomerization of azobenzene moieties.[151] Figure 2.12 shows the light response of a liquid crystalline polymer functionalized with azobenzene moieties. Another class of stimuli-responsive polymare are those that respond to changes in electric field. These electrosensitive polymers have been investigated for applications in modern medicine.[154] For example, polythiophene-based conductive polymer gel was shown to undergo swelling–deswelling transition in response to applied potential over −0.8 to 0.5 square wave potential.[155] When confined in a well, the gel developed a pressure of 10 KPa, which can be used in small-scale actuators or valves in microsystems. Any of the stimuli-responsive polymers described could potentially be used to tailor nanotube dispersion state. This dissertation focuses on pH and temperature-controlled dispersion, whose polymers are stable and well studied.

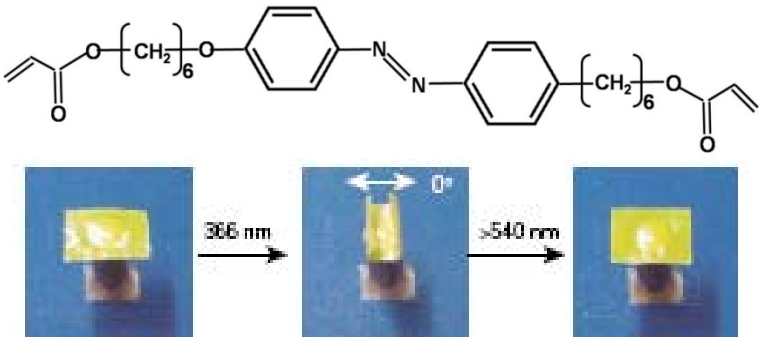

Figure 2.12. Photoactive effect of liquid-crystal film containing azobenzene exposed to linearly polarized light.[151]

CHAPTER III

pH-TAILORED CARBON NANOTUBE DISPERSION

3.1. Introduction

Single-walled carbon nanotubes offer attractive properties that could be used in variety of applications.[1] However, as produced nanotubes exist in bundles that contain numerous tubes, which create problems for their efficient utilization. Covalent and non-covalent functionalization of SWNTs is shown to an effective way to exfoliate (i.e., break bundles to yield individual tubes) nanotube bundles.[9-18] Covalent functionalization usually disrupts the conjugated π structure and degrades electrical and optical properties of SWNTs, whereas, non-covalent functionalization better preserves nanotube structure, as described in the Chapter II.[19,103-105] When stimuli-responsive polymers are used to non-covalently functionalize SWNTs, there is an opportunity to control the level of exfoliation of nanotubes as a function of applied stimulus while preserving their structure. Earlier studies on non-covalently functionalized SWNTs using pH responsive polymers suggested a pH tailored microstructure of nanotubes in aqueous suspensions.[21-22] Unfortunately, the underlying mechanism responsible for such a controlled dispersion of nanotubes is not well understood and needs further attention.

In this chapter, four different pH-responsive polymers, PAA, PMAA, poly(allylamine) (PAAm), and branched polyethylene-imine (BPEI) were used to stabilize aqueous SWNT suspensions. These polymers exhibit a transition between completely neutral and fully charged states with changing pH. PAA and PMAA are

weak polyanions, exhibiting negative and neutral charge at high and low pH,[21,156-157] respectively. PAAm and BPEI are weak polycations, exhibiting neutral and positive charge at high and low pH,[158] respectively. The focus of this work is to evaluate the effectiveness of these polymers in dispersing SWNTs in water and to understand the pH-responsive behavior of the stabilized suspensions. Various techniques (rheology, conductivity, microscopy and zeta potential) were used to characterize these stabilized SWNT suspensions stabilized using pH-responsive polymers. The results indicate that pH-responsive polymers are useful for controlling the microstructure of SWNTs in water as a function of pH. Furthermore, polyanions were found to stabilize SWNTs more effectively relative to polycations. Based on the results obtained, a stabilizing mechanism is proposed to explain the pH-responsive dispersion and aggregation of SWNTs in aqueous suspensions that are stabilized using weak polyelectrolytes. This work expands the scope of previous work and provides fresh insights on the dispersion and stabilization of SWNTs in water using weak polyelectrolytes.[21-22] Additionally, this pH tailorability of SWNT dispersion is expected to impact the microstructure and final properties of solution-processed polymer composites.

3.2. Experimental Section

3.2.1. Materials and Methods

Raw single-walled carbon nanotubes (SWNTs) [batch number R0487] were purchased from Carbon Nanotechnologies (Houston, TX) containing 27 wt% impurity (mostly Fe-based catalyst). These nanotubes were used without further purification. PAA (M_w= 100,000 g/mol) and BPEI (M_w = 25,000 g/mol) were purchased from Aldrich (Milwaukee, WI), while PAAm (M_w=15,000 g/mol) and PMAA (M_w=100,000 g/mol) were purchased from PolyScience Inc (Warrington, PA). Aqueous suspensions were prepared by mixing dry SWNTs in 1wt% aqueous solutions of polymers at their natural (unaltered) pH, followed by sonication for 10 minutes at 50 W using a VirTis Virsonic 100 ultrasonic cell disrupter (SP industries, Warminster, PA). pH adjustments were made using 1M NaOH and HCl purchased from Aldrich. Suspensions were sonicated for 5 minutes at 50 W after pH adjustment. Composites used for electrical conductivity measurements were made by drying 5 ml of suspension on a quartz slide at room temperature (20 ^{o}C) for 24 hours followed by storing the samples in a dry box for a week before measurements. Dried films were on the order of 0.5 mm thick.

3.2.2. Characterization

To investigate the relative stability of suspensions, centrifugation was performed at 4500 RPM for 15 minutes with an accuSpin 400 (Fisher Scientific, Pittsburgh PA). Cryo-TEM images were taken with an FEI Tecnai G2 F20 (Hillsboro, OR) operated at

200 kV and equipped with cryogenic accessories. The samples were frozen in liquid ethane using an FEI Vitrobot apparatus. Images were recorded with a Gatan Tridiem GIF-CCD camera attached to the microscope. UV-Vis measurements were made with a USB2000 UV−vis spectrometer (Ocean Optics, Dunedin, FL) using a quartz cuvette. Suspensions that originally contained 1 wt% of polymer and 0.11 wt% SWNT were diluted 10 times for UV-Vis measurements. Viscosity of the suspensions as function of shear rate was measured using an AR-G2 rheometer (TA Instruments, Newcastle, DE) equipped with a 40 mm parallel plate geometry. A gap of 1000 μm was maintained for the measurements shown here. Sheet resistance of the composites was measured using a custom-built 4-point probe apparatus. The details of this system and measurement technique has been published elsewhere.[159] The data presented in Figure 7 are the average values of 16 measurements per sample. Volume conductivity was calculated by taking the inverse of the product of the sheet resistance and composite thickness. To determine suspension stability, zeta potential measurements were made with a Zeta Phase Angle Light Scattering (ZETA PALS) system (Brookhaven Instruments Corporation, Holtsville, NY) using a quartz cuvette. The test chamber was maintained at 25^{o}C and zeta potentials were determined following the standard operating procedure of the instrument. Scanning electron microscopy was performed with an FEI Quanta 600 FE-SEM on the surface of composites coated with a 5nm layer of Pt.

3.3 Results and Discussion

Figure 3.1 shows a schematic of conformational changes as a function of pH for the polymers studied here. All of these polymers exhibit a transition between completely neutral and fully charged states as pH increases or decreases. In their fully ionized state these polymers exist in an *"extended"* (i.e, looser coil) form and transition to a more coiled (i.e., globule-like) conformation as the chain becomes neutralized. It should be noted here that the weak polycations (PAAm and BPEI) and weak polyanions (PAA and PMAA) used in this study achieve neutrality on opposite ends of the pH spectrum. Higher charge density causes the polymer chain to repel itself and leads to a more extended conformation. PAA and PMAA are protonated (neutral) weak polyacids at low pH and exhibit significant intramolecular hydroden bonding resulting in a globular conformation. At high pH, these polyacids are deprotonated, leading to buildup of negative charge along the polymer backbone that causes extension of the polymer chain through self-repulsion. In contrast, PAAm and BPEI are weak polybases that exhibit globular conformation at high pH and assume an extended conformation with decreasing pH due to ionization. It is this combination of changes in polymer chemistry and conformation that alters their interaction with carbon nanotubes and produces macroscopic changes in suspension properties, as described below.

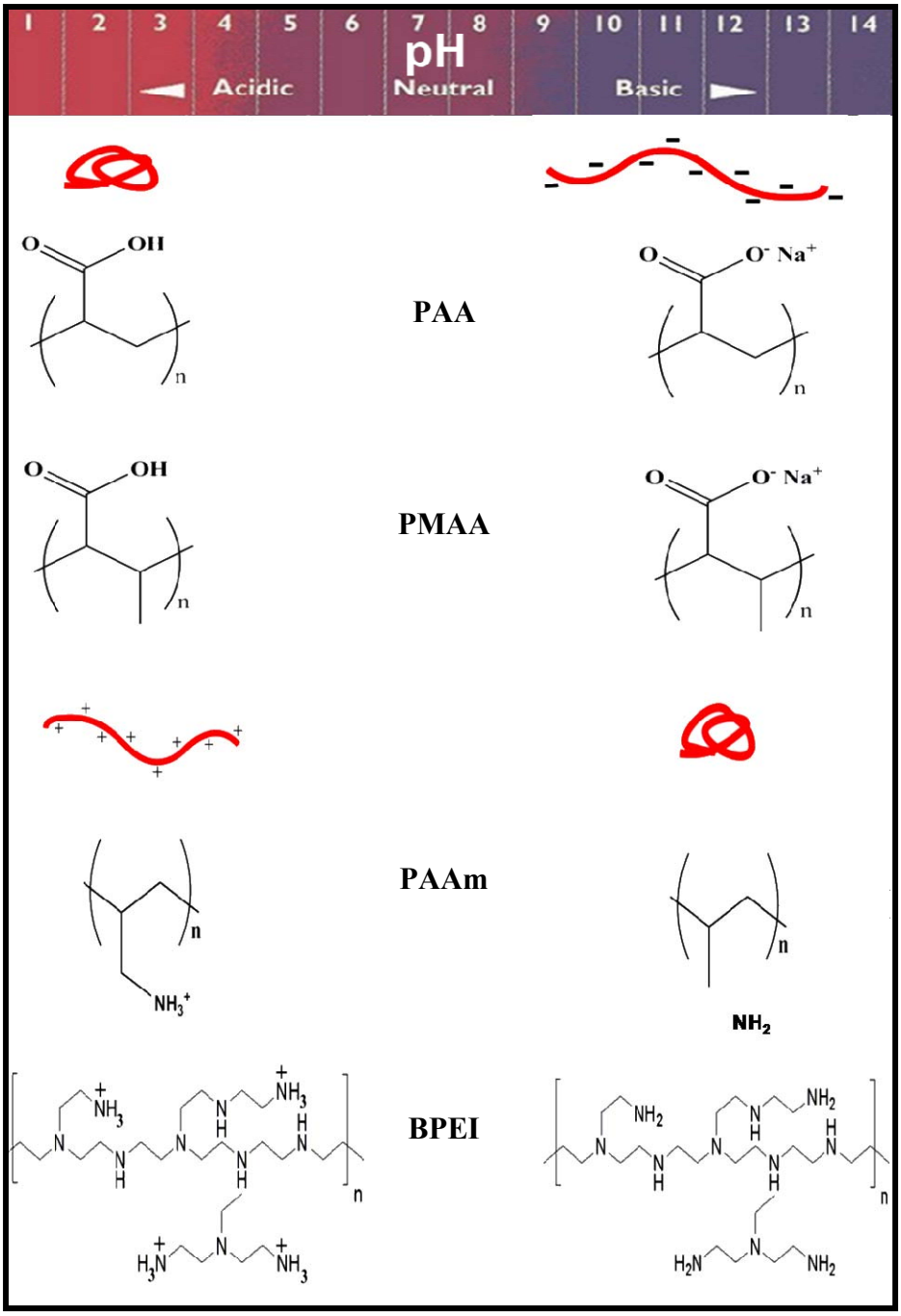

Figure 3.1. Effect of pH on the chain conformations of PAA, PMAA, PAAm and BPEI. PAA and PMAA have neutral charge at low pH and become negatively charged at high pH. PAAm and BPEI are neutral at high pH and attain positive charge at low pH.

It was previously shown that suspensions containing exfoliated SWNTs have higher UV absorbance compared to the suspensions containing bundles.[160-161] Individual SWNTs are active in UV-Vis region and exhibit characteristic bands corresponding to additional absorption due to 1D van Hove singularities.[162-164] On the other hand, the carrier dynamics in SWNT bundles are dominated by tunnel coupling between semi-conducting and metallic SWNTs, which results in diminished interaction with light. As a result, only individual SWNTs can provide a UV-Vis signature that suggests an increase in absorbance corresponds to the presence of more exfoliated SWNTs. To investigate this aspect, UV-Vis spectroscopy was performed on weak polyelectrolyte suspensions containing SWNTs and the results are shown in Figure 3.2. It can be seen that the UV absorption is greater for PAA-stabilized SWNT suspensions at pH 7 as compared to those stabilized at pH 5 and pH 9. This is attributed to the presence of more exfoliated SWNTs at pH 7, than at pH 5 or pH 9 in PAA stabilized suspensions. A similar observation was made for PAA-stabilized multi-walled carbon nanotubes, where suspensions at pH 5 show better dispersion than those at lower or higher pH.[165] The SWNT suspensions stabilized with PMAA at pH 5 have more absorbance than those at pH 7 and pH 9 suggesting the presence of more exfoliated SWNTs at pH 5. Furthermore, PAAm-stabilized SWNT suspensions have higher absorbance at pH 11 than those at pH 3 or pH 5, suggesting better SWNT exfoliation at high pH. BPEI stabilized suspensions show only a small increase in absorbance as a function of pH that may be due to the branched structure of BPEI causing weaker interaction with the nanotubes. It was previously shown that dispersion of SWNTs by amines is sensitive to steric hindrance

around the nitrogen atom.[166] It should be noted that pH-dependent differences in UV-Vis absorption are more prominent for polyanion-stabilized SWNTs as compared to polycations. Furthermore, it was observed that polyanion-based suspensions were stable for a longer period of time relative to polycation-based. Better stabilization of SWNTs with polyanions is presumably because of the Lewis-base character of the graphene side-walls of SWNTs, which results in stronger adsorption of polyacids.[167]

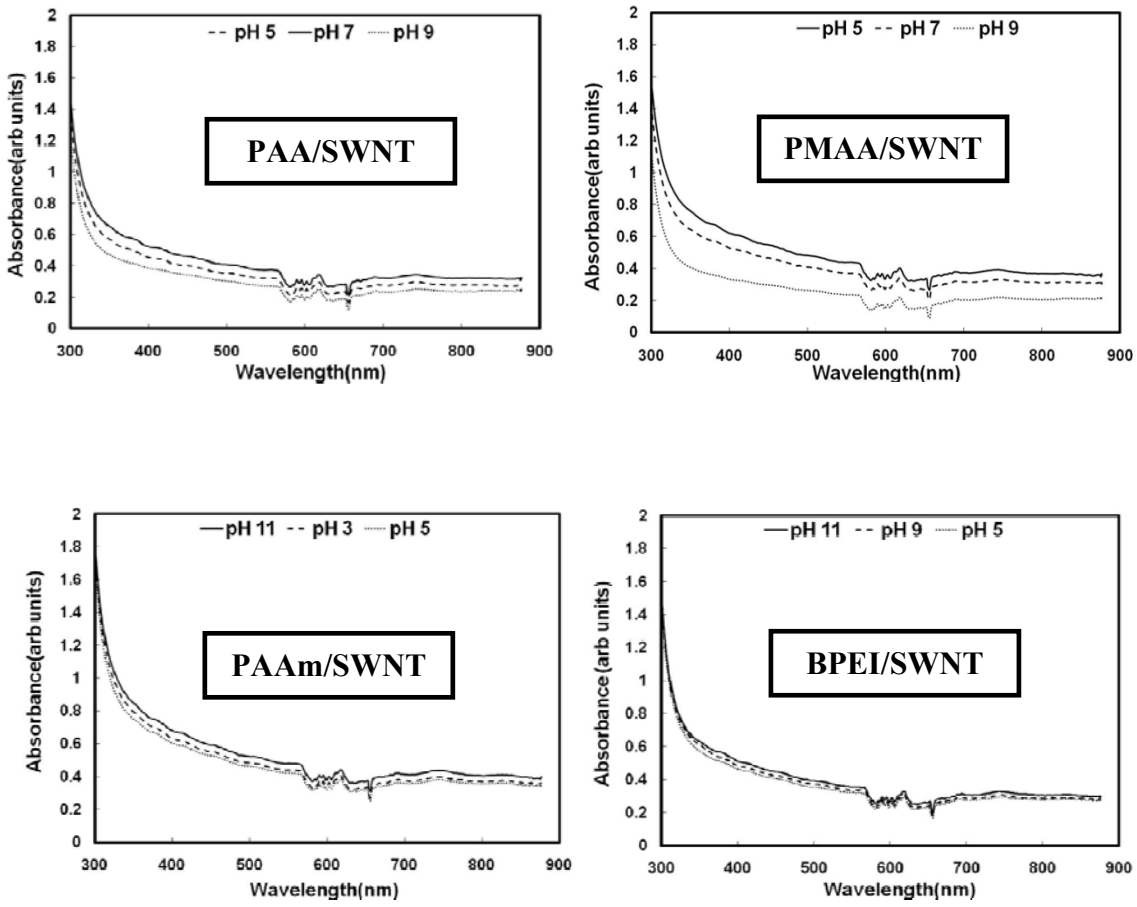

Figure 3.2. UV-Vis spectra of aqueous suspensions containing 0.01 wt% pH-responsive polymer and 0.0011wt% SWNTs at various pH levels.

Suspensions at pH levels corresponding to maximum and minimum UV-Vis absorption were chosen for further characterization. Figure 3.3 shows the relative stability of SWNT- stabilized suspensions at different pH. The suspensions were sonicated for 10 minutes at 50 W prior to centrifugation at 4500 rpm for 15 minutes. As shown in Fig.3.3, PAA-stabilized suspensions at pH 7 are relatively homogeneous after centrifugation, but those at pH 9 show significant sedimentation. It should be noted here that PAA/SWNT suspensions at pH < 7 were slightly less stable than those at pH 7, although they are relatively similar compared to the pH 9 suspensions. The PMAA-stabilized suspensions show similar pH-dependent stability, with suspensions at pH 5 being stable after centrifugation, while those at pH 9 show significant sedimentation. As expected, PAAm stabilized suspensions show the opposite trend. PAAm-based suspensions are stable at pH 11, while those at pH 5 show significant sedimentation. BPEI stabilized suspensions show poor stabilization at both high and low pH. As already mentioned, this may be due to the branched structure of BPEI that sterically diminishes interaction.

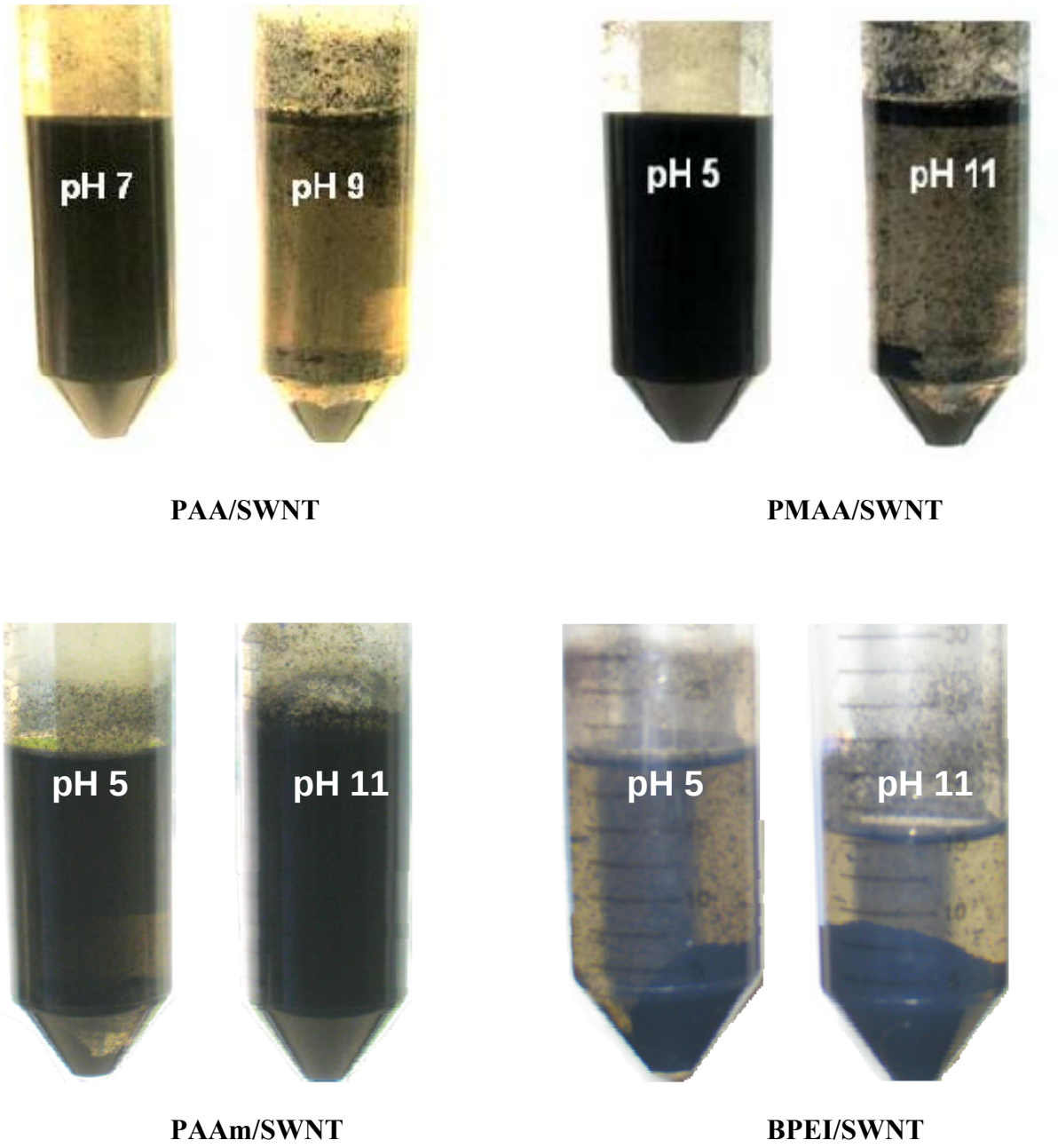

Figure 3.3. Images of aqueous nanotube suspensions after centrifugation at different pH. All suspensions contained 0.11 wt% of SWNT in 1 wt% of the aqueous polymer solution.

In an effort to visualize the SWNT nanostructure in water, cryo-TEM was done with SWNT/PAA and SWNT/PAAm suspensions. Figure 3.4 shows these images, where it is obvious that PAA-stabilized SWNTs exist in a relatively exfoliated state at pH 7 and are more bundled at pH 9. The images of PAAm-stabilized SWNT suspensions show more exfoliation at pH 11(Fig. 3.4(c)) than at pH 5 (Fig. 3.4(d)). Significant exfoliation of nanotubes is possible when sufficient inter-tube repulsion is introduced by the dispersant. The repulsion can be electrostatic, steric or a combination of both (i.e., electrosteric) based on the charged state and conformation of the adsorbed dispersant.[168] Since the polyelectrolytes used in this study are weak polyacids and polybases, the electrostatic stabilization mechanism alone may be not sufficient for stable dispersion of SWNTs. The observation of aggregated SWNTs at the pH corresponding to the charged state of PAA and PAAm strengthens this claim. Exfoliated nanotubes observed at conditions corresponding to more globular polymer conformation suggests the presence of a thicker steric layer on the SWNT surface. Both PAA and PAAm have globule like conformation at low and high pH, respectively, that can lead to thicker steric layer coverage on the nanotubes. Additionally, these polymers undergo pH-dependent ionization that leads to a charge buildup along the polymer backbone. The presence of a steric layer of partially ionized polymers on SWNTs counteracts the inter-tube van der Waals force of attraction through what is believed to be an electrosteric stabilization mechanism. The cryo-TEM micrographs of PMAA stabilized suspensions (not shown here) also show exfoliated and aggregated SWNTs as a function of pH. The observation of exfoliated and aggregated SWNTs, depending on the type of stabilizing polymer used,

as a function of pH (in the cryo-TEM micrographs) provides direct evidence of pH-responsive SWNT-stabilization in water.

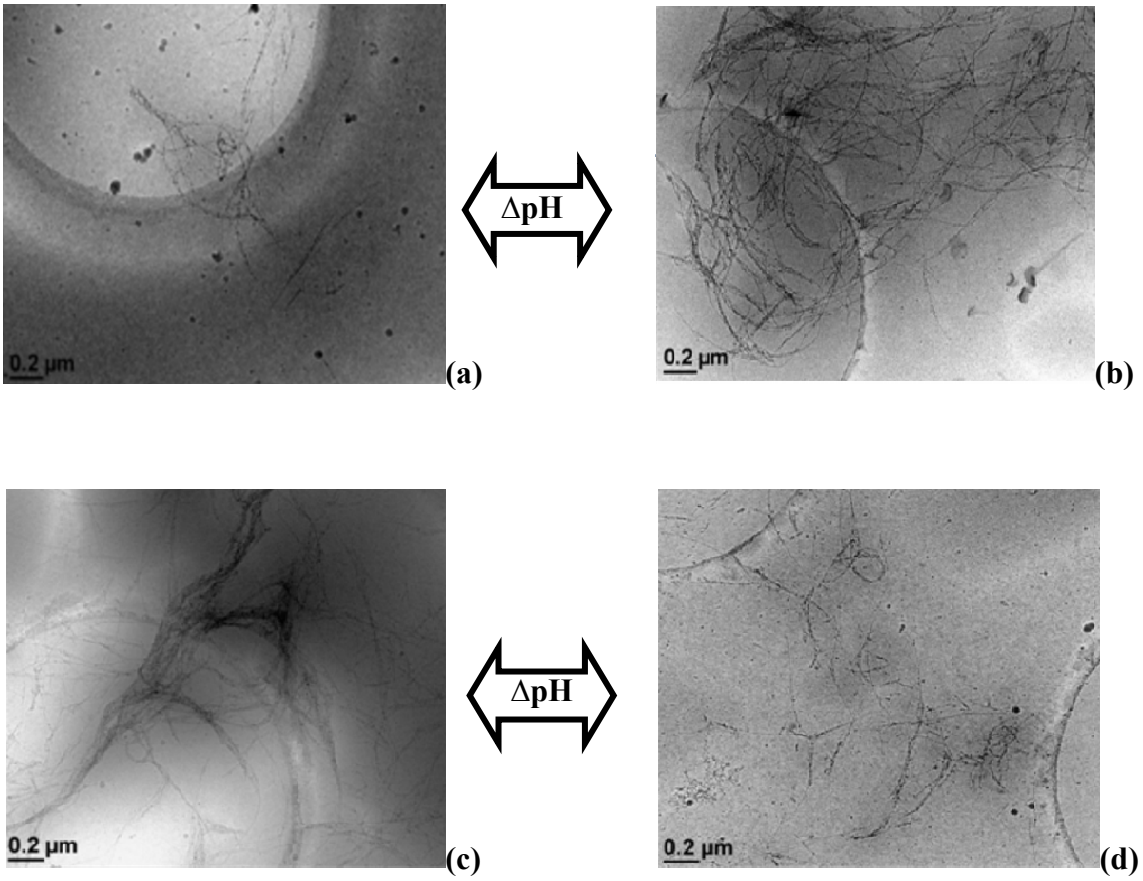

Figure 3.4. Cryo-TEM images of SWNT/PAA suspensions at pH 7 (a) and pH 9 (b) and SWNT/PAAm suspensions at pH 5 (c) and pH 11 (d).

Suspensions with well-dispersed SWNTs are known to have lower viscosities as compared to those that have agglomerated or bundled tubes, due to lack of entanglements.[22] Furthermore, it was shown that concentrated solutions of nanotubes show *shear-thinning* behavior because of the high degree of physical entanglements that are akin to polymeric solutions.[169] The observation of shear-thinning behavior in SWNT

suspensions stabilized with pH-responsive polymers should therefore suggest the presence of highly networked SWNT structure. At high shear rates these networks are broken, which results in lower suspension viscosity. On the other hand, the absence of a networked SWNT structure, found in suspensions containing highly exfoliated SWNTs, should lead to a more shear rate independent behavior (i.e., Newtonian). In an effort to investigate this pH-dependent behavior, viscosity measurements were made on aqueous suspensions containing 0.11 wt% SWNTs and 1 wt% of the stabilizing polymer as shown in Figure 3.5. Both PAA and PMAA-stabilized SWNT suspensions show *shear-thinning* behavior at pH 9, further confirming the presence of a networked structure. Newtonian behavior arising due to the presence of exfoliated nanotubes is observed at low pH (i.e, pH 7 for PAA and pH 5 for PMAA). PAAm and BPEI stabilized SWNT suspensions show strong *shear-thinning* behavior at pH 5 and pH 3, respectively, also suggesting the presence of networked SWNTs. At high pH, the PAAm-based suspension still shows *shear-thinning* behavior, although it is closer to Newtonian than low pH. BPEI-based suspensions actually get slightly more shear thinning at high pH. This lack of transition to fully Newtonian behavior suggests weaker polymer-nantube interaction for weak polycations, which may be expected due to both entities having basic chemistry. It should be noted here that aggregated and exfoliated microstructure of SWNTs was observed in cryo-TEM images (see Fig. 3.4) for suspensions showing shear-thinning and Newtonian behavior, respectively. Therefore, it is reasonable to suggest that SWNTs stabilized with pH-responsive polymers exhibit pH dependent dispersion in aqueous suspensions.

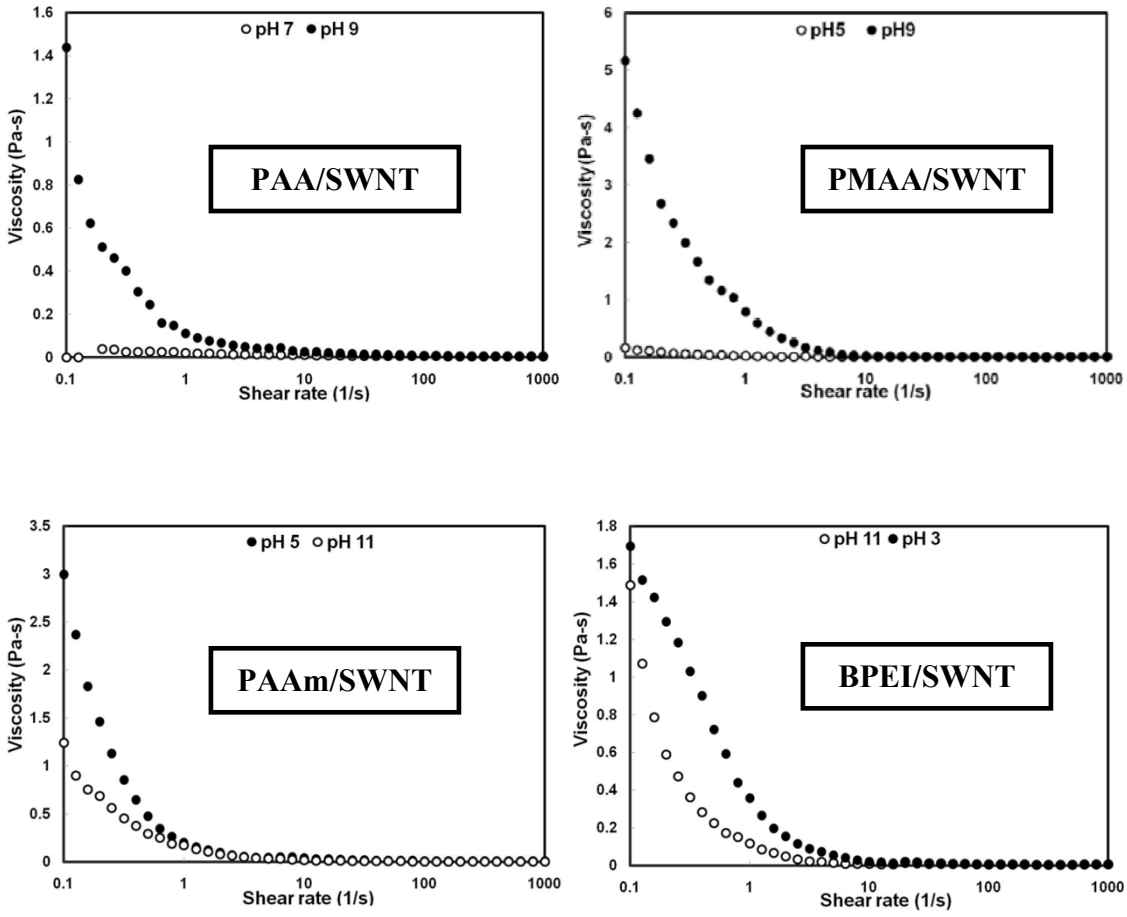

Figure 3.5. Viscosity as a function of shear-rate at varying pH levels for PAA, PMAA, PAAm and BPEI-stabilized aqueous suspensions of SWNTs.

Zeta potential is another property used to characterize the stability of colloidal suspensions. Suspensions with large zeta potential values (> + 25 mV or < - 25 mV) signify good stability.[170] Furthermore, the sign of the potential may indicate the nature of the stabilizing species. Table 3.1 shows the zeta potential results for the SWNT suspensions studied here. As expected, suspensions stabilized using PAA and PMAA have high negative zeta potential, whereas those stabilized using PAAm and BPEI show positive zeta potential values. It should be noted that zeta potential measurements were

made only on the suspensions that contained highly exfoliated SWNTs, as the suspensions containing more bundled and aggregated SWNTs were too irreproducible. One of the most interesting observations is the stabilizing polymer dependent polarity of the zeta potential values. The use of negatively-charged polymers (PAA and PMAA) and positively-charged polymers (PAAm and BPEI) results in negative and positive zeta potentials, respectively. It is known that the polarity of the zeta potential is dependent on the charge of the adsorbed polymer on particles.[171-172] This suggests that the weak polyelectrolytes used in this study are adsorbed onto the SWNT surface, which imparts surface charge depending on the nature of the polymer. Although the BPEI stabilized SWNTs show positive zeta potential values, significant scatter was observed in the measurements. This is attributed to weaker stability of BPEI-based suspensions that results in variable SWNT aggregation during measurements.

Table 3.1. Zeta potentials of aqueous SWNT suspensions stabilized with pH-responsive polymers.

Suspension	pH	Zeta Potential (mV)
PAA/SWNT	**7**	**-82**
PMAA/SWNT	**5**	**-62**
PAAm/SWNT	**11**	**43**
BPEI	**11**	**14 – 74**

It was previously shown that this dispersion state of SWNTs in solution influences their microstructure in solid polymer composites upon drying the suspension.[22,165] To investigate the solid state microstructure of SWNTs in polymer composites, suspensions containing 1 wt% of a pH-responsive polymer and 0.11 wt% SWNT, at different pH, were dried at room temperature. Scanning electron microscopy was perfomed on the surface of PAA and PAAm matrix composites and the images obtained are shown in Figure 3.6. As expected, nanotube microstructure in these composites is dependent on the pH of the suspensions used. It is clear that the PAA-based composite made with a pH-7 suspension has fairly homogenous and uniform SWNT dispersion (Fig. 3.6(a)), whereas that made with pH 9 show extensively aggregated SWNTs (Fig. 3.6(b)). PAAm-based composites also shows similar behavior, where composites made with pH 11 and pH 5 suspensions have homogeneous and aggregated SWNT dispersion, respectively. It should be noted here that PAA-based composites have better overall SWNT distribution as compared to PAAm based composites at both pH levels. This again suggests that polyacids are better stabilizers for SWNTs than polybases. BPEI based composites exhibited non-uniform SWNT distribution where large areas with no nanotubes can be seen. This is because of poor interaction between SWNTs and BPEI.

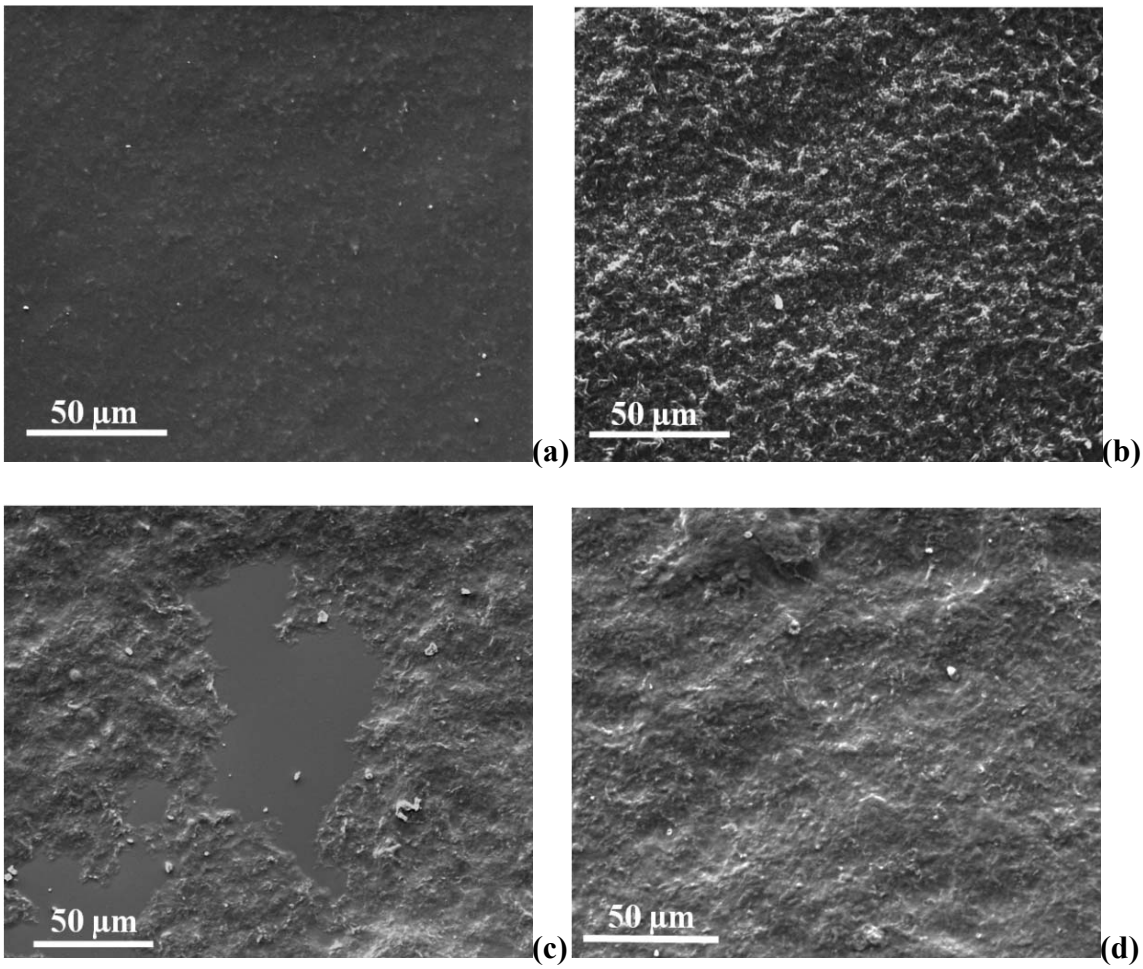

Figure 3.6. SEM images of composites containing 10 wt% SWNT that were made by drying aqueous PAA- based suspension at pH 7 (a) or pH 9 (b) and PAAm-based suspensions at pH5 (c) or pH 11(d).

Electrical conductivity measurements were made on these dried composite films and the results are shown in Figure 3.7. It can be seen that the pH of the SWNT/polymer suspensions ultimately influences the electrical conductivity of the composite. The SWNT/PAA composite prepared at pH 7 has an order of magnitude lower conductivity as compared to that made from a pH 9 suspension. Similar observations were made for SWNT/PMAA and SWNT/PAAm composites. It should be pointed out that all

composite films contained 10 wt% of SWNT, which is well above the percolation threshold reported for nanotube-polymer composites.[173-174] This point suggests the difference in the electrical conductivity in these composites is the result of altered nanotube-nanotube interaction and network formation in the presence of the stabilizing polymer. The increased conductivity for the composites made from suspensions that contained bundled SWNTs is attributed to more intimate nanotube-nanotube contacts resulting from the extended structure of the polymer. When the polymer assumes an extended conformation, the steric hindrance necessary for generating exfoliated SWNTs is reduced, which leads to SWNT aggregation and a greater number of contacts for electrical transport.[24] The observed lower conductivities for the composites made from the suspensions containing exfoliated SWNTs is due to the presence of a thicker layer of adsorbed polymer, which results in effective shielding of the nanotubes-nanotube contacts and also reduces the total number of contacts due to better dispersion. Much like with viscosity (see Fig. 3.5), BPEI/SWNT composites show only a small difference in electrical conductivity as a function of pH. This may be due to poor interaction between BPEI and SWNT. The results obtained from these measurements suggest that interactions and microstructure in the liquid suspensions are at least partially preserved in the solid composites. This method of tailoring microstructure in the liquid state to control the microstructure in the solid state holds significant potential for the preparation of polymer nanocomposites.

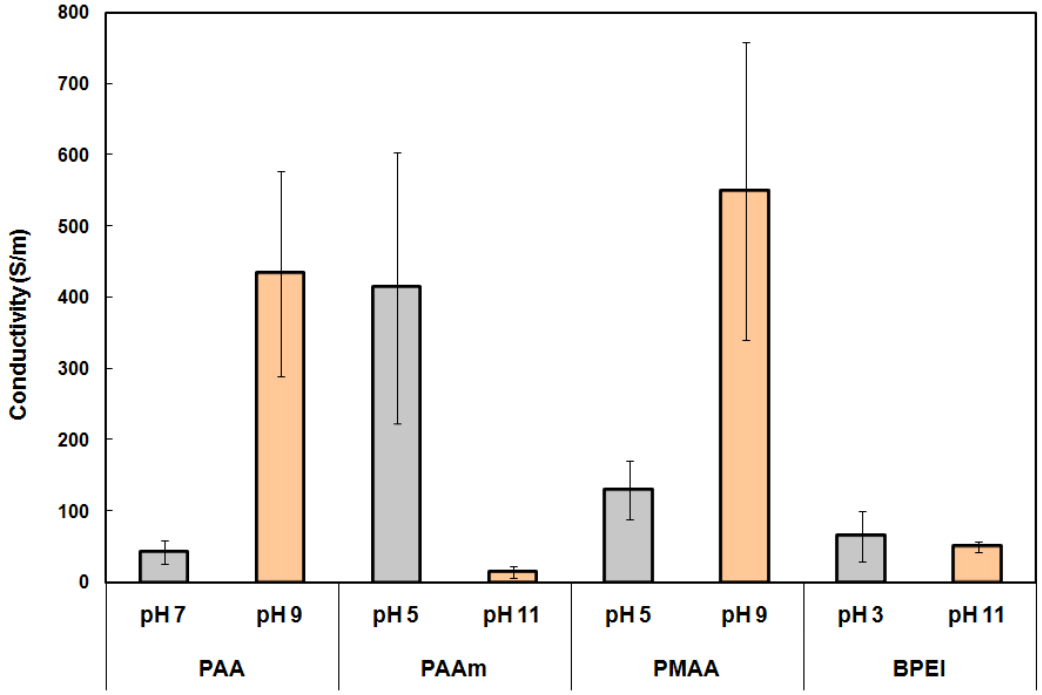

Figure 3.7. Electrical conductivity of solution-processed 10 wt% SWNT/pH-responsive polymer composites as a function of pH.

Based on the above results, the scheme shown in Figure 3.8 is postulated to explain the stabilizing mechanism by pH-responsive polymers. SWNT stabilization with polymers is believed to be due to polymer wrapping on the nanotube surfaces, which results in extended coverage of the polymer along the tube axis.[104,106] Despite this generally accepted mechanism, at low ionizations, weak polyelectrolytes assume a coiled conformation at the adsorbed surface in order to maximize configurational entropy and assume a random walk configuration.[175] Therefore, at these conditions it would be difficult for the polymer to wrap around the SWNTs. Superior stability of SWNT suspensions, stabilized with partially ionized polymers, suggests that polymers

are adsorbed on to the SWNT surface in globular form, as shown schematically in Fig. 3.8. The globular conformation of the polymer results in a smaller radius of gyration (R_g) that creates a thicker steric layer on the SWNT sidewall. Upon complete ionization, the polymer assumes an extended conformation and results in a flatter coverage on the SWNT sidewall. This conformation of the polymer reduces the steric layer thickness and results in SWNT aggregation. It is true that fully ionized polymers adsorbing on the SWNT sidewall should impart inter-tube electrostatic repulsion, thereby preventing aggregation, but at these conditions the nanotubes exist in aggregated state (as evidenced in cryo-TEM images shown in Fig. 3.4). This suggests that electrostatic repulsion alone is not sufficient for exfoliation of SWNTs. The SWNT microstructure in these suspensions is believed to be influenced by a combination of electrostatic and steric forces and is more sensitive to the steric layer thickness variations. A similar steric layer thickness dependent stabilization was observed for polystyrene latex stabilized with acidic polysaccharides.[176]

SWNT suspensions stabilized using polyanions show superior stability as compared to those stabilized with polycations (see Fig. 3.2). This may be due to better interaction between polyanions and SWNTs owing to the Lewis base character of the nanotube graphene sidewalls.[167] Additionally, the stabilizing polymer charge, observed in zeta potential measurements (see Table 3.1) on the suspensions, suggests the adsorption of the stabilizing polymer onto the SWNT sidewalls. Therefore, it is reason-

able to assume that polyanions are adsorbed more strongly to the SWNT surface than polycations. Furthermore, the weak polyelectrolytes used in this study (PAA, PMAA, PAAm and BPEI) exist in a partially ionized state at the pH corresponding to high SWNT exfoliation (i.e, low pH for polyanions and high pH for polycations), so it is reasonable to assume a conformation of the polymer that is intermediate between tight globule and extended coil (i.e, a combination of *coiled and uncoiled* domains shown in Fig. 3.8). These polymer conformations result in thicker steric layer coverage on the SWNT surface, thereby providing superior stability of suspensions. On the contrary, the weaker adsorption of polycations to the SWNT surface may result in desorption upon standing. Sedimentation of SWNT upon standing is observed in both PAAm and BPEI-stabilized suspensions at high pH, which is attributed to desorption of polymer from the SWNT surface. When these polyelectolytes are fully charged, they assume an extended conformation, thereby reducing the steric layer thickness on the SWNT surface that leads to the aggregated microstructure shown in Fig. 3.8.

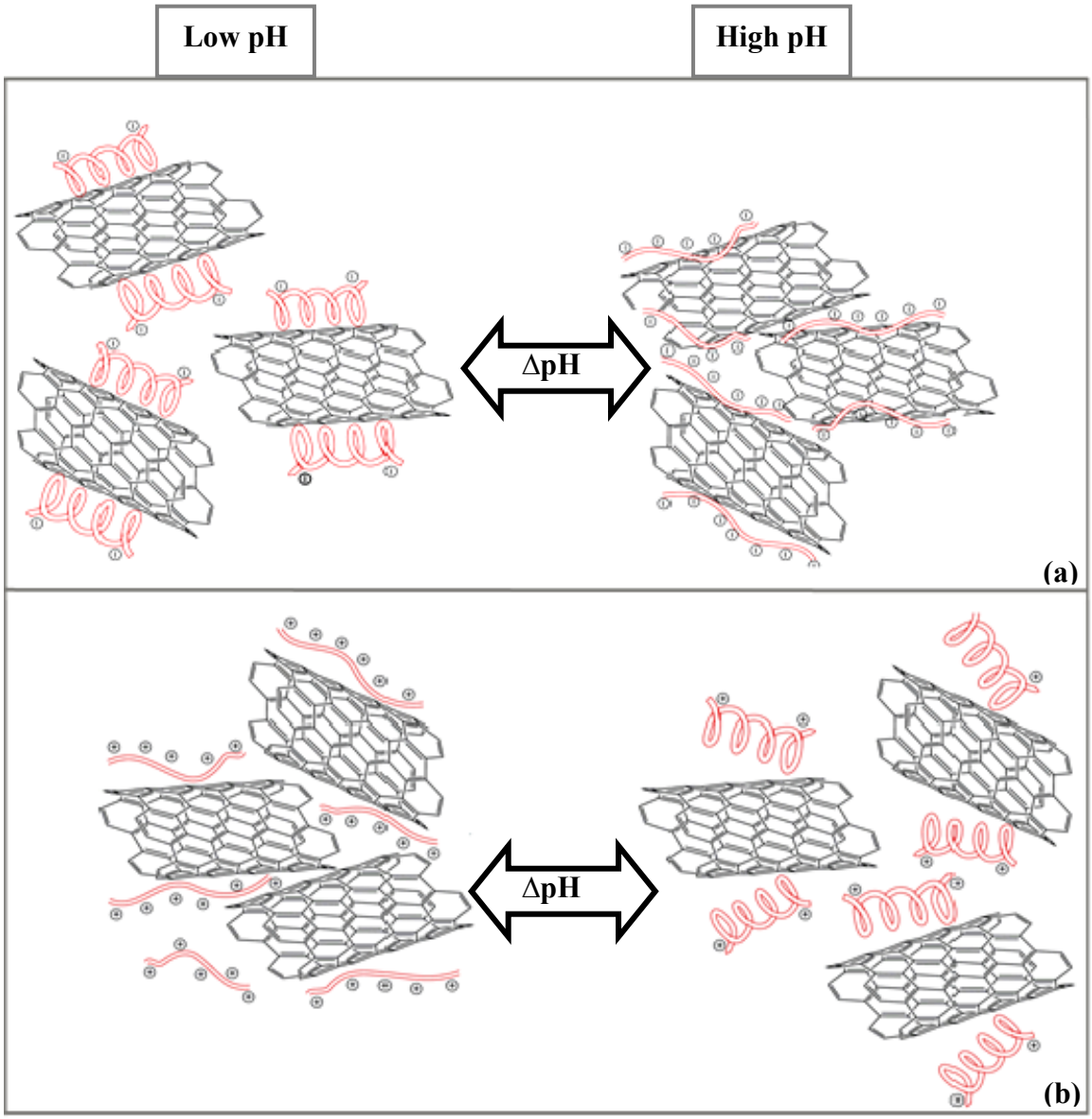

Figure 3.8. Schematic of SWNT dispersion and aggregation as a function of pH in aqueous suspensions using weak polyanions (a) and weak polycations (b). Both polycations and polyanions transition between weakly and fully ionized states along the pH spectrum. In the weakly ionized state, these polyelectrolytes exfoliate and stabilize SWNTs in water, whereas aggregated and bundled nanotubes are observed when polymer electrolytes are fully ionized.

CHAPTER IV

TEMPERATURE-TAILORED CARBON NANOTUBE DISPERSION

4.1 Introduction

Chapter III demonstrated the use of weak polyelectrolytes to tailor SWNT dispersion state as a function of pH. The ability to use temperature to control the level of nanotube exfoliation is perhaps a more convenient extension of this powerful concept. Unfortunately, the most widely used temperature responsive polymers, such as poly(*N*-isopropylacrylamide), have very low affinity for SWNTs and cannot effectively stabilize/disperse nanotubes in water.[25] Adding pyrene increases the affinity between these temperature responsive polymer and carbon nanotubes. Pyrene moieties interact strongly with SWNT sidewalls through a π-π stacking mechanism, as described in Chapter II (Section 2.2.2). In this chapter, the use of a thermoresponsive poly(*N*-cyclopropylacrylamide) (PNCPA) and poly (*N*-isopropylacrylamide) (PNIPAM), copolymerized with pyrene side groups, are shown to stabilize aqueous SWNT suspensions. Detailed synthesis and characterization of the polymers containing varying amounts of pyrene groups is presented. Lower critical solution temperature (LCST) of the polymers is determined by turbidity measurements and light scattering. Nanotube dispersion state in suspensions stabilized with these polymers is characterized using cryo-TEM, viscosity measurements, and settling behavior. Nanotube dispersion state in the composites made by drying the suspensions is characterized using SEM and electrical conductivity measurements of dried suspensions. It is shown that nanotubes

stabilized with pyrene functional thermoresponsive polymers exhibit altered dispersion state as a function of temperature. The changes in polymer conformation (i.e., *coil to globule* transformation) as a function of temperature is believed to influence the dispersion state of SWNTs (i.e., stabilized or bundled) in water and composites prepared by drying these suspensions.

4.2 Experimental Section

4.2.1. Materials and Methods

All chemicals and solvents were commercially available and used as received unless otherwise stated. Tetrahydrofuran (THF) was distilled over sodium. Spectra/Por 3 (MWCO 3500) were used as dialysis membranes. Poly(pentafluorophenylacrylate) PPFPA, with a molecular weight of 25000 g/mol (M_w/M_n = 1.32) was synthesized according to a published procedure.[177] The PNCPA series with 1,3,5 mol% pyrene side groups (i.e. 1p-PNCPA, 3p-PNCPA, 5p-PNCPA), PNIPAM with 1 mol% pyrene side groups (i.e., 1p-PNIPAM) and pure PNIPAM were synthesized according to the Schemes 1 and 2, respectively (Section 4.3). Raw single-walled carbon nanotubes (SWNTs) [batch number R0487] were purchased from Carbon Nanotechnologies (Houston, TX), containing 27 wt% impurity (mostly Fe-based catalyst). These nanotubes were used without further purification. Multi-walled nanotubes (purity > 95%, ID 5-10nm, OD 20-30nm, length 10-30 μm) were purchased from Cheap Tubes Inc. (Brattleboro, VT). Nanotube suspensions were prepared by mixing dry tubes in 0.1 wt%

aqueous solutions of p-PNCPA and p-PNIPAM, followed by sonication for 10 minutes at 50 W using a VirTis Virsonic 100 ultrasonic cell disrupter (SP industries, Warminster, PA). Composites of p-PNCPA and 1p-PNIPAM were made by drying 5 ml of a given nanotube suspension on a quartz slide at a given temperature.

All ^{1}H-NMR spectra were recorded on a Bruker 300 MHz FT-NMR spectrometer in deuterated solvents. Chemical shifts are given in ppm relative to TMS. Gel permeation chromatography (GPC) was performed in THF to determine molecular weights and molecular weight distributions (M_w/M_n) of polymer samples with respect to polystyrene standards. Calibration was done using polystyrene standards. UV/Vis spectra were recorded on a Jasco V-630 photo spectrometer. Fluorescence measurements were performed on a Perkin Elmer LS 50B luminescence spectrometer. IR spectra were recorded on a Bruker Vector 22 FT-IR spectrometer, using an ATR unit. FD-masses were measured on a MAT 95 Finnigan mass spectrometer. Viscosity of the suspensions as function of shear rate was measured using an AR-G2 rheometer (TA Instruments, Newcastle, DE) equipped with 40 mm parallel plate geometry. A gap of 1000 μm was maintained as per the recommended procedure for the instrument. This rheometer is equipped with a Peltier control system that provides accurate control of temperature (±0.1^{o}C) between 10 and 90^{o}C. Turbidity measurement was made with a USB2000 UV/Vis spectrometer (Ocean Optics, Dunedin, FL) using a quartz couvette containing 0.1 wt% polymer solution. Scanning electron microscopy was performed with a FEI Quanta 600 FE-SEM on composites coated with a 5 nm layer of Pt/Pd. Sheet resistance of the composites was measured using a custom-built 4-point probe apparatus. The

details of the instrument and measurement technique have been published elsewhere.[159] Volume conductivity was calculated by taking the inverse of the product of the sheet resistance and composite thickness.

4.2.2. Synthesis of p-PNCPA Series and 1p-PNIPAM

Synthesis of pentafluorophenyl-4-(pyren-4-yl)butanoate: 3.00 g (0.010 mol) 4-(pyren-4-yl)butanoic acid and 4.31 mL (0.031 mol) triethylamine (TEA) were dissolved in 25 mL dry THF and 8.74 g (0.031 mol) pentafluorophenyl trifluoracetate was added drop wise. The solution was stirred for 12 h at room temperature, then diluted with 300 mL dichloromethane and transferred into a separation funnel. The organic phase was washed three times with 50 mL of water, dried with sodium sulfate and concentrated under vacuum. The product was isolated through precipitation into hexane. After filtration and drying in vacuum at 40°C, 3.23 g (0.0071 mol – 71 %) yellow colored pentafluorophenyl-4-(pyren-4-yl)butanoate was obtained. ^{1}H-NMR ($CDCl_3$): δ /ppm: 8.27 (d, 1H), 8.13 (m, 4H), 8.03 (s, 2H), 7.99 (t, 1H), 7.86 (d, 1H), 3.47 (t, 2H), 2.77 (t, 2H), 2.32 (quin, 2H); FT-IR (ATR-mode): 2944 cm^{-1} (C-H – valence), 1774 cm^{-1} (C=O reactive ester band), 1517 cm^{-1} (PFP - C=C aromatic band), 1100 cm^{-1} (C-O ester band); MS (FD) m/z (%): 454.3 (100.00), 455.3 (27.58), 456.3 (4.51).

Synthesis of *N*-(6-aminohexyl)-4-(pyren-4-yl)butanamide: 7.77 g (0.067 mol) hexamethylenediamine and 0.93 mL (0.0067 mol) TEA were dissolved in 80 mL dry THF and 3.04 g (0.0067 mol) pentafluorophenyl-4-(pyren-4-yl)butanoate dissolved in 30 ml dry THF was added drop wise. The solution was stirred for 12 h at room temperature,

then diluted with 400 mL dichloromethane and extracted four times with 80 mL of water, respectively. The organic phase was separated and dried with sodium sulfate. After removal of the solvent in vacuum, 2.07 g (0.0054 mol – 80 %) yellow colored *N*-(6-aminohexyl)-4-(pyren-4-yl)butanamide was obtained. ^{1}H-NMR (DMSO): δ /ppm: 8.35 (d, 1H), 8.22 (m, 4H), 8.10 (s, 2H), 8.02 (t, 1H), 7.90 (d, 1H), 7.83 (t, 1H), 3.29 (t, 2H), 3.06 (q, 2H), 2.46 (t, 2H), 2.24 (t, 2H), 2.00 (quin, 2 H), 1.35 (t, 2H), 1.23 (m, 6H); FT-IR (ATR-mode): 3300 cm^{-1} (N-H – amide valence), 2928 cm^{-1} (C-H – valence), 1643 cm^{-1} (C=O amide band I), 1550 cm^{-1} (C=O amide band II); MS (FD) m/z (%): 386.3 (89.14), 387.4 (58.24), 774.0 (100.00), 775.0 (62.55), 776.0 (3.09).

Synthesis of p-PNCPA series (see Scheme 1, Route B): 2 g PPFPA and 2 mL (0.0143 mol) TEA were dissolved in 20 mL dry THF and 162 mg ($4.201 * 10^{-4}$ mol) *N*-(6-aminohexyl)-4-(pyren-4-yl)butanamide was subsequently added. This solution was stirred 3 h under nitrogen atmosphere at room temperature. Afterwards, 2 mL (0.029 mol) cyclopropylamine was added. After an additional 12 hours of stirring, the solvent was removed by evaporation in vacuum. The residue was suspended in 10 mL of water and dialyzed against diluted ammonia for ~12 h. The clear dialyzed solution was evaporated and the residue was twice dissolved in 5 mL of methanol and precipitated into diethyl ether. After centrifugation and drying in vacuum at 40°C, 0.61 g of colorless p-PNCPA was obtained. ^{1}H-NMR (MeOD): δ /ppm: 8.13 (m), 3.21 (s), 2.71 (s), 2.38 (s), 2.06 (br s), 1.59 (br s), 0.67 (d); FT-IR (ATR-mode): 3280 cm^{-1} (N-H – amide valence), 2940 cm^{-1} (C-H – valence), 1643 cm^{-1} (C=O amide band I), 1540 cm^{-1} (C=O amide band II). *N*-(6-aminohexyl)-4-(pyren-4-yl)butanamide was synthesised in two steps. First, 4-

(pyren-4-yl)butanoic acid was activated with pentafluorophenyl trifluoracetate and then reacted with an excess amount of hexamethylenediamine resulting in *N*-(6-aminohexyl)-4-(pyren-4-yl)butanamide (Route A). p-PNCPA was synthesized through a polymer analogous to PPFPA with *N*-(6-aminohexyl)-4-(pyren-4-yl)butanamide and cyclopropylamine (Route B).

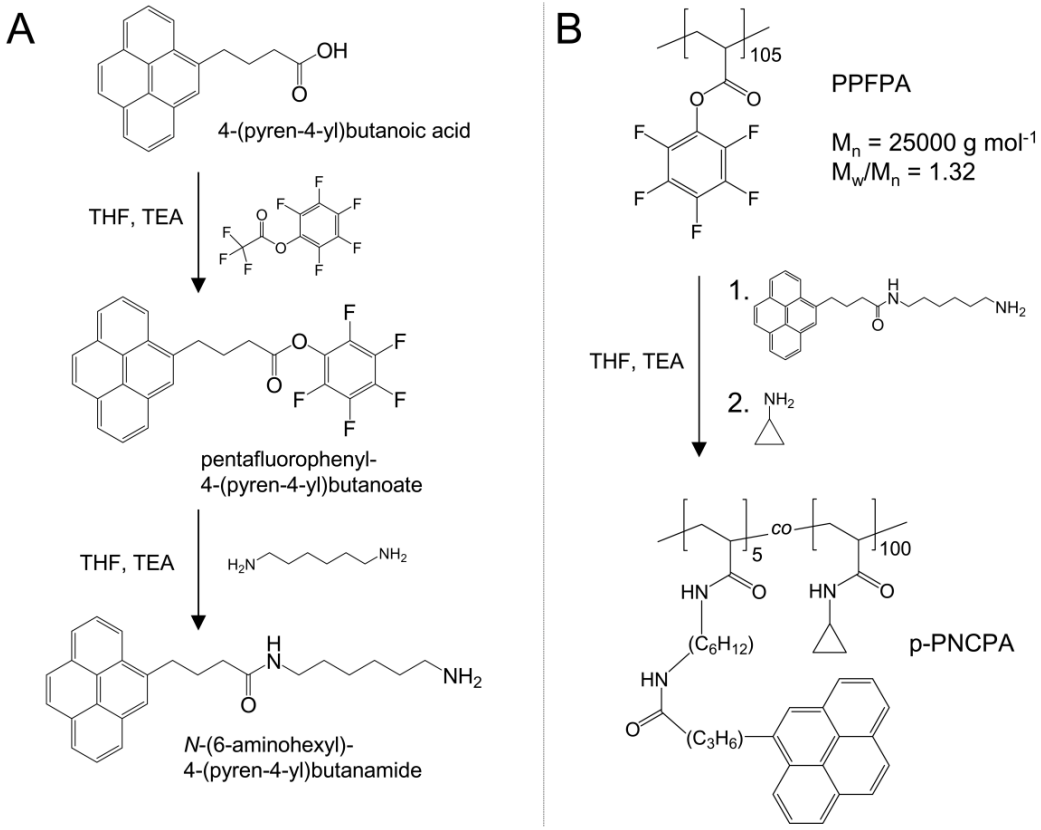

Scheme 1. Overview of pyrene-functionalized PNCPA synthesis.

Synthesis of PNIPAM (see scheme 2, route A): 1.5 g PPFPA and 2 mL (0.0143 mol) triethylamine (TEA) were dissolved in 20 mL dry THF. Afterwards, 2 mL (0.0233

mol) isopropylamine were added and the solution was stirred for 12 hours under nitrogen atmosphere at room temperature. Next, the solvent was removed by evaporation in vacuum. The residue was suspended in 10 mL of water and dialyzed against diluted ammonia over night. The clear dialyzed solution was evaporated and the residue was twice dissolved in 5 mL of THF and precipitated into hexane. After centrifugation and drying in vacuum at 40°C, 0.41 g of colorless PNIPAM was obtained. ^{1}H-NMR ($CDCl_3$): δ /ppm: 6.45 (br s), 3.97 (br s), 2.10 (br s), 1.77 (br s), 1.59 (br s), 1.34 (br s), 1.10 (br s); FT-IR (ATR-mode): 3298 cm^{-1} (N-H – amide valence), 2970 cm^{-1} (C-H – valence), 1642 cm^{-1} (C=O amide band I), 1540 cm^{-1} (C=O amide band II).

Synthesis of 1p-PNIPAM (see scheme 1, route B): 2 g PPFPA and 2 mL (0.0143 mol) TEA were dissolved in 20 mL dry THF and 32 mg ($8.290 * 10^{-5}$ mol) *N*-(6-aminohexyl)-4-(pyren-4-yl)butanamide were added, subsequently. The solution was stirred 3 h under nitrogen atmosphere at room temperature. Afterwards, 2 mL (0.0233 mol) isopropylamine were added. After additional 12 hours of stirring, the solvent was removed by evaporation in vacuum. The residue was suspended in 10 mL of water and dialyzed against diluted ammonia over night. The clear dialyzed solution was evaporated and the residue was twice dissolved in 5 mL of THF and precipitated into hexane. After centrifugation and drying in vacuum at 40°C, 0.52 g of colorless p-PNIPAM was obtained. ^{1}H-NMR (MeOD): δ /ppm: 8.42-7.92 (br m), 7.72 (br s) 4.02 (br s), 2.14 (br s), 1.90 (br s), 1.63 (br s), 1.33 (br s), 1.19 (br s); FT-IR (ATR-mode): 3298 cm^{-1} (N-H – amide valence), 2970 cm^{-1} (C-H – valence), 1642 cm^{-1} (C=O amide band I), 1540 cm^{-1}

(C=O amide band II). Poly(pentafluorophenylacrylate) (PPFPA) with a molecular weight of M_n = 25000 g/mol (M_w/M_n = 1.32) and *N*-(6-aminohexyl)-4-(pyren-4-yl)butanamide were synthesized as described previously.[177-178] PNIPAM and 1p-PNIPAM were synthesized through a polymer analogous reaction of PPFPA (route A and B).

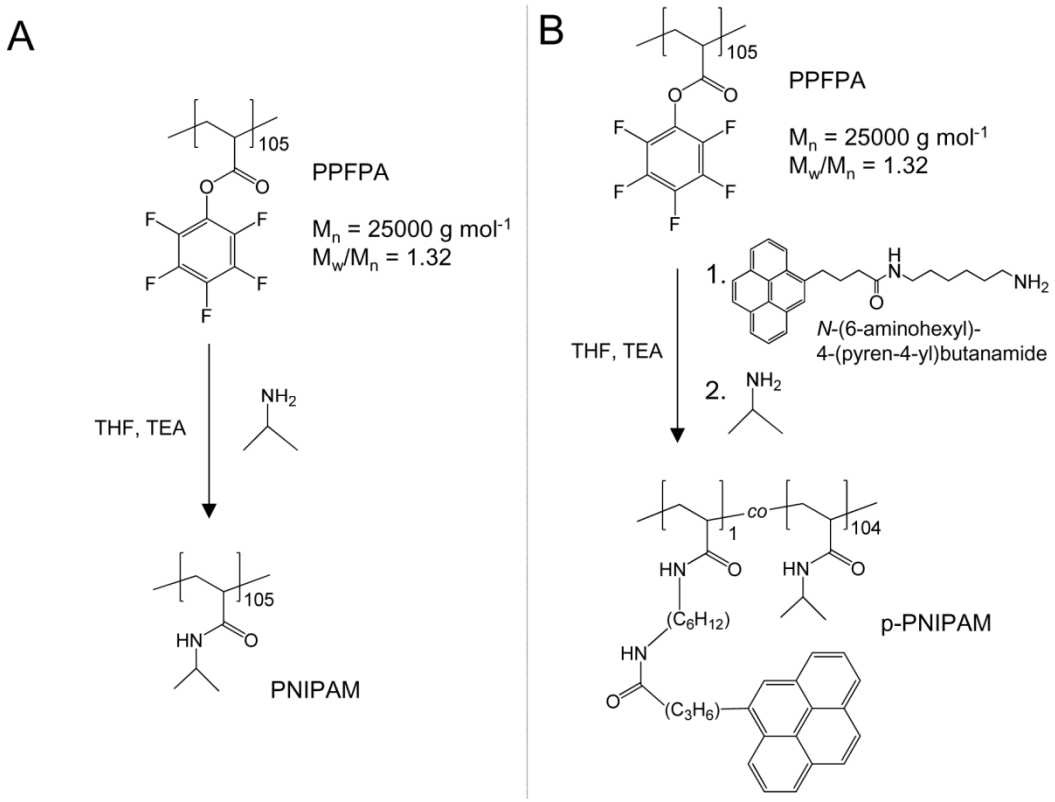

Scheme 2. Overview of pyrene-functionalized PNIPAM synthesis.

4.3 Results and Discussion

4.3.1. Characterization of p-PNCPA Series and 1p-PNIPAM

^{1}H NMR spectroscopy confirmed a successful synthesis of the p-PNCPA copolymers series and 1p-PNIPAM. The characteristic signals of the aromatic pyrene side groups at 8.13 ppm, as well as the cyclopropylamide repeating units at 2.71 ppm and 0.67 ppm, were assigned as illustrated for 5p-PNCPA in Figure 4.1(a). The characteristic signals of the isopropylamide repeating unit protons at 4.02 ppm and 1.19 ppm were assigned for 1p-PNIPAM, as shown in Figure 4.1(b). The amount of incorporated pyrene side groups was determined by calculating the ratio of the integrals of the aromatic pyrene protons to the single signal of the cyclopropyl proton at 2.71 ppm and isopropyl proton at 4.02 ppm for p-PNCPA and p-PNIPAM, respectively. It is noteworthy that, the calculated values from NMR measurements fit to the theoretical values, indicating the high accuracy of the polymer analogous reaction. UV-Vis and fluorescence emission spectra of the p-PNCPA series were collected to investigate the synthesized copolymers. Both spectra in Figure 4.2 clearly show the characteristic peaks of the pyrene side groups. Furthermore, with increasing pyrene content in PNCPA, UV absorption and fluorescence emission increases. This suggests that the pyrene groups have been incorporated in the polymer. Figure 4.3 shows the UV/Vis absorption (black solid curve, conc. 0.190 mg/mL methanol) and fluorescence emission spectroscopy (grey dashed curve, conc. 0.00190 mg/mL methanol, λ_{ex} = 340 nm) of the synthesized p-

PNIPAM. Additonally, both spectra show the characteristic peaks of the pyrene side groups of the copolymer, indicating a successful reaction.

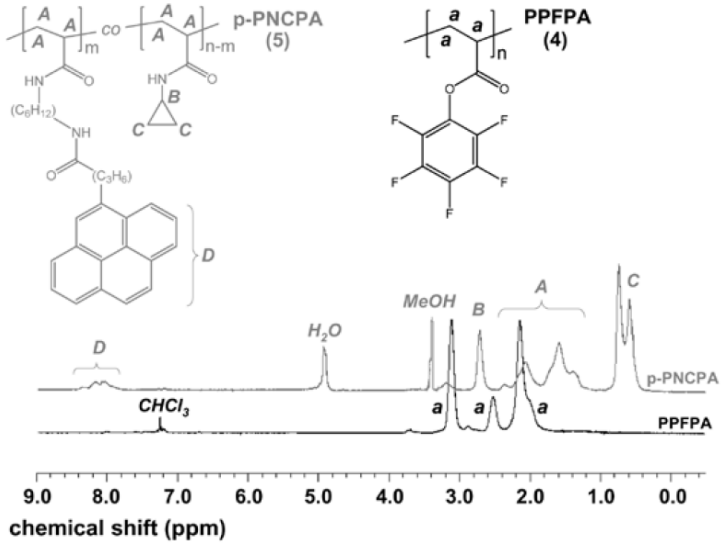

(a)

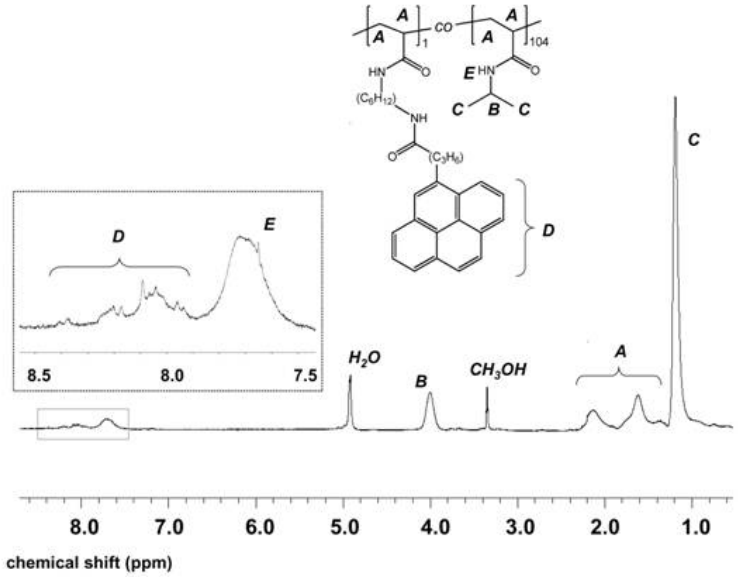

(b)

Figure 4.1. ^{1}H NMR spectra of PPFPA (black line) and p-PNCPA with 5 mol% pyrene moieties (5p-PNCPA, gray line) measured in deuterated solvents $CDCl_3$ and MeOD, respectively (a) and ^{1}H NMR spectra of p-PNIPAM measured in deuterated methanol (b).

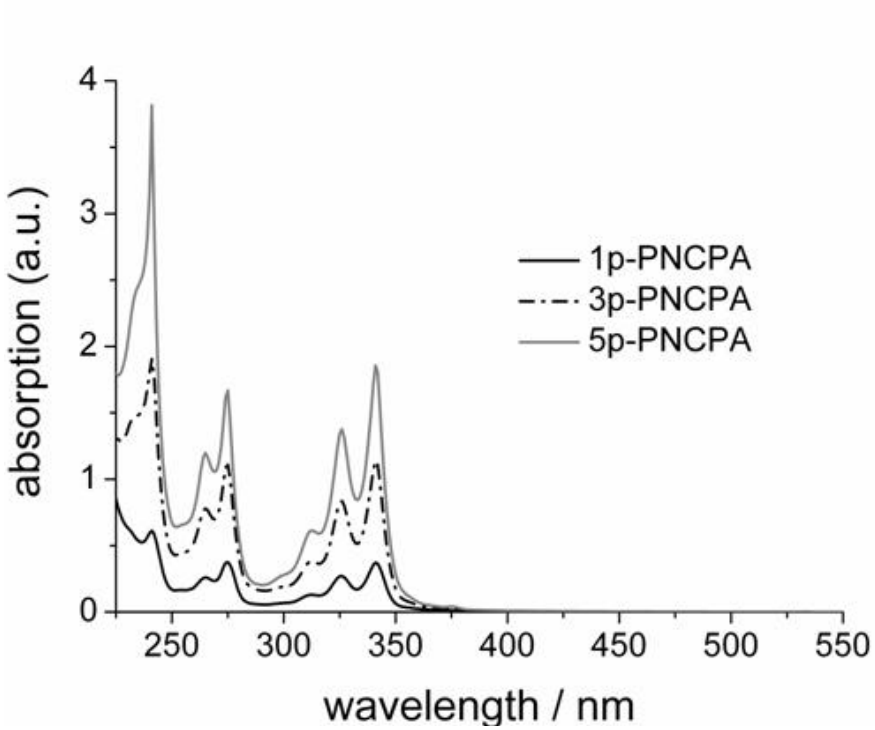

(a)

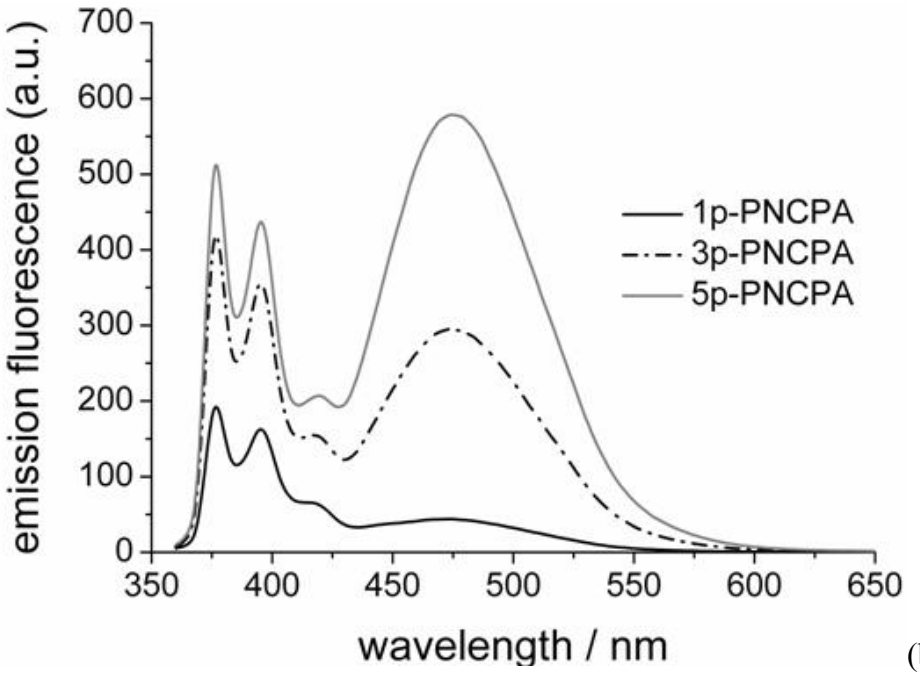

(b)

Figure 4.2. UV/Vis absorption spectra of the p-PNCPA series measured at constant concentration (0.16 mg/mL in methanol) (a) and fluorescence emission spectra (λ_{ex} = 340 nm) of the p-PNCPA series measured at constant concentration (0.0032 mg/mL in methanol).

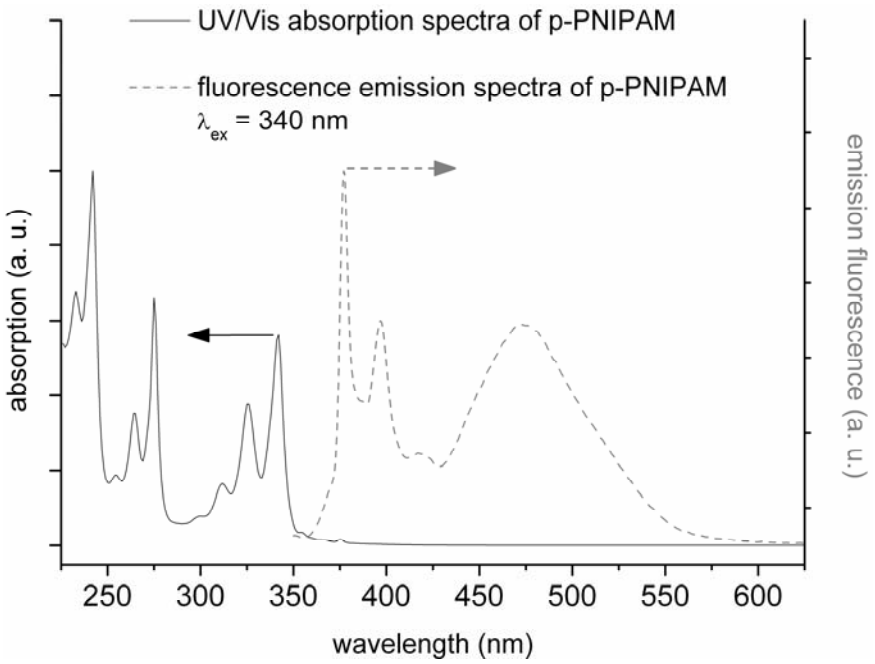

Figure 4.3. UV/Vis absorption and fluorescence emission spectra of p-PNIPAM measured in methanol.

4.3.2 LCST of p-PNCPA and 1p-PNIPAM

In order to reveal the temperature responsive characteristics of the polymers, light scattering measurements were made. In dynamic light scattering, the diffusive motion of particles in solution gives rise to fluctuations in the intensity of the scattered light on the μs timescale. The fluctuating signal is processed by forming an autocorrelation function, $g(\tau)$, where τ is the time delay. This experimentally obtained autocorrelation function is used to calculate the translational diffusion coefficient (D). The hydrodynamic radius (R_H) of the polymer is then calculated using the Stokes-Einstein equation:

$$R_H = \frac{k_B T}{6\pi\eta(\tau)D} \quad (1)$$

where k_B is the Boltzmann's constant, T is temperature (in K), η (τ) is the viscosity of liquid medium and D is the translational diffusion coefficient. This procedure was carried out automatically using the instruments own software. The data shown in Figure 4.4 is the average of 5 measurements. The R_H value of 1p-PNIPAM and 5p-PNCPA decreases sharply between 25 and 30°C and 30 and 40°C, respectively. This decrease is due to the coil-globule transition of the polymer and suggests that temperature-responsive behavior of PNCPA and PNIPAM is preserved in the presence of pyrene.

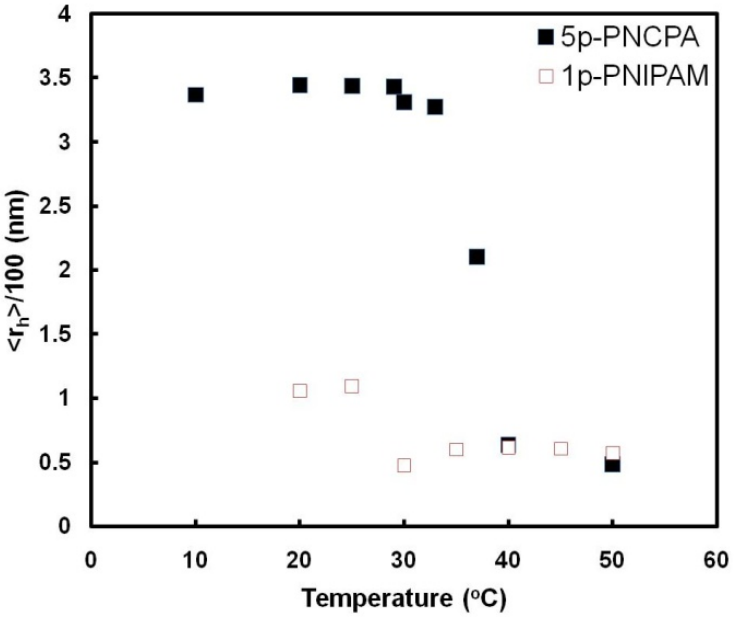

Figure 4.4. Hydrodynamic radius of 5p-PNCPA and 1p-PNIPAM as a function of temperature in water. The concentration of polymer in the solution was 0.1 wt% and the scattering angle was set at 90°C.

In an effort to determine the influence of pyrene addition on the LCST of p-PNCPA and p-PNIPAM, turbidity measurements (actually decadic absorbance at 400nm) were made on dilute aqueous solutions as a function of temperature. These solutions become turbid near the LCST (referred to as the cloud point temperature), which is defined as the temperature corresponding to a 10% reduction in the original transmittance of the solution.[179] Figure 4.5 shows that the LCST of p-PNCPA series in water is dependent on pyrene content and decreases with increasing pyrene content. This reduction of LCST with pyrene addition has been observed by others and is attributed to the increasing hydrophobic character of the polymer.[180-183] Similar observations were made for p-PNIPAM where addition of 1 mol% pyrene lowered LCST by 4^{o}C. Tailoring the LCST of polymer through incorporation of hydrophobic compounds may actually be desirable for applications requiring a specific transition temperature.

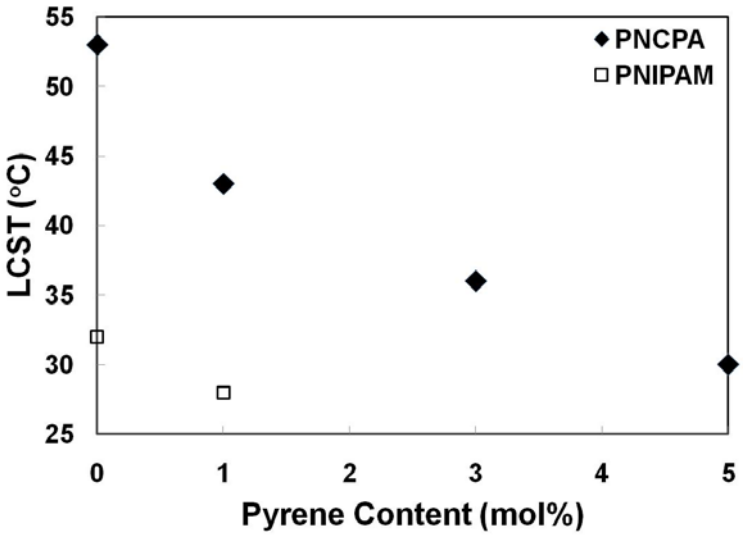

Figure 4.5. Lower critical solution temperatures (LCST) of 0.1 wt% solutions of pyrene-functionalized PNCPA and PNIPAM, as a function of pyrene content.

4.3.3 SWNT/p-PNCPA Aqueous Suspensions

In an effort to visualize the nanotube microstructure in aqueous SWNT suspensions stabilized with pyrene functionalized PNCPA, cryo-TEM microscopy was performed on thin frozen sections of suspensions, as shown in Figure 4.6. It can be seen that nanotubes exhibit more exfoliated and more bundled microstructures at temperatures below and above the LCST of the polymer, respectively. This temperature-dependent SWNT microstructure in suspensions is attributed to the conformational transitions of the adsorbed polymer on the nanotube sidewalls that counteracts the inter-tube van der Waals force of attraction. At temperatures lower than the LCST, polymer is water-soluble, but becomes more hydrophobic and immiscible at temperatures above the LCST. This temperature-dependent solubility of 5p-PNCPA in water is presumably due to the *coil-to-globule* transition exhibited by neat PNCPA, which is primarily due to changes in hydrogen bonding and hydrophobic interactions between polymer and water molecules.[184] Accordingly, the transition of polymer chains anchored to the nanotube sidewall, because of the presence of pyrene moieties, changes the dispersion state of SWNTs as illustrated in Figure 4.6 (c) and (d). Similar steric layer dependent dispersions were also observed for polystyrene latex stabilized with acidic polysaccharides.[176,185]

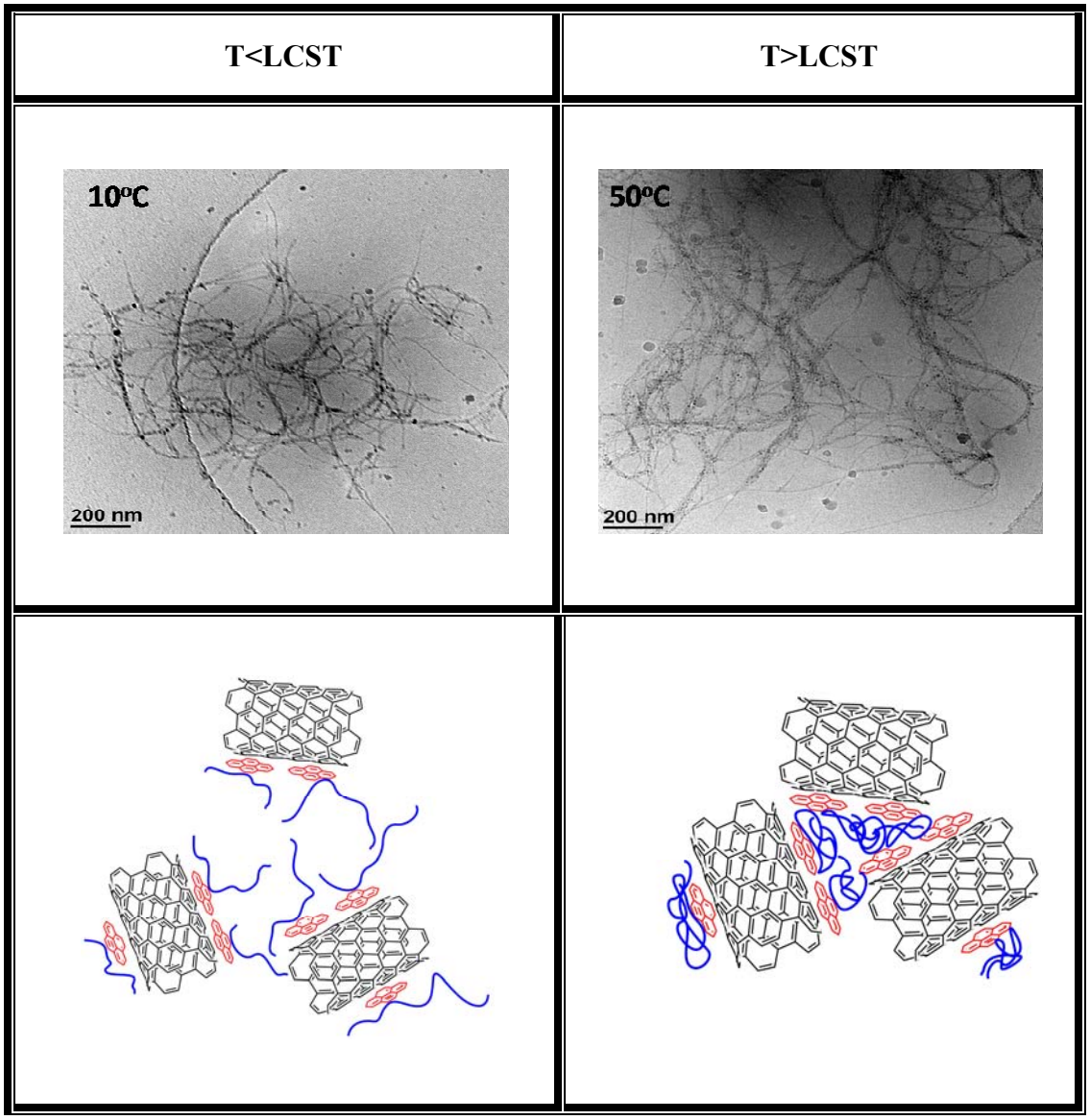

Figure 4.6. Cryo-TEM of 5p-PNCPA/SWNT suspensions at temperatures below and above the LCST of the polymer (a),(b) and a schematic of observed microstructure (c),(d).

Suspensions with well-dispersed SWNTs are known to have lower viscosities as compared to those that have agglomerated or bundled SWNTs, due to lack of entanglements.[22] Viscosity measurements were made both below and above the LCST of

the copolymers, as shown in Figure 4.7. It can be seen that both 1p-PNCPA and 5p-PNCPA-stabilized SWNT suspensions exhibit a shear thinning behavior (i.e., decreasing viscosity with increasing shear) at temperatures above the LCST of the polymer. Furthermore, unmodified PNCPA treated nanotube suspensions are shear thinning both above and below the LCST of the polymer. Shear thinning behavior is observed in concentrated nanotube suspensions that exhibit a high degree of entanglements and resemble polymer-like solutions. With this understanding, it is reasonable to suggest that SWNTs are more networked and entangled above LCST in suspensions stabilized with 1p-PNCPA and 5p-PNCPA. It should be noted that below the LCST of the polymer, SWNT/5p-PNCPA and SWNT/3p-PNCPA suspensions exhibit nearly Newtonian behavior (shear-independent viscosity). This behavior in these suspensions arises due the lack of bundled and networked nanotube microstructure. Below the LCST, the polymer chain is fully dissolved and able to interact with and exfoliate the nanotubes. As the polymer coagulates out of the solution above the LCST, the polymer-polymer interactions increase, and leading to more nanotube bundling/networking (Fig. 4.6 (c) and (d)).

SWNT/3p-PNCPA suspensions exhibited anomalous Newtonian behavior at a temperature above the LCST of the polymer. This anomalous behavior is attributed to the presence of excess pyrene in this polymer. In contrast, SWNT/1p-PNCPA suspensions also show shear-thinning behavior below LCST, but they exhibit lower viscosities at every shear rate examined. This suggests that 1p-PNCPA is relatively less effective than 5p-PNCPA and 3p-PNCPA, but certainly better than unmodified PNCPA,

for stabilizing nanotubes. One reason for this may be the low pyrene content that produces weaker interactions between 1p-PNCPA and SWNTs, as only pyrene moieties can interact with nanotubes through π-π stacking. Similar observations were made with nanotubes stabilized with pyrene-containing block copolymers, where higher concentration of pyrene resulted in greater solubility in water.[186]

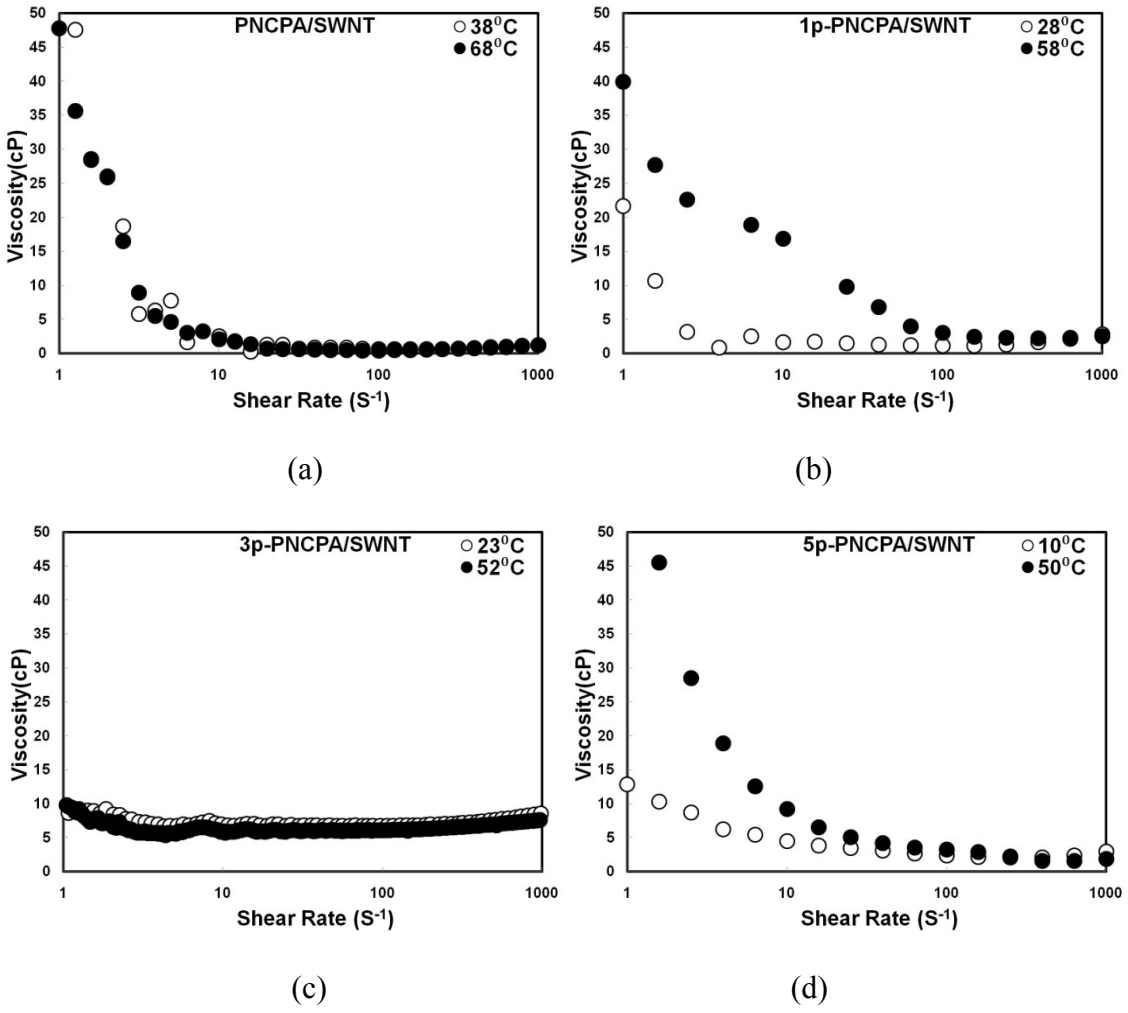

Figure 4.7. Viscosity as a function of shear rate of 0.011 w% aqueous SWNT suspensions stabilized by 0.1wt% of PNCPA (a), 1p-PNCPA (b), 3p-PNCPA (c) and 5p-PNCPA (d), at temperatures below and above the LCST.

In an effort to understand the temperature response of pyrene functionalized PNCPA in the presence of SWNTs, turbidity (actually decadic absorbance at 400nm) was examined in the absence and presence of SWNTs, as shown in Figure 4.8. It can be seen that there is a significant increase in optical absorption of the 5p-PNCPA solution at 30^{o}C due to the coil-globule transition of p-PNCPA. The 5p-PNCPA/SWNT suspensions also show a small but significant increase near 30^{o}C, which corresponds to the transition temperature of 5p-PNCPA. Similar observations could be made for 1p-PNCPA in presence and absence of SWNTs. Based on these results, it is reasonable to suggest that the thermo-responsive characteristics of pyrene functionalized copolymers of PNCPA are preserved in the presence of SWNTs.

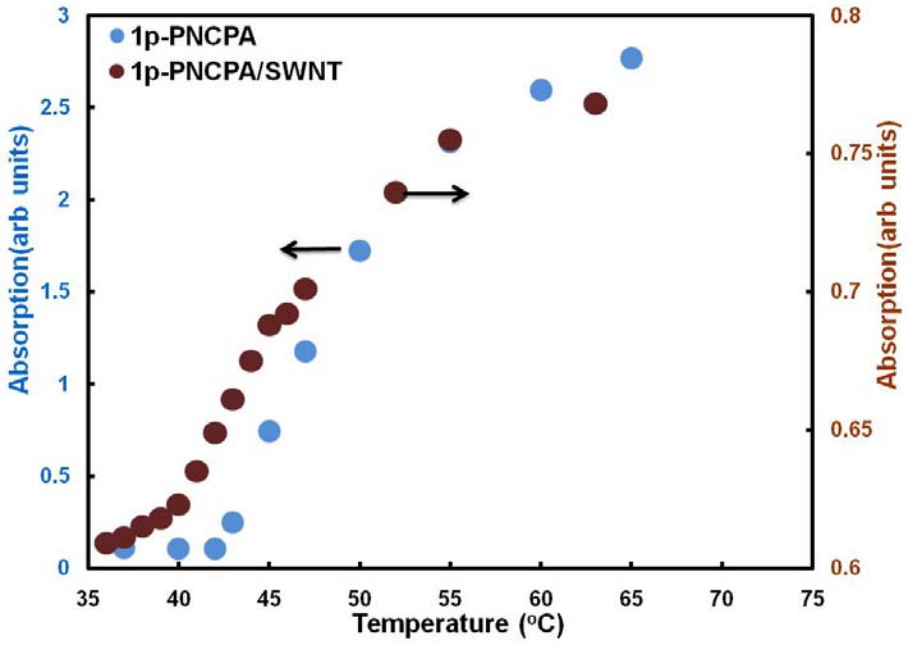

(a)

Figure 4.8. Turbidity (decadic absorption at 400nm) as a function of temperature for aqueous 1p-PNCPA/SWNT (a) and 5p-PNCPA/SWNT (b) suspensions and 1p-PNCPA and 5p-PNCPA solutions in water.

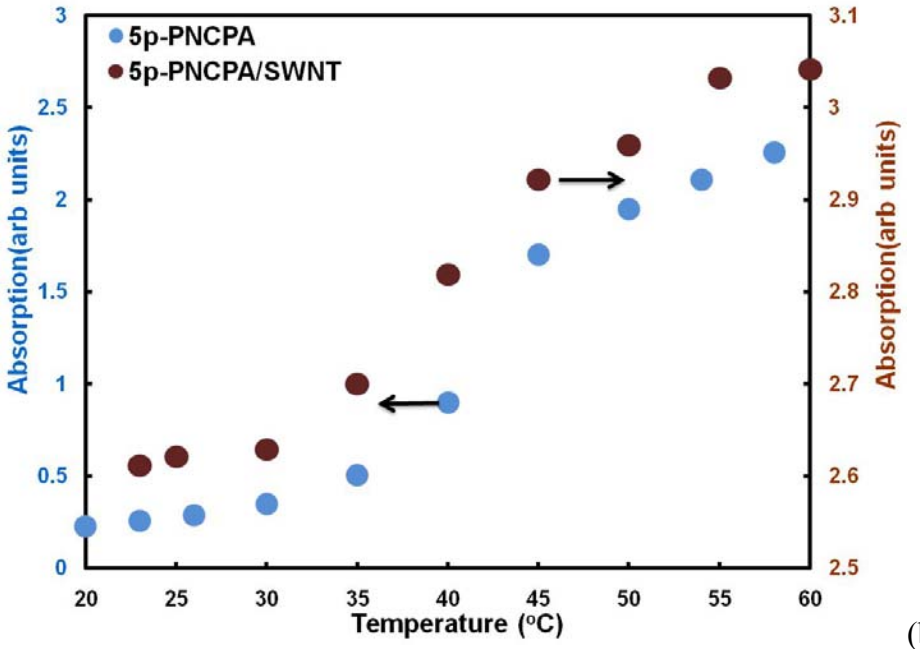

(b)

Figure 4.8. Continued.

The stability of these SWNT suspensions was further investigated with zeta potential measurements, as shown in Figure 4.9. Large zeta potential values (> + 25 mV or < - 25 mV) generally signify good suspension stability (i.e., no significant sedimentation).[170] Figure 4.9 shows that 1p-PNCPA stabilized SWNTs have zeta potential values that are significantly lower than 3p-PNCPA or 5p-PNCPA-stabilized nanotubes. However, 3p-PNCPA-stabilized SWNTs show higher zeta potential values as compared to those stabilized with 5p-PNCPA. As already mentioned, this may be because of excess pyrene present in 3p-PNCPA, which is adsorbed on the SWNT surface and provides hindrance to nanotube aggregation. Based on the above results, it is clear that 1p-PNCPA is not as effective as higher pyrene-containing copolymers of PNCPA (i.e., 3p-PNCPA and 5p-PNCPA) for stabilizing SWNTs.

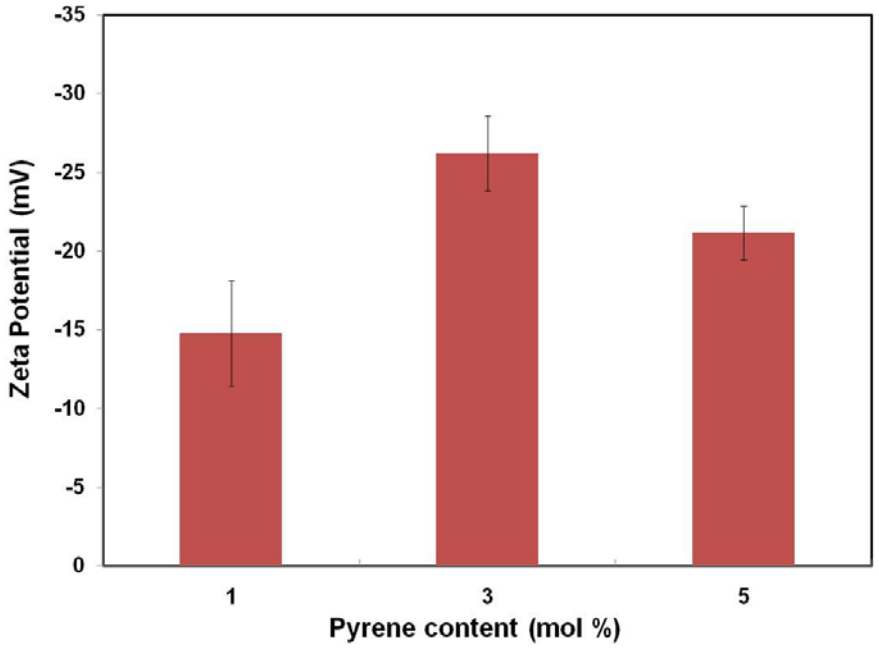

Figure 4.9. Zeta potential values of SWNTs stabilized with p-PNCPA as a function of pyrene content.

To further characterize the stability of SWNT suspensions, UV-Vis measurements were made, as shown in Figure 4.10. As already mentioned in Chapter III, the carrier dynamics in SWNT bundles are dominated by tunnel coupling between semi-conducting and metallic SWNTs, which results in reduced interaction with light and therefore, only individual SWNTs can provide a UV-Vis signature.[160-164] In other words, greater UV-Vis absorbance corresponds to the presence of more exfoliated SWNTs in the suspension. SWNT suspensions statbilized with 1p-PNCPA exhibit significantly lower optical absorption as compared to higher pyrene-containing copolymers. This further suggests that 1p-PNCPA is not as effective as 3p-PNCPA and 5p-PNCPA in stabilizing SWNTs.

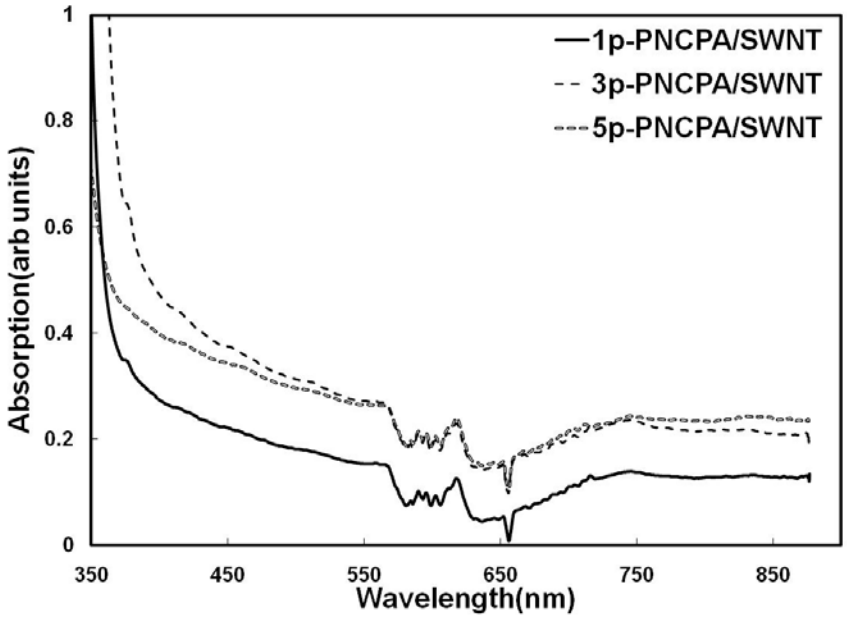

Figure 4.10. UV-Vis spectra of aqueous suspensions containing 0.011 wt% SWNT and 0.1 wt% polymer.

4.3.4. SWNT/p-PNCPA Composites

It was mentioned in Chapter III that nanotube dispersion state in liquid suspensions is largely preserved in composites prepared upon drying these suspensions.[22,165] In an effort to characterize nanotube microstructure in the liquid state, SWNT suspensions stabilized with pyrene-functionalized PNCPA were dried on glass substrates at temperatures above and below the LCST of the polymer. Scanning electron microscopy was performed on these composite films, as shown in Figure 4.11. It can be seen that nanotube dispersion state in these composites is dependent on temperature.

Nanotubes are well dispersed in 1p-PNCPA/SWNT composites dried at a temperature below the LCST of the polymer, but exhibit a heavily bundled and networked microstructure in composites made above the LCST. These images indicate that SWNTs are exfoliated and more bundled at temperatures below and above the LCST of 1p-PNCPA, respectively. Similar temperature-dependent dispersion state is also seen in 5p-PNCPA/SWNT composites. The presence of more aggregated nanotube microstructure in 1p-PNCPA composites, as compared to 5p-PNCPA composites dried below the LCST, should be noted. These images compliment the viscosity data and cryo-TEM results (See Fig.4.6 and Fig. 4.7) and suggest that SWNTs are better stabilized by 5p-PNCPA than 1p-PNCPA at temperatures below the LCST. As already mentioned, this improved stabilization is attributed to the greater pyrene content of 5p-PNCPA. This method of controlling the nanotube dispersion state in solid composites with drying temperature could be a useful tool for tailoring the behavior of solution-processed, nanotube-filled polymer composites.

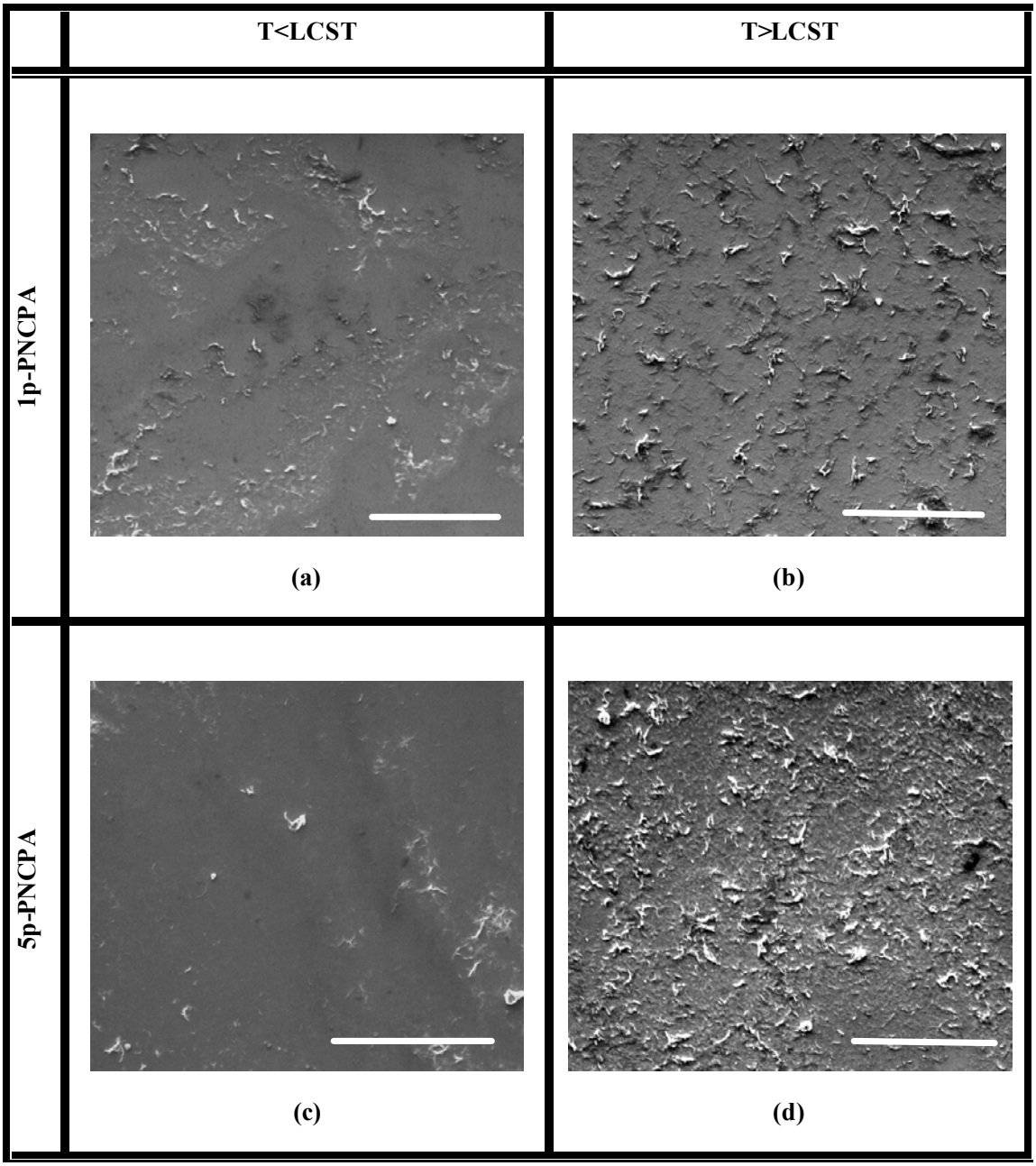

Figure 4.11. Surface SEM images of 1p-PNCPA (a),(b) and 5p-PNCPA (c),(d) composites containing 1 wt% SWNTs at temperatures below (left) and above (right) the LCST of the polymer. The scale bar in these images is 20μm.

To further characterize solid state (i.e., composite) microstructure, electrical conductivity measurements were made on the dried SWNT suspensions. Figure 4.12 shows that suspensions dried at temperatures above the LCST exhibit significantly higher electrical conductivity than those dried at lower temperatures. This increased electrical conductivity is attributed to a greater number of nanotube-nanotube contacts in these composites. The suspensions above the LCST of the polymer exhibit a highly entangled nanotube microstructure that is preserved upon drying and results in a greater number of tube-tube contacts. In contrast, the suspensions below the LCST have better dispersed (and debundled) nanotubes that have fewer connections with each other, resulting in lower composite electrical conductivity. Fig. 4.12 also shows that electrical conductivity decreases with increasing pyrene content of PNCPA in these composites. Moreover, this decrease in conductivity is more significant in films made at temperatures above the LCST. Greater interaction between the polymer and nanotube with increasing pyrene content may account for this behavior. The association of polymer with nanotube acts as a barrier to electron movement by shielding the nanotube surface, leading to a lower number of contacts, which results in decreased electrical conductivity. It was previously shown that non-covalently functionalized nanotubes exhibit lower electrical conductivities than pristine nanotubes.[187]

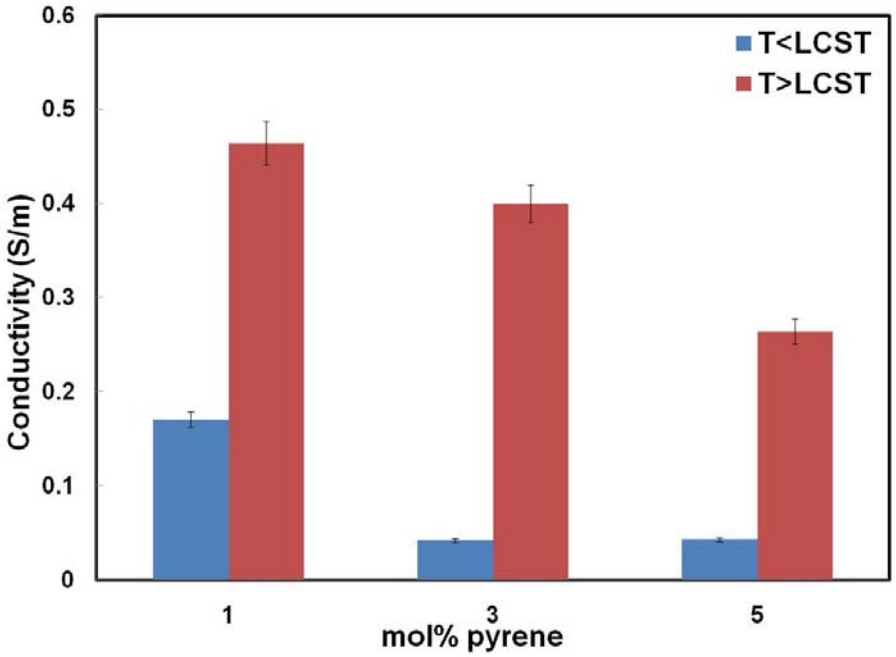

Figure 4.12. Electrical conductivity of 10 wt% SWNTs in pyrene-functionalized PNCPA composites, made at temperatures below (blue) and above (red) the LCST, as a function of pyrene concentration.

4.3.5. SWNT/1p-PNIPAM Suspensions

Temperature tailoring of SWNT dispersion state in water using PNIPAM should be of significant interest due to the extensive study of PNIPAM for various biological applications.[188-191] Successful combination of PNIPAM and SWNTs in aqueous solution may lead to thermoresponsive materials (e.g, hydrogels) with improved properties.[192-194] Despite its potential, PNIPAM has only modest affinity for CNTs, which is not sufficient for effective stabilization of aqueous suspensions.[25] In contrast, 1 mol% pyrene functionalized PNIPAM (1p-PNIPAM) acts as an excellent stabilizer for both single and multi-walled nanotubes, as shown in Figure 4.13. It can be seen that 1p-PNIPAM stabilized suspensions are homogeneous with no visible sedimentation 24 hours after

ultra-sonication, whereas pure PNIPAM treated suspensions exhibit extensive sedimentation. Similar observations were made for MWNTs stabilized with 1p-PNIPAM. As already mentioned, this enhanced stability of carbon nanotube suspensions, stabilized with 1p-PNIPAM is due to the presence of pyrene moieties that interact strongly with the nanotubes.

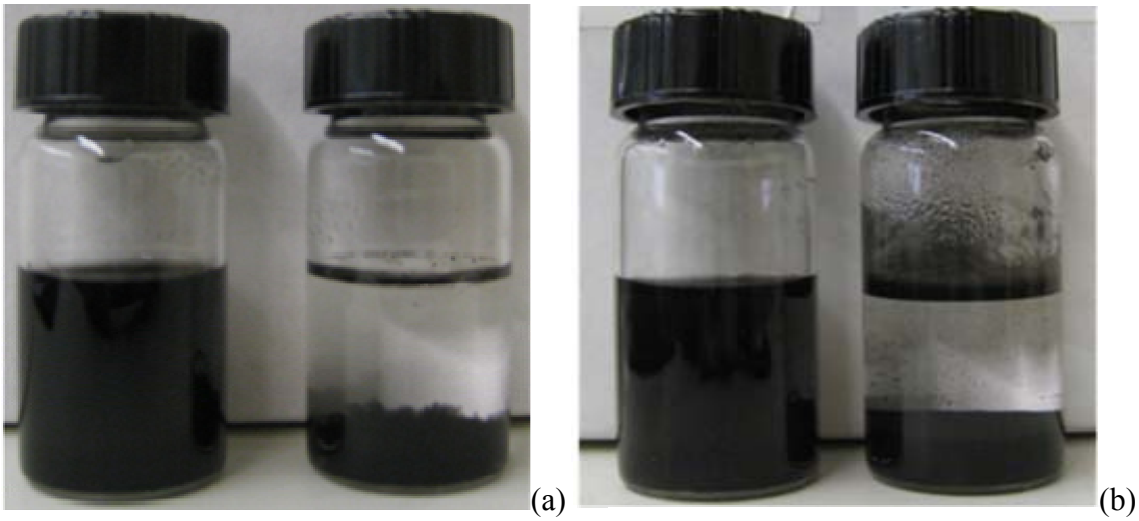
(a) (b)

Figure 4.13. Aqueous suspensions containing 0.011 wt% SWNT (a) or MWNT (b), stabilized with p-PNIPAM (left vial) and PNIPAM (right vial), after 24 hours of sonication. These suspensions were kept at room temperature during a 24 hour period.

In an effort to investigate the temperature responsive characteristics of these suspensions, viscosity measurements were made, as shown in Figure 4.14. Nanotube suspensions treated with PNIPAM show shear-thinning behavior at temperatures both above and below the LCST of the polymer, suggesting bundled nanotube microstructure without a temperature responsive behavior. This further suggests the inability of unmodified PNIPAM to effectively stabilize nanotubes. In contrast, 1p-PNIPAM stabilized nanotube suspensions are Newtonian at temperatures below the LCST and shear-thinning at temperatures above the LCST of the polymer, respectively, revealing a thermoresponsive behavior. It should be pointed out that 1p-PNCPA stabilized SWNTs suspensions exhibit shear thinning behavior at temperatures both below and above the LCST of the polymer, but 1p-PNIPAM stabilized nanotubes show temperature-responsive behavior. One reason for this may be the structural difference between PNIPAM and PNCPA, which influences the conformational transitions of the polymer. The strain of the bond angles of the cyclopropyl group reduces the overlap of electron clouds, which makes PNCPA more hydrophilic than PNIPAM and increases it LCST.[195] Furthermore, presence of more hydrophilic groups along the polymer chain will diminish their interaction with SWNTs.

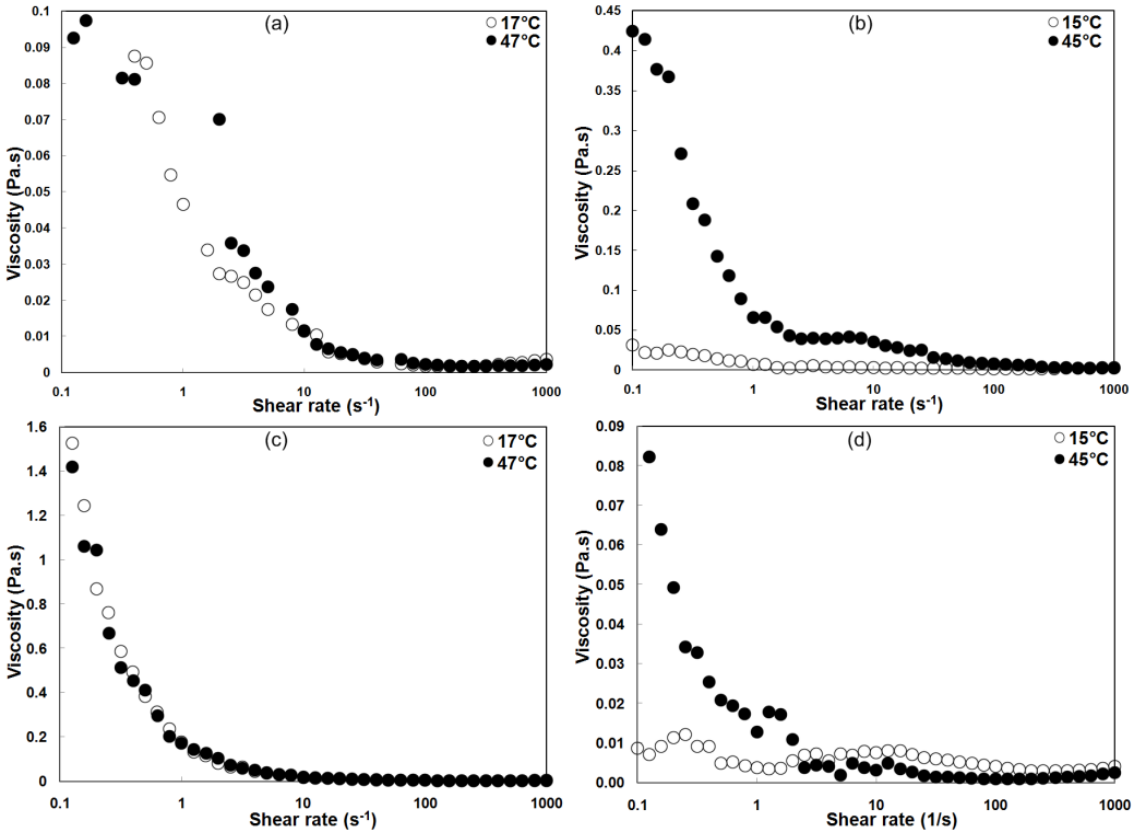

Figure 4.14. Viscosity as a function of shear rate of aqueous suspensions containing 0.011 wt% SWNT and 1 wt% of PNIPAM (a) or p-PNIPAM (b) and 0.011 wt% MWNT and 1 wt% of PNIPAM (c) or p-PNIPAM (d) at temperatures above and below the LCST.

Cryo-TEM was used to visualize nanotube microstructures in SWNT suspensions, as shown in Figure 4.15. As expected, SWNTs in suspensions treated with PNIPAM exist in a bundled state at temperatures above and below the LCST of the polymer. In contrast, 1p-PNIPAM-stabilized suspensions contain more exfoliated and bundled SWNTs at temperatures below and above the LCST of the polymer, respectively. As already mentioned, this temperature-dependent SWNT microstructure in 1p-PNIPAM-stabilized suspensions is attributed to the conformational transitions of

the adsorbed polymer on the nanotube sidewalls that counteracts the inter-tube van der Waals force of attraction. The results obtained from viscosity measurements and cryo-TEM images are complementary, so it is reasonable to assume that SWNTs stabilized using 1p-PNIPAM are more exfoliated at 15^{o}C and more bundled at 47^{o}C.

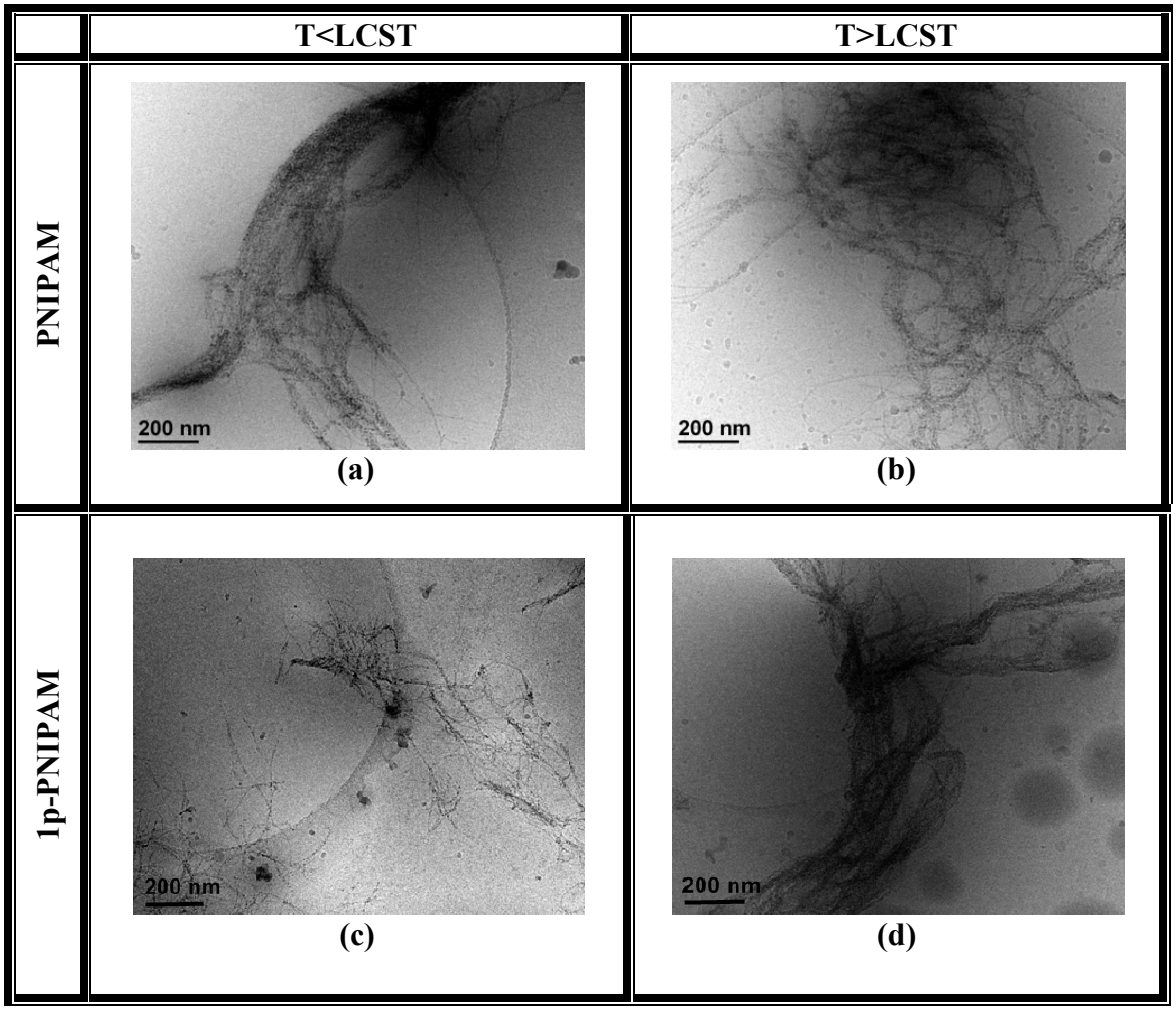

Figure 4.15. Cryo-TEM images of aqueous suspensions containing 0.011 wt% SWNT and 0.1 wt% PNIPAM (a), (b) or 0.1 wt% p-PNIPAM (c), (d) as a function of temperature.

In an effort to better characterize and understand the temperature sensitivity of nanotube suspensions stabilized with 1p-PNIPAM, turbidity measurements (actually decadic absorbance at 400 nm) were conducted on these suspensions. It can be seen in Figure 4.16 shows that there is a significant increase in turbidity of the aqueous 1p-PNIPAM solution at 28°C, suggesting a coil-to-globule transition of the polymer. Similar trends were also observed for SWNT/1p-PNIPAM and MWNT/1p-PNIPAM suspensions, where a small but significant increase in turbidity was observed around 28°C. This suggests that the temperature-responsive characteristics of 1p-PNIPAM are preserved in the presence of nanotubes and their dispersion quality is influenced by the conformational transitions of the polymer as a function of temperature.

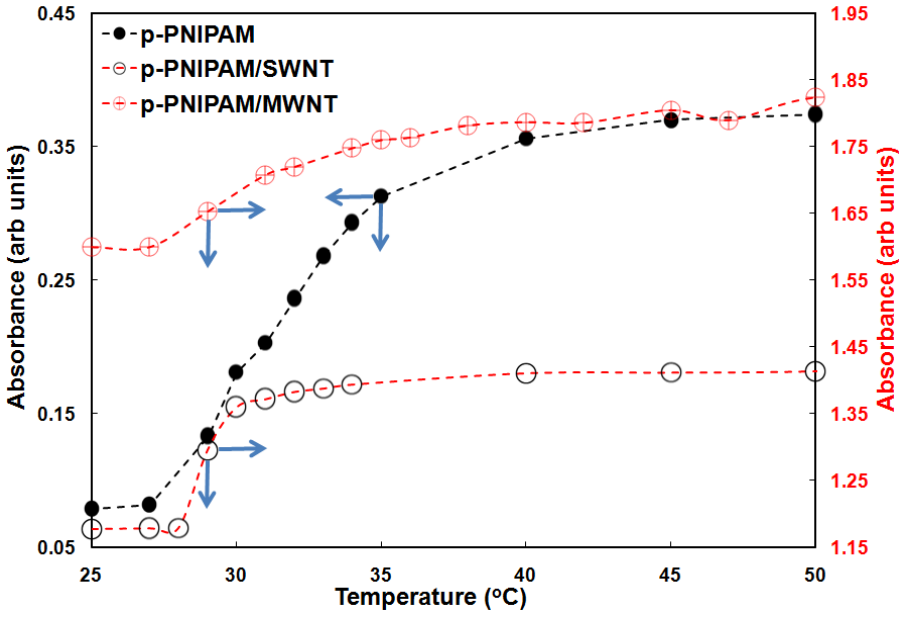

Figure 4.16. Turbidity as a function of temperature for p-PNIPAM/SWNT, p-PNIPAM/MWNT neat suspensions and p-PNIPAM solution in water.

4.3.6 SWNT/1p-PNIPAM Composites

The nanotube microstructure in 1p-PNIPAM composites was investigated by drying SWNT suspensions, stabilized with 1p-PNIPAM or treated with PNIPAM, at temperatures above and below the LCST of the polymer. It is true that the LCST decreases with increasing concentration of polymer, but PNIPAM LCST decreases by only 10^{o}C over a wide concentration range.[179] SEM and digital images of the composite surfaces are shown in Figures 4.17 and 4.18, respectively. As expected, PNIPAM/SWNT composites have regions containing heavily aggregated SWNTs and no SWNTs at both temperatures investigated. This demonstrates the inability of PNIPAM to effectively stabilize SWNTs. In contrast, 1p-PNIPAM/SWNT suspensions dried at 20^{o}C have a homogenous SWNT distribution, suggesting well dispersed nanotubes in the suspension at 20^{o}C. Furthermore, aggregated SWNT microstructure was observed in 1p-PNIPAM/SWNT suspensions dried at 47^{o}C. The temperature dependent SWNT microstructure observed in SWNT/1p-PNIPAM composites suggests that nanotube microstructure in composites can be tailored as a function of temperature. As already mentioned, this method of tailoring nanotube microstructure in the solid state could be a useful tool for solution-processed nanotube filled polymer composite preparation.

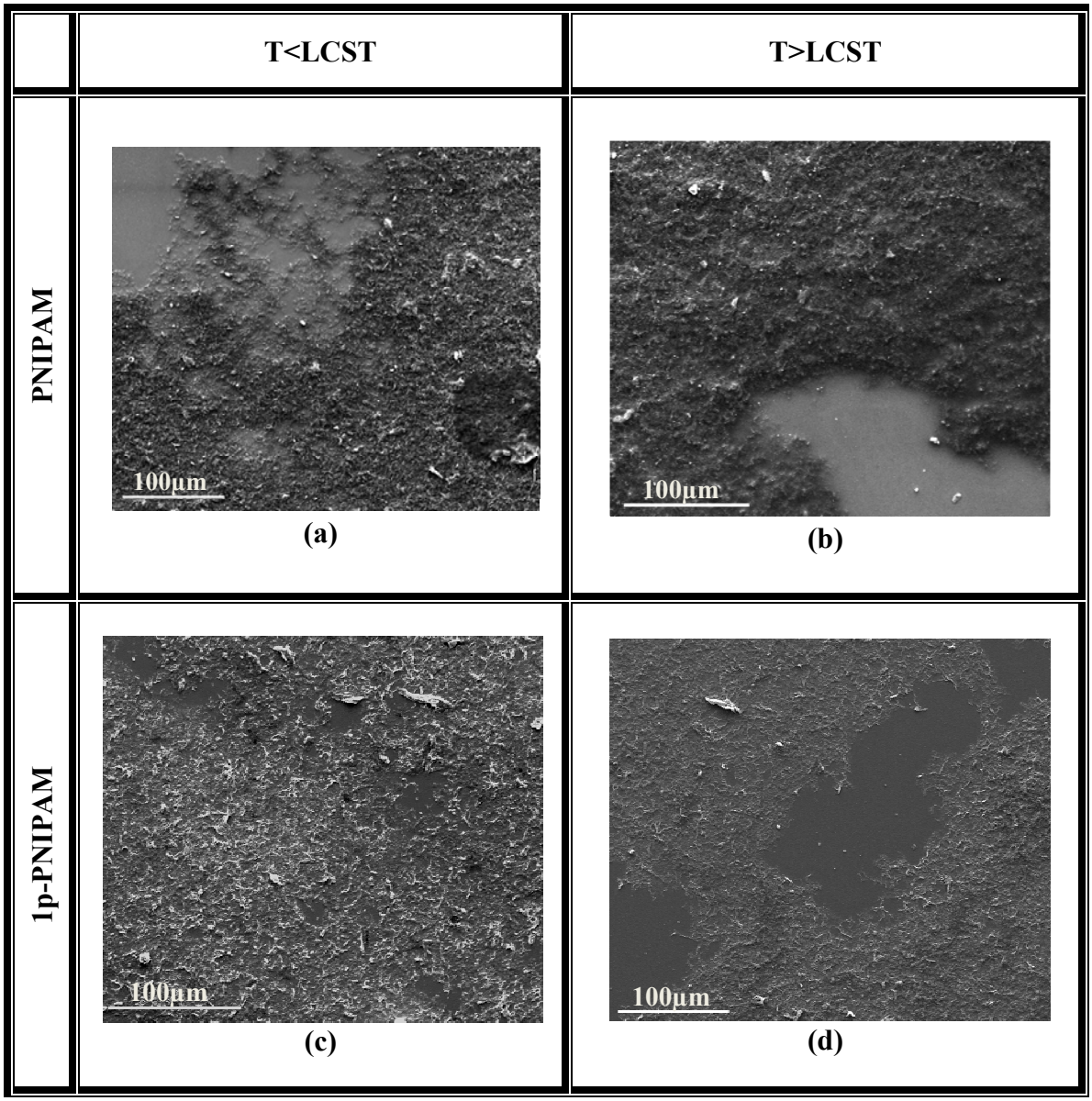

Figure 4.17. SEM images of PNIPAM ((a),(b)) and p-PNIPAM ((c),(d)) dried suspensions, containing 10 wt% SWNT, as a function of temperature. (a) and (c) were made at 20^{o}C and (b) and (d) were made at 47^{o}C.

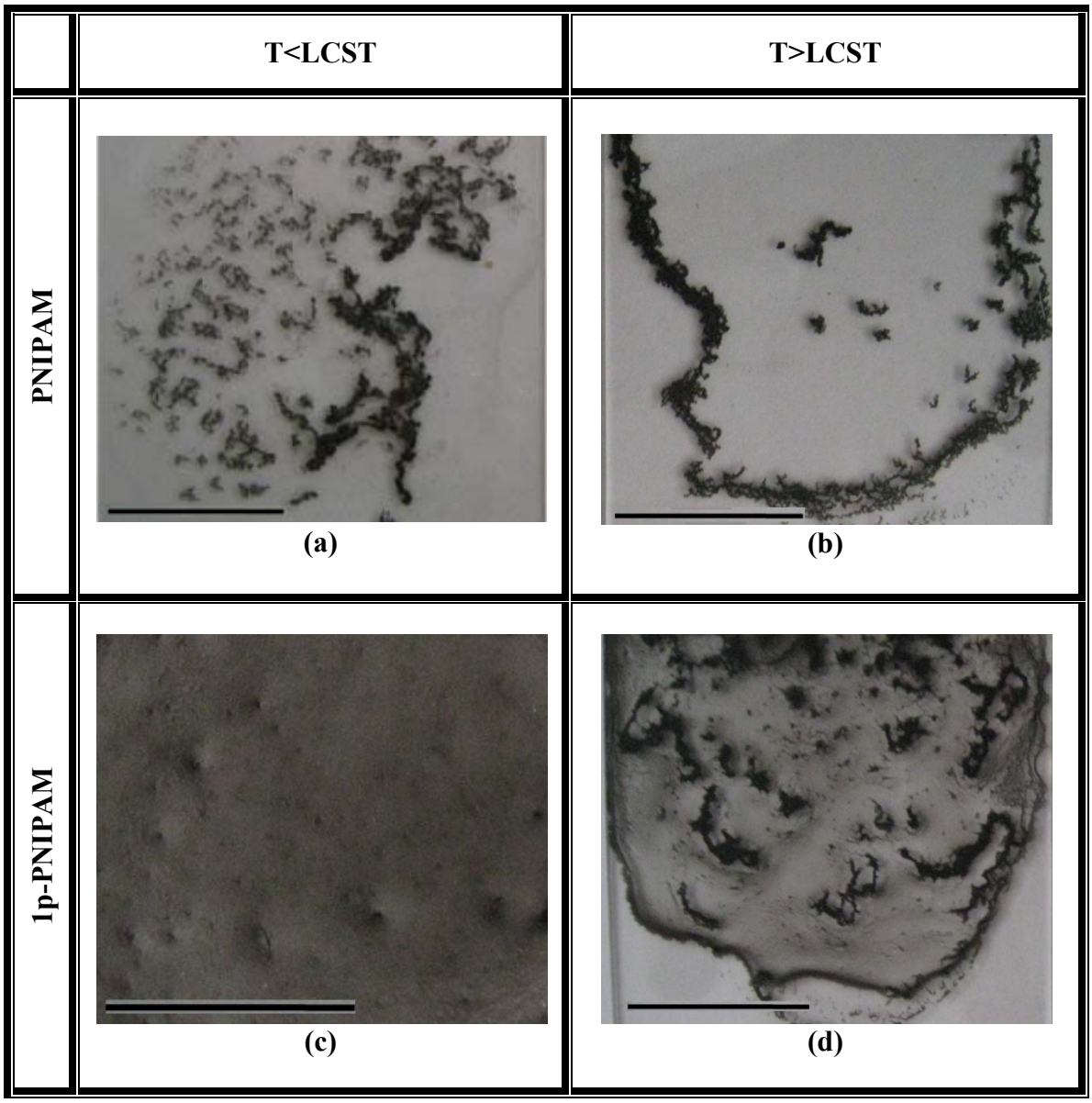

Figure 4.18. Digital images of suspensions containing 10 wt% SWNTs in PNIPAM (a) (b) or p-PNIPAM (c), (d) dried at the temperatures 20^{o}C (a) and (c) and 47^{o}C (c) and (d). Scale bar in these images is 2 cm.

CHAPTER V

CONCLUSIONS AND FUTURE WORK

The overall goal of this research was to demonstrate the effectiveness of stimuli-responsive polymers in stabilizing aqueous SWNT-based suspensions and to tailor the nanotube dispersion state in these suspensions as a function of applied external stimulus. A variety of water soluble pH and temperature-responsive polymers were used as nanotube stabilizers and the resulting suspensions were characterized using a range of techniques. Special emphasis was placed upon gaining a fundamental understanding of the mechanism associated with stabilization and tailoring of nanotube dispersion state in these suspensions.

5.1. pH-Tailored Carbon Nanotube Dispersions

The ability to control the dispersion state of carbon nanotubes in water was demonstrated with four different pH-reponsive polymers (PAA, PMAA, PAAm and BPEI). These weak polyelectrolytes exhibit pH-dependent conformational transitions in water (i.e, extended coil-to-globule) with changing pH. The stability of SWNT suspensions was characterized using UV-Vis spectroscopy, cryo-TEM and centrifugation. Suspensions containing exfoliated SWNTs show greater UV-Vis absorption than those having larger bundles. Viscosity measurements of aqueous suspensions indicate that nanotubes exists in exfoliated and aggregated states depending upon pH. Zeta potential measurements of these same suspensions suggest adsorption of

polymer on the SWNT surface. Electrical conductivity measurements on the composites made by drying the suspensions, demonstrate that nanotube microstructure in the liquid state is preserved to a large extent in the solid state. These results suggest that SWNTs can be stabilized in water using pH-responsive polymers and the dispersion state can be tailored between more bundled and exfoliated states as a function of pH. Based on these results, a stabilization mechanism was hypothesized, where pH induced conformational changes of a polymer adsorbed on the SWNT sidewalls influences their dispersion state. This ability to control nanotube microstructure in the liquid state using pH holds significant promise for the processing of solution-based composites. Tailoring SWNT structure in this manner should allow composite properties (conductivity, strength, etc.) to be precisely tailored, which could lead to improved materials.

5.2. Temperature-Tailored Carbon Nanotube Dispersions

Novel temperature responsive copolymers based on PNCPA and PNIPAM containing 1,3,5 and 1 mol% pyrene moieties, respectively, were synthesized to stabilize aqueous SWNT suspensions. These polymers were characterized using ^{1}H-NMR, UV-Vis and fluorescence emission spectroscopy. ^{1}H NMR spectroscopy confirmed a successful synthesis of the p-PNCPA copolymers series and 1p-PNIPAM and UV-Vis and fluorescence emission spectra clearly show the characteristic peaks of the pyrene side groups. Furthermore, with increasing pyrene content in PNCPA, UV absorption and fluorescence emission were found to increase. Increasing pyrene content

in the PNCPA copolymer series was found to reduce the LCST and increase the polymer-nanotube affinity.

Nanotube dispersion state in the aqueous suspension stabilized with the synthesized polymers, at temperatures above and below the LCST of the polymer, was characterized using a variety of techniques. Cryo-TEM images of 5p-PNCPA stabilized SWNT suspensions at temperatures above and below the LCST of the polymer suggest more individualized and more bundled SWNTs, respectively. Similar observation was made in cryo-TEM image of 1p-PNIPAM stabilized suspensions that exhibited more individualized and more entangled nanotube microstructure at temperatures below and above the LCST of polymer. Viscosity measurements made on the 5p-PNCPA and 1p-PNIPAM stabilized SWNTs suspensions show shear thinning and Newtonian behavior above and below the LCST of the polymer, respectively. The inefficiency of pure PNIPAM in stabilizing SWNTs and MWNTs was demonstrated using images of aqueous suspensions, where the PNIPAM treated suspensions exhibit extensive nanotube sedimentation. The influence of pyrene content in PNCPA on stabilization efficiency of aqueous SWNT suspensions was studied by comparing the viscosity, UV-Vis spectra and zeta potentials. 1p-PNCPA was relatively less effective than 3p-PNCPA and 5p-PNCPA in stabilizing and tailoring SWNT dispersion state in aqueous suspensions. In contrast, 1p-PNIPAM stabilized SWNTs exhibited good stability and thermosensitive dispersion state. Based on the results obtained, a stabilization mechanism involving conformational changes of adsorbed polymer on the nanotube

surface was proposed to explain the observed nanotube dispersion state in these suspensions.

Nanotube microstructure in composites, which were made by drying aqueous SWNT suspensions at temperatures above and below the LCST of the polymer, was characterized using SEM, digital images and electrical conductivity measurements. SEM images of 1p-PNCPA and 5p-PNCPA composites containing SWNTs exhibit more exfoliated and more entangled nanotube microstructure in composites made below and above the LCST of the polymer, respectively. Furthermore, electrical conductivity measurements show that composites made above the LCST of the polymer exhibit higher electrical conductivity. Moreover, the electrical conductivity in composites was influenced by the pyrene content in PNCPA, decreasing with increasing pyrene content. 1p-PNIPAM/SWNT composites also exhibited similar behavior, where composites made below and above the LCST of the polymer show more dispersed and more entangled nanotube microstructure in SEM images, respectively. Furthermore, extensive nanotube phase segregation was seen in PNIPAM/SWNT composites. Based on the results obtained, it appears that nanotube microstructure in suspensions is preserved to a large extent in solid composites made by drying these suspensions. This method of controlling nanotube dispersion state in water, using temperature to influence the properties of solid state composites, will be very useful for the synthesizing nanotube-polymer composites with tailorable properties.

5.3 Future Research Direction

The research presented in this dissertation was focused on the use of pH and temperature-responsive polymers to tailor SWNT dispersion state in water and polymer composites. Assuming, the methods described here are universal, they could be extended to other interesting nanoparticles, such as fullerenes,[33,39] graphene[196-198] and inorganic nanowires.[199-200] Also, there are a variety of other polymers that respond to pH[136,201-203], temperature[204-208] and other kinds of stimuli, such as light,[181-183,209-212] ionic strength,[209] and magnetic field[209]. The use of these polymers to tailor dispersion state of carbon nanotubes and other types of nanoparticles could be very interesting. The following sections touch on these topics by providing some preliminary results and outlining future directions.

5.3.1 Temperature-Tailored Fullerene Suspensions

Fullerenes were briefly described in Chapter II. Owing to their unique atomic structure and nano-sized dimentions, these nanoparticles can be used in many potential applications, such as photovoltaic devices,[213-214] organic electronics,[215-216] and biopharmaceuticals.[217-218] Poly(2-ethyl-2-oxazoline) (PEtOx) is a temperature responsive polymer that exhibits LCST at 62^{o}C in water.[136] Preliminary studies using PEtOx to stabilize C_{60} fullerenes suggest an affinity between them. Figure 5.1 shows the UV-Vis and viscosity data of this C_{60} suspension. Dilute fullerene suspensions obey the Beer-Lambert law, which correlates greater optical absorption to better suspension stability. Figure 5.1 (a) shows that C_{60} stabilized with PEtOx is more stable that C60 alone in

water, while Figure 5.1(b) shows that PEtOx stabilized fullerenes exhibit shear thinning and more Newtonian behavior at temperatures below and above the LCST of the polymer, respectively. Based on these results, it appears that PEtOx stabilized aqueous C_{60} suspensions are thermoresponsive. It would be interesting to further investigate this system by probing the fullerene dispersion state in these suspensions. Furthermore, the ability of PEtOx in stabilizing other interesting nanofillers such as garphene, inorganic nanowires and carbon nanofibers would be interesting to investigate. These temperature responsive suspensions may find potential applications in sensors and responsive interfaces.

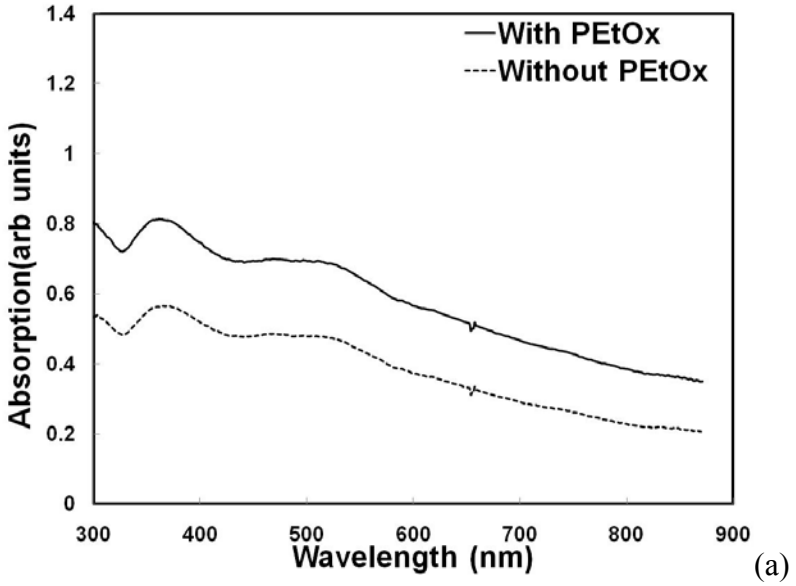

Figure 5.1. UV-Vis spectra (a) and viscosity (b) of aqueous C60 suspensions, containing 0.11 wt% fullerene and 1 wt% PEtOx.

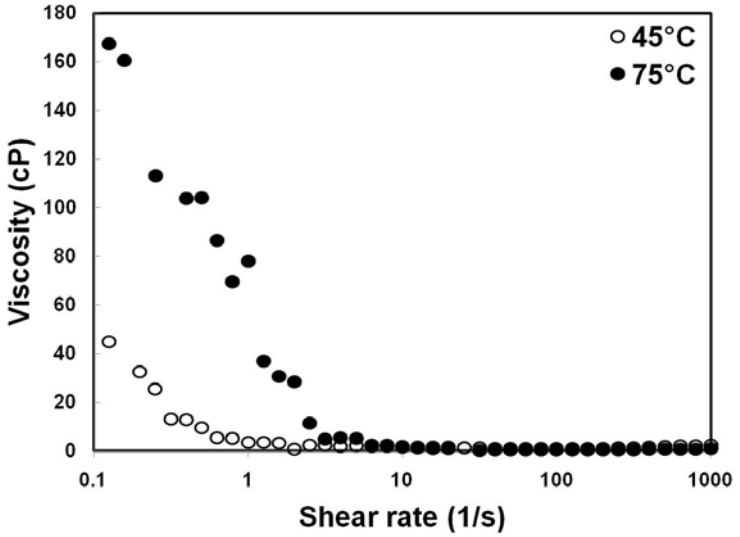

(b)

Figure 5.1. Continued.

5.3.2. Light-Tailored SWNT Dispersion State

Tailoring carbon nanotube dispersion state using light could be an even more interesting extension of the concepts presented in this dissertation. A variety of polymers, such as poly (aryl ether ketone amide) (PAEKA)[219-220] and azobenze containing polymers, that respond to light could also be used to tailor nanotube dispersion state. In an effort to achieve the above mentioned objective, PNIPAM-based polymer containing 8 mol% azobenzene and 5 mol% pyrene moieties was synthesized. The structure of polymer is shown in Figure 5.2. As mentioned in Chapter II, the presence of azobenzene groups makes this polymer UV responsive. An initial experiment showed that this polymer stabilizes nanotubes in water, but the nanotube dispersion state was not found to be influenced by light. One reason for this was likely the low concentration of azobenzene in these polymers that was set arbitrarily to 8

mol%. It is believed that low azobenzene content in this polymer results in insufficient conformational transitions of the polymer which diminishes its dispersion ability. The ability of higher azobenzene containing polymers to tailor nanotube dispersion state would be very interesting to investigate. Furthermore, many of the light-responsive polymers[181-183,209-212,221] are soluble in common organic solvents, which expands the types of composites that could be made with tailored properties (eg., epoxy).

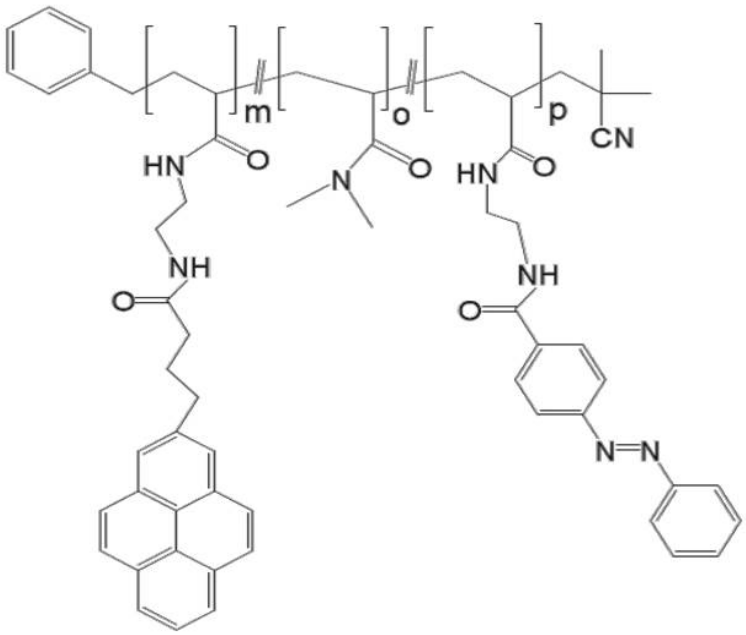

Figure 5.2. Structure of PNIPAM-based azobenzene and pyrene-containing block copolymer synthesized to tailor SWNT dispersion state as a function of light.

REFERENCES

(1) Terrones, M. *An. Rev. Mater. Res.* **2003**, *33*, 419-501.

(2) Ajayan, P. M.; Schadler, L. S.; Giannaris, C.; Rubio, A. *Adv. Mater.2***000**, *12*, 750-753.

(3) Kam, N. W. S.; O'Connell, M.; Wisdom, J. A.; Dai, H. J. *Proc. Nat. Acad. Sci. U.S.A* **2005**, *102*, 11600-11605.

(4) Bhirde, A. A.; Patel, V.; Gavard, J.; Zhang, G. F.; Sousa, A. A.; Masedunskas, A.; Leapman, R. D.; Weigert, R.; Gutkind, J. S.; Rusling, J. F. *Acs Nano* **2009**, *3*, 307-316.

(5) Douroumis, D.; Fatouros, D. G.; Bouropoulos, N.; Papagelis, K.; Tasis, D. *Int. J. Nanomedicine* **2007**, *2*, 761-766.

(6) Barone, P. W.; Baik, S.; Heller, D. A.; Strano, M. S. *Nat. Mater.* **2005**, *4*, 86-92.

(7) Bandyopadhyaya, R.; Nativ-Roth, E.; Regev, O.; Yerushalmi-Rozen, R. *Nano Lett.* **2002**, *2*, 25-28.

(8) Islam, M. F.; Rojas, E.; Bergey, D. M.; Johnson, A. T.; Yodh, A. G. *Nano Lett.* **2003**, *3*, 269-273.

(9) Chen, J.; Hamon, M. A.; Hu, H.; Chen, Y. S.; Rao, A. M.; Eklund, P. C.; Haddon, R. C. *Science* **1998**, *282*, 95-98.

(10) Khabashesku, V. N.; Billups, W. E.; Margrave, J. L. *Acc. Chem. Res* **2002**, *35*, 1087-1095.

(11) Bahr, J. L.; Yang, J. P.; Kosynkin, D. V.; Bronikowski, M. J.; Smalley, R. E.; Tour, J. M. *J. Am. Chem. Soc.* **2001**, *123*, 6536-6542.

(12) Coleman, K. S.; Bailey, S. R.; Fogden, S.; Green, M. L. H. *J. Am. Chem. Soc.* **2003**, *125*, 8722-8723.

(13) Liang, F.; Sadana, A. K.; Peera, A.; Chattopadhyay, J.; Gu, Z. N.; Hauge, R. H.; Billups, W. E. *Nano Lett.* **2004**, *4*, 1257-1260.

(14) Bandow, S.; Rao, A. M.; Williams, K. A.; Thess, A.; Smalley, R. E.; Eklund, P. C. *J. Phys. Chem. B* **1997**, *101*, 8839-8842.

(15) Chen, R. J.; Zhang, Y. G.; Wang, D. W.; Dai, H. J. *J. Am. Chem. Soc.* **2001**, *123*, 3838-3839.

(16) Star, A.; Stoddart, J. F.; Steuerman, D.; Diehl, M.; Boukai, A.; Wong, E. W.; Yang, X.; Chung, S. W.; Choi, H.; Heath, J. R. *Angew. Chem.-Int. Ed.* **2001**, *40*, 1721-1725.

(17) Chen, R. J.; Bangsaruntip, S.; Drouvalakis, K. A.; Kam, N. W. S.; Shim, M.; Li, Y. M.; Kim, W.; Utz, P. J.; Dai, H. J. *Proc. Nat. Acad. Sci. U.S.A.* **2003**, *100*, 4984-4989.

(18) Huang, W. J.; Fernando, S.; Allard, L. F.; Sun, Y. P. *Nano Lett.* **2003**, *3*, 565-568.

(19) Dyke, C. A.; Tour, J. M. *J. Phys. Chem. A* **2004**, *108*, 11151-11159.

(20) Ajayan, P. M.; Tour, J. M. *Nature* **2007**, *447*, 1066-1068.

(21) Grunlan, J. C.; Liu, L.; Regev, O. *J. Colloid Interface Sci.* **2008**, *317*, 346-349.

(22) Grunlan, J. C.; Liu, L.; Kim, Y. S. *Nano Lett.* **2006**, *6*, 911-915.

(23) Etika, K. C.; Cox, M. A.; Grunlan, J. C. *Polymer* **2010**, *51*, 1761-1770.

(24) Etika, K. C.; Jochum, F. D.; Theato, P.; Grunlan, J. C. *J. Am. Chem. Soc.* **2009**, *131*, 13598-13599.

(25) Wang, D.; Chen, L. W. *Nano Lett.* **2007**, *7*, 1480-1484.

(26) Umeyama, T.; Kawabata, K.; Tezuka, N.; Matano, Y.; Miyato, Y.; Matsushige, K.; Tsujimoto, M.; Isoda, S.; Takano, M.; Imahori, H. *Chem. Commun.* **2010**, *46*, 5969-5971.

(27) Galaev, I. Y.; Mattiasson, B. *Trends Biotechnol.* **1999**, *17*, 335-340.

(28) Nath, N.; Chilkoti, A. *Adv. Mater.* **2002**, *14*, 1243-1347.

(29) Siegel, R. A. *Adv. Polym. Sci.* **1993**, *109*, 233-267.

(30) Barone, P. W.; Strano, M. S. *Angew. Chem.-Int. Ed.* **2006**, *45*, 8138-8141.

(31) Bromberg, A. V.; Lukyanovich, V. M.; Nemtsova, V. V.; Radushkevich, L. V.; Chmutov, K. V. *Zhurnal Fizicheskoi Khimii* **1953**, *27*, 379-388.

(32) Bykov, V. T.; Lukyanovich, V. M.; Radushkevich, L. V. *Izvestiya Akademii Nauk Sssr-Seriya Khimicheskaya* **1952**, 406-408.

(33) Kroto, H. W.; Heath, J. R.; Obrien, S. C.; Curl, R. F.; Smalley, R. E. *Nature* **1985**, *318*, 162-163.

(34) Oberlin, A.; Endo, M.; Koyama, T. *J. Crystal Growth* **1976**, *32*, 335-349.

(35) Dresselhaus, M. S.; Dresselhaus, G.; Saito, R. *Phys. Rev. B* **1992**, *45*, 6234-6242.

(36) Iijima, S. *Nature* **1991**, *354*, 56-58.

(37) Iijima, S.; Ichihashi, T. *Nature* **1993**, *363*, 603-605.

(38) Bethune, D. S.; Kiang, C. H.; Devries, M. S.; Gorman, G.; Savoy, R.; Vazquez, J.; Beyers, R. *Nature* **1993**, *363*, 605-607.

(39) Kroto, H. W.; Allaf, A. W.; Balm, S. P. *Chem. Rev.* **1991**, *91*, 1213-1235.

(40) Odom, T. W.; Huang, J. L.; Kim, P.; Lieber, C. M. *Nature* **1998**, *391*, 62-64.

(41) Berber, S.; Kwon, Y. K.; Tomanek, D. *Phys. Rev. Lett.* **2000**, *84*, 4613-4616.

(42) Salvetat, J. P.; Briggs, G. A. D.; Bonard, J. M.; Bacsa, R. R.; Kulik, A. J.; Stockli, T.; Burnham, N. A.; Forro, L. *Phys. Rev. Lett.* **1999**, *82*, 944-947.

(43) Ge, M. H.; Sattler, K. *Appl. Phys. Lett.* **1994**, *65*, 2284-2286.

(44) Odom, T. W.; Huang, J. L.; Kim, P.; Ouyang, M.; Lieber, C. M. *J. Mater.Res.* **1998**, *13*, 2380-2388.

(45) Baughman, R. H.; Zakhidov, A. A.; de Heer, W. A. *Science* **2002**, *297*, 787.

(46) Dai, H. J. *Acc. Chem. Res.* **2002**, *35*, 1035-1044.

(47) Zhou, O.; Fleming, R. M.; Murphy, D. W.; Chen, C. H.; Haddon, R. C.; Ramirez, A. P.; Glarum, S. H. *Science* **1994**, *263*, 1744-1747.

(48) Journet, C.; Maser, W. K.; Bernier, P.; Loiseau, A.; delaChapelle, M. L.; Lefrant, S.; Deniard, P.; Lee, R.; Fischer, J. E. *Nature* **1997**, *388*, 756-758.

(49) Thess, A.; Lee, R.; Nikolaev, P.; Dai, H. J.; Petit, P.; Robert, J.; Xu, C. H.; Lee, Y. H.; Kim, S. G.; Rinzler, A. G.; Colbert, D. T.; Scuseria, G. E.; Tomanek, D.; Fischer, J. E.; Smalley, R. E. *Science* **1996**, *273*, 483-487.

(50) Rinzler, A. G.; Liu, J.; Dai, H.; Nikolaev, P.; Huffman, C. B.; Rodriguez-Macias, F. J.; Boul, P. J.; Lu, A. H.; Heymann, D.; Colbert, D. T.; Lee, R. S.; Fischer, J.

E.; Rao, A. M.; Eklund, P. C.; Smalley, R. E. *Appl. Phys. a-Mater. Sci. & Process,* **1998**, *67*, 29-37.

(51) Bronikowski, M. J.; Willis, P. A.; Colbert, D. T.; Smith, K. A.; Smalley, R. E. *J. Vac. Sci. Technol. A* **2001**, *19*, 1800-1805.

(52) Nikolaev, P. *J. Nanosci. Nanotechnol.* **2004**, *4*, 307-316.

(53) Saito, Y.; Inagaki, M. *Jpn. J. of Appl. Phys. Part 2-Lett.* **1993**, *32*, L954-L957.

(54) Yakobson, B. I.; Smalley, R. E. *Am. Scientist* **1997**, *85*, 324-337.

(55) Chiang, I. W.; Brinson, B. E.; Huang, A. Y.; Willis, P. A.; Bronikowski, M. J.; Margrave, J. L.; Smalley, R. E.; Hauge, R. H. *J. Phys. Chem. B* **2001**, *105*, 8297-8301.

(56) Walters, D. A.; Ericson, L. M.; Casavant, M. J.; Liu, J.; Colbert, D. T.; Smith, K. A.; Smalley, R. E. *Appl. Phys. Lett.* **1999**, *74*, 3803-3805.

(57) Yu, M. F.; Files, B. S.; Arepalli, S.; Ruoff, R. S. *Phys. Rev. Lett.* **2000**, *84*, 5552-5555.

(58) Chesnokov, S. A.; Nalimova, V. A.; Rinzler, A. G.; Smalley, R. E.; Fischer, J. E. *Phys. Rev. Lett.* **1999**, *82*, 343.

(59) Moniruzzaman, M.; Winey, K. I. *Macromolecules* **2006**, *39*, 5194-5205.

(60) Zheng, M.; Jagota, A.; Semke, E. D.; Diner, B. A.; Mclean, R. S.; Lustig, S. R.; Richardson, R. E.; Tassi, N. G. *Nat. Mater.* **2003**, *2*, 338-342.

(61) Girifalco, L. A.; Hodak, M.; Lee, R. S. *Phys. Rev. B* **2000**, *62*, 13104-13110.

(62) Ajayan, P. M.; Banhart, F. *Nat. Mat.* **2004**, *3*, 135-136.

(63) Hamon, M. A.; Itkis, M. E.; Niyogi, S.; Alvaraez, T.; Kuper, C.; Menon, M.; Haddon, R. C. *J. Am. Chem. Soc.* **2001**, *123*, 11292-11293.

(64) Niyogi, S.; Hamon, M. A.; Hu, H.; Zhao, B.; Bhowmik, P.; Sen, R.; Itkis, M. E.; Haddon, R. C. *Acc. Chem. Res.* **2002**, *35*, 1105-1113.

(65) Khlobystov, A. N.; Britz, D. A.; Briggs, G. A. D. *Acc. Chem. Res.* **2005**, *38*, 901-909.

(66) Hirsch, A. *Angew. Chem-Int. Ed.* **2002**, *41*, 1853-1859.

(67) Xu, G. D.; Zhu, B.; Han, Y.; Bo, Z. S. *Polymer* **2007**, *48*, 7510-7515.

(68) Kitano, H.; Tachimoto, K.; Anraku, Y. *J. Colloid Interface Sci.* **2007**, *306*, 28-33.

(69) Yuen, S. M.; Ma, C. C. M.; Teng, C. C.; Wu, H. H.; Kuan, H. C.; Chiang, C. L. *J. Polym. Sci. Part B-Polym. Phys.* **2008**, *46*, 472-482.

(70) Lu, X.; Chen, Z. F.; Schleyer, P. V. *J. Am. Chem. Soc.* **2005**, *127*, 20-21.

(71) Bockrath, M.; Liang, W. J.; Bozovic, D.; Hafner, J. H.; Lieber, C. M.; Tinkham, M.; Park, H. K. *Science* **2001**, *291*, 283-285.

(72) Mawhinney, D. B.; Naumenko, V.; Kuznetsova, A.; Yates, J. T.; Liu, J.; Smalley, R. E. *Chem. Phys. Lett.* **2000**, *324*, 213-216.

(73) Chiang, I. W.; Brinson, B. E.; Smalley, R. E.; Margrave, J. L.; Hauge, R. H. *J. Phys. Chem. B* **2001**, *105*, 1157-1161.

(74) Niyogi, S.; Hu, H.; Hamon, M. A.; Bhowmik, P.; Zhao, B.; Rozenzhak, S. M.; Chen, J.; Itkis, M. E.; Meier, M. S.; Haddon, R. C. *J. Am. Chem. Soc.* **2001**, *123*, 733-734.

(75) Hamon, M. A.; Hui, H.; Bhowmik, P.; Itkis, H. M. E.; Haddon, R. C. *Appl. Phys. a-Mater. Sci. & Process.* **2002**, *74*, 333-338.

(76) Qu, L. W.; Martin, R. B.; Huang, W. J.; Fu, K. F.; Zweifel, D.; Lin, Y.; Sun, Y. P.; Bunker, C. E.; Harruff, B. A.; Gord, J. R.; Allard, L. F. *J. Chem. Phys.* **2002**, *117*, 8089-8094.

(77) Li, B.; Shi, Z. J.; Lian, Y. F.; Gu, Z. N. *Chem. Lett.* **2001**, 598-599.

(78) Pompeo, F.; Resasco, D. E. *Nano Lett.* **2002**, *2*, 369-373.

(79) Azamian, B. R.; Coleman, K. S.; Davis, J. J.; Hanson, N.; Green, M. L. H. *Chem. Commun.* **2002**, 366-367.

(80) Banerjee, S.; Wong, S. S. *Nano Lett.* **2002**, *2*, 195-200.

(81) Sun, Y. P.; Fu, K. F.; Lin, Y.; Huang, W. J. *Acc. Chem. Res.* **2002**, *35*, 1096-1104.

(82) Serp, P.; Corrias, M.; Kalck, P. *Appl. Catalysis A* **2003**, *253*, 337-358.

(83) Hemraj-Benny, T.; Banerjee, S.; Wong, S. S. *Chem. Mater.* **2004**, *16*, 1855-1863.

(84) Banerjee, S.; Wong, S. S. *J. Am. Chem. Soc.* **2002**, *124*, 8940-8948.

(85) Banerjee, S.; Hemraj-Benny, T.; Wong, S. S. *Adv. Mater.* **2005**, *17*, 17-29.

(86) Bahr, J. L.; Tour, J. M. *J. Mater. Chem.* **2002**, *12*, 1952-1958.

(87) Chen, Z. F.; Thiel, W.; Hirsch, A. *Chem. phys. chem* **2003**, *4*, 93-97.

(88) Dyke, C. A.; Tour, J. M. *J. Am. Chem. Soc.* **2003**, *125*, 1156-1157.

(89) Mickelson, E. T.; Huffman, C. B.; Rinzler, A. G.; Smalley, R. E.; Hauge, R. H.; Margrave, J. L. *Chem. Phys. Lett.* **1998**, *296*, 188-194.

(90) Kelly, K. F.; Chiang, I. W.; Mickelson, E. T.; Hauge, R. H.; Margrave, J. L.; Wang, X.; Scuseria, G. E.; Radloff, C.; Halas, N. J. *Chem. Phys. Lett.* **1999**, *313*, 445-450.

(91) Mickelson, E. T.; Chiang, I. W.; Zimmerman, J. L.; Boul, P. J.; Lozano, J.; Liu, J.; Smalley, R. E.; Hauge, R. H.; Margrave, J. L. *J. Phys. Chem. B* **1999**, *103*, 4318-4322.

(92) Boul, P. J.; Liu, J.; Mickelson, E. T.; Huffman, C. B.; Ericson, L. M.; Chiang, I. W.; Smith, K. A.; Colbert, D. T.; Hauge, R. H.; Margrave, J. L.; Smalley, R. E. *Chem. Phys. Lett.* **1999**, *310*, 367-372.

(93) Holzinger, M.; Vostrowsky, O.; Hirsch, A.; Hennrich, F.; Kappes, M.; Weiss, R.; Jellen, F. *Angew. Chem.-Int. Ed.* **2001**, *40*, 4002-4005.

(94) Georgakilas, V.; Voulgaris, D.; Vazquez, E.; Prato, M.; Guldi, D. M.; Kukovecz, A.; Kuzmany, H. *J. Am. Chem. Soc.* **2002**, *124*, 14318-14319.

(95) Viswanathan, G.; Chakrapani, N.; Yang, H. C.; Wei, B. Q.; Chung, H. S.; Cho, K. W.; Ryu, C. Y.; Ajayan, P. M. *J. Am. Chem. Soc.* **2003**, *125*, 9258-9259.

(96) Qin, S. H.; Qin, D. Q.; Ford, W. T.; Resasco, D. E.; Herrera, J. E. *Macromolecules* **2004**, *37*, 752-757.

(97) Sano, M.; Kamino, A.; Okamura, J.; Shinkai, S. *Langmuir* **2001**, *17*, 5125-5128.

(98) Lin, Y.; Zhou, B.; Fernando, K. A. S.; Liu, P.; Allard, L. F.; Sun, Y. P. *Macromolecules* **2003**, *36*, 7199-7204.

(99) Blake, R.; Gun'ko, Y. K.; Coleman, J.; Cadek, M.; Fonseca, A.; Nagy, J. B.; Blau, W. J. *J. Am. Chem. Soc.* **2004**, *126*, 10226-10227.

(100) Shaffer, M. S. P.; Koziol, K. *Chem. Commun.* **2002**, 2074-2075.

(101) Xin, T.; Chang, L.; Cheng, H. M.; Zhao, H. C.; Feng, Y.; Zhang, X. Q. *J. Appl. Polym. Sci.* **2004**, *92*, 3697-3700.

(102) Yao, Z. L.; Braidy, N.; Botton, G. A.; Adronov, A. *J. Am. Chem. Soc.* **2003**, *125*, 16015-16024.

(103) Chen, J.; Liu, H. Y.; Weimer, W. A.; Halls, M. D.; Waldeck, D. H.; Walker, G. C. *J. Am. Chem. Soc.* **2002**, *124*, 9034-9035.

(104) O'Connell, M. J.; Boul, P.; Ericson, L. M.; Huffman, C.; Wang, Y. H.; Haroz, E.; Kuper, C.; Tour, J.; Ausman, K. D.; Smalley, R. E. *Chem. Phys. Lett.* **2001**, *342*, 265-271.

(105) Liu, L.; Etika, K. C.; Liao, K. S.; Hess, L. A.; Bergbreiter, D. E.; Grunlan, J. C. *Macromol. Rapid Commun.* **2009**, *30*, 627-632.

(106) Didenko, V. V.; Moore, V. C.; Baskin, D. S.; Smalley, R. E. *Nano Lett.* **2005**, *5*, 1563-1567.

(107) Satake, A.; Miyajima, Y.; Kobuke, Y. *Chem. Mater.* **2005**, *17*, 716-724.

(108) Kim, O. K.; Je, J. T.; Baldwin, J. W.; Kooi, S.; Pehrsson, P. E.; Buckley, L. J. *J. Am. Chem. Soc.* **2003**, *125*, 4426-4427.

(109) Star, A.; Steuerman, D. W.; Heath, J. R.; Stoddart, J. F. *Ang. Chem.-Int. Ed.* **2002**, *41*, 2508-2512.

(110) Ortiz-Acevedo, A.; Xie, H.; Zorbas, V.; Sampson, W. M.; Dalton, A. B.; Baughman, R. H.; Draper, R. K.; Musselman, I. H.; Dieckmann, G. R. *J. Am. Chem. Soc.* **2005**, *127*, 9512-9517.

(111) Zheng, M.; Jagota, A.; Strano, M. S.; Santos, A. P.; Barone, P.; Chou, S. G.; Diner, B. A.; Dresselhaus, M. S.; McLean, R. S.; Onoa, G. B.; Samsonidze, G. G.; Semke, E. D.; Usrey, M.; Walls, D. J. *Science* **2003**, *302*, 1545-1548.

(112) Badaire, S.; Zakri, C.; Maugey, M.; Derre, A.; Barisci, J. N.; Wallace, G.; Poulin, P. *Adv. Mater.* **2005**, *17*, 1673-1676.

(113) Duesberg, G. S.; Burghard, M.; Muster, J.; Philipp, G.; Roth, S. *Chem. Commun.* **1998**, 435-436.

(114) Krstic, V.; Duesberg, G. S.; Muster, J.; Burghard, M.; Roth, S. *Chem. Mater.* **1998**, *10*, 2338-2340.

(115) Wiltshire, J. G.; Li, L. J.; Khlobystov, A. N.; Padbury, C. J.; Briggs, G. A. D.; Nicholas, R. J. *Carbon* **2005**, *43*, 1151-1155.

(116) Britz, D. A.; Khlobystov, A. N. *Chem. Soc. Rev.* **2006**, *35*, 637-659.

(117) Singh, I.; Bhatnagar, P. K.; Mathur, P. C.; Bharadwaj, L. M. *J. Mater. Res.* **2008**, *23*, 632-636.

(118) Li, L. J.; Nicholas, R. J.; Chen, C. Y.; Darton, R. C.; Baker, S. C. *Nanotechnol.* **2005**, *16*, S202-S205.

(119) Angelikopoulos, P.; Gromoy, A.; Leen, A.; Nerushev, O.; Bock, H.; Campbell, E. E. B. *J. Phys. Chem. C* **2010**, *114*, 2-9.

(120) Sun, Z.; Nicolosi, V.; Rickard, D.; Bergin, S. D.; Aherne, D.; Coleman, J. N. *J. Phys. Chem. C* **2008**, *112*, 10692-10699.

(121) Moore, V. C.; Strano, M. S.; Haroz, E. H.; Hauge, R. H.; Smalley, R. E.; Schmidt, J.; Talmon, Y. *Nano Lett.* **2003**, *3*, 1379-1382.

(122) Grunlan, J. C.; Kim, Y. S.; Ziaee, S.; Wei, X.; Abdel-Magid, B.; Tao, K. *Macromol. Mater. Eng.* **2006**, *291*, 1035-1043.

(123) Grunlan, J. C.; Bannon, M. V. *Nanotube-Based Devices* **2003**, *772*, 233-236.

(124) Nativ-Roth, E.; Levi-Kalisman, Y.; Regev, O.; Yerushalmi-Rozen, R. *J. Polym. Eng.* **2002**, *22*, 353-368.

(125) Wenseleers, W.; Vlasov, I. I.; Goovaerts, E.; Obraztsova, E. D.; Lobach, A. S.; Bouwen, A. *Adv. Funct. Mater.* **2004**, *14*, 1105-1112.

(126) Lukaszczuk, P.; Borowiak-Palen, E.; Rummeli, M. H.; Kalenczuk, R. J. *Appl. Phys. A* **2010**, *100*, 505-510.

(127) Park, Y. T.; Ham, A. Y.; Grunlan, J. C. *J. Phys. Chem. C* **2010**, *114*, 6325-6333.

(128) Zhao, Y. L.; Stoddart, J. F. *Acc. Chem. Res.* **2009**, *42*, 1161-1171.

(129) Tomonari, Y.; Murakami, H.; Nakashima, N. *Chem.- A Eur. J.l* **2006**, *12*, 4027-4034.

(130) Nakashima, N.; Tomonari, Y.; Murakami, H. *Chem. Lett.* **2002**, 638-639.

(131) Chen, J. Y.; Collier, C. P. *J. Phys. Chem. B* **2005**, *109*, 7605-7609.

(132) Star, A.; Liu, Y.; Grant, K.; Ridvan, L.; Stoddart, J. F.; Steuerman, D. W.; Diehl, M. R.; Boukai, A.; Heath, J. R. *Macromolecules* **2003**, *36*, 553-560.

(133) Ramasubramaniam, R.; Chen, J.; Liu, H. Y. *Appl. Phys. Lett.* **2003**, *83*, 2928-2930.

(134) Star, A.; Stoddart, J. F. *Macromolecules* **2002**, *35*, 7516-7520.

(135) Yang, M. J.; Koutsos, V.; Zaiser, M. *J. Phys. Chem. B* **2005**, *109*, 10009-10014.

(136) Schmaljohann, D. *Adv. Drug Delivery Rev.* **2006**, *58*, 1655-1670.

(137) Stuart, M. A. C.; Huck, W. T. S.; Genzer, J.; Muller, M.; Ober, C.; Stamm, M.; Sukhorukov, G. B.; Szleifer, I.; Tsukruk, V. V.; Urban, M.; Winnik, F.; Zauscher, S.; Luzinov, I.; Minko, S. *Nat. Mater.* **2010**, *9*, 101-113.

(138) Roy, I.; Gupta, M. N. *Chem. Biol.* **2003**, *10*, 1161-1171.

(139) Qiu, Y.; Park, K. *Adv. Drug Delivery Rev.* **2001**, *53*, 321-339.

(140) Sajeesh, S.; Sharma, C. P. *J. Biomater. Sci.-Polym. Ed.* **2007**, *18*, 1125-1139.

(141) Jeong, B.; Gutowska, A. *Trends Biotechnol.* **2002**, *20*, 305-311.

(142) Sajeesh, S.; Sharma, C. P. *J. Biomedical Mater. Res. B-Appl. Biomater.* **2006**, *76B*, 298-305.

(143) Zhang, J.; Chu, L. Y.; Li, Y. K.; Lee, Y. M. *Polymer* **2007**, *48*, 1718-1728.

(144) Galaev, I. Y.; Mattiasson, B. *Enzyme and Microbial Technol.* **1993**, *15*, 354-366.

(145) Jeong, B.; Kim, S. W.; Bae, Y. H. *Adv. Drug Delivery Rev.* **2002**, *54*, 37-51.

(146) Bhattarai, N.; Ramay, H. R.; Gunn, J.; Matsen, F. A.; Zhang, M. Q. *J. Controlled Release* **2005**, *103*, 609-624.

(147) Raucher, D.; Chilkoti, A. *Cancer Res.* **2001**, *61*, 7163-7170.

(148) Betre, H.; Liu, W.; Zalutsky, M. R.; Chilkoti, A.; Kraus, V. B.; Setton, L. A. *J. Controlled Release* **2006**, *115*, 175-182.

(149) Markvicheva, E. A.; Kuzkina, I. F.; Pashkin, I. I.; Plechko, T. N.; Kirsh, Y. E.; Zubov, V. P. *Biotechnol. Tech.* **1991**, *5*, 223-226.

(150) Alarcon, C. D. H.; Pennadam, S.; Alexander, C. *Chem. Soc. Rev.* **2005**, *34*, 276-285.

(151) Finkelmann, H.; Nishikawa, E.; Pereira, G. G.; Warner, M. *Phys. Rev. Lett.* **2001**, *8701,* 015501-1–015501-4.

(152) Andreopoulos, F. M.; Deible, C. R.; Stauffer, M. T.; Weber, S. G.; Wagner, W. R.; Beckman, E. J.; Russell, A. J. *J. Am. Chem. Soc.* **1996**, *118*, 6235-6240.

(153) Camacho-Lopez, M.; Finkelmann, H.; Palffy-Muhoray, P.; Shelley, M. *Nat. Mater.* **2004**, *3*, 307-310.

(154) Schmidt, C. E.; Shastri, V. R.; Vacanti, J. P.; Langer, R. *Proc. Nat. Acad. Sci. U. S.A.* **1997**, *94*, 8948-8953.

(155) Irvin, D. J.; Goods, S. H.; Whinnery, L. L. *Chem. Mater.* **2001**, *13*, 1143-1145.

(156) Zhang, J.; Peppas, N. A. *Macromolecules* **2000**, *33*, 102-107.

(157) Grunlan, M. A.; Lee, N. S.; Mansfeld, F.; Kus, E.; Finlay, J. A.; Callow, J. A.; Callow, M. E.; Weber, W. P. *J. Polym. Sci. A-Poly. Chem.* **2006**, *44*, 2551-2566.

(158) Suh, J.; Paik, H. J.; Hwang, B. K. *Bioorg. Chem.* **1994**, *22*, 318-327.

(159) Etika, K. C.; Liu, L.; Hess, L. A.; Grunlan, J. C. *Carbon* **2009**, *47*, 3128-3136.

(160) Grossiord, N.; Loos, J.; Meuldijk, J.; Regev, O.; Miltner, H. E.; Van Mele, B.; Koning, C. E. *Composites Sci. Technol.* **2007**, *67*, 778-782.

(161) Grossiord, N.; Regev, O.; Loos, J.; Meuldijk, J.; Koning, C. E. *Anal. Chem.* **2005**, *77*, 5135-5139.

(162) Hamada, N.; Sawada, S.; Oshiyama, A. *Phys. Rev. Lett.* **1992**, *68*, 1579-1581.

(163) Saito, R.; Fujita, M.; Dresselhaus, G.; Dresselhaus, M. S. *Appl. Phys. Lett.* **1992**, *60*, 2204-2206.

(164) Kataura, H.; Kumazawa, Y.; Maniwa, Y.; Umezu, I.; Suzuki, S.; Ohtsuka, Y.; Achiba, Y. *Syn. Met.* **1999**, *103*, 2555-2558.

(165) Saint-Aubin, K.; Poulin, P.; Saadaoui, H.; Maugey, M.; Zakri, C. *Langmuir* **2009**, *25*, 13206-13211.

(166) Maeda, Y.; Kimura, S.; Hirashima, Y.; Kanda, M.; Lian, Y. F.; Wakahara, T.; Akasaka, T.; Hasegawa, T.; Tokumoto, H.; Shimizu, T.; Kataura, H.; Miyauchi, Y.; Maruyama, S.; Kobayashi, K.; Nagase, S. *J. Phys. Chem. B* **2004**, *108*, 18395-18397.

(167) Schaefer, D.; Brown, J. M.; Anderson, D. P.; Zhao, J.; Chokalingam, K.; Tomlin, D.; Ilavsky, J. *J. Appl. Crystallograp.* **2003**, *36*, 553-557.

(168) Napper, D. H. *Polymeric stabilization of colloidal dispersions*; Academic Press: London ; 1983.

(169) Shaffer, M. S. P.; Windle, A. H. *Macromolecules* **1999**, *32*, 6864-6866.

(170) Tang, F. Q.; Huang, X. X.; Zhang, Y. F.; Guo, J. K. *Ceram. Int.* **2000**, *26*, 93-97.

(171) White, B.; Banerjee, S.; O'Brien, S.; Turro, N. J.; Herman, I. P. *J. Phys. Chem. C* **2007**, *111*, 13684-13690.

(172) Chen, Z. C.; Ring, T. A.; Lemaitre, J. *J. Am. Ceram. Soc.* **1992**, *75*, 3201-3208.

(173) Regev, O.; ElKati, P. N. B.; Loos, J.; Koning, C. E. *Adv. Mater.* **2004**, *16*, 248-251.

(174) Liu, L.; Grunlan, J. C. *Adv. Funct. Mater.* **2007**, *17*, 2343-2348.

(175) Sarkar, D.; Somasundaran, P. *Langmuir* **2004**, *20*, 46574664.

(176) Yokoyama, A.; Srinivasan, K. R.; Fogler, H. S. *Langmuir* **1989**, *5*, 534-538.

(177) Eberhardt, M.; Theato, P. *Macromol. Rapid Commun.* **2005**, *26*, 1488-1493.

(178) Eberhardt, M.; Mruk, R.; Zentel, R.; Theato, P. *Eur. Polym. J.* **2005**, *41*, 1569-1575.

(179) Boutris, C.; Chatzi, E. G.; Kiparissides, C. *Polymer* **1997**, *38*, 2567-2570.

(180) Taylor, L. D.; Cerankowski, L. D. *J. Polym. Sci. A-Polym. Chem.* **1975**, *13*, 2551-2570.

(181) Jochum, F. D.; Theato, P. *Macromolecules* **2009**, *42*, 5941-5945.

(182) Jochum, F. D.; Theato, P. *Polymer* **2009**, *50*, 3079-3085.

(183) Jochum, F. D.; zur Borg, L.; Roth, P. J.; Theato, P. *Macromolecules* **2009**, *42*, 7854-7862.

(184) Zhu, P. W.; Napper, D. H. *J. Colloid Interface Sci.* **1996**, *177*, 343-352.

(185) Yokoyama, A.; Srinivasan, K. R.; Fogler, H. S. *Langmuir* **1990**, *6*, 702-706.

(186) Bahun, G. J.; Wang, C.; Adronov, A. *J. Polym. Sci. A-Polym. Chem.* **2006**, *44*, 1941-1951.

(187) Li, X.; Wong, S. Y.; Tjiu, W. C.; Lyons, B. P.; Oh, S. A.; Bin He, C. *Carbon* **2008**, *46*, 829-831.

(188) Wei, H.; Cheng, S. X.; Zhang, X. Z.; Zhuo, R. X. *Prog. Polym. Sci.* **2009**, *34*, 893-910.

(189) Ozturk, N.; Girotti, A.; Kose, G. T.; Rodriguez-Cabello, J. C.; Hasirci, V. *Biomater.* **2009**, *30*, 5417-5426.

(190) Akiyama, Y.; Kushida, A.; Yamato, M.; Kikuchi, A.; Okano, T. *J Nanosci Nanotechnol* **2007**, *7*, 796-802.

(191) Ohya, S.; Sonoda, H.; Nakayama, Y.; Matsuda, T. *Biomater.* **2005**, *26*, 655-659.

(192) Nie, J. J.; Du, B. Y.; Oppermann, W. *Macromolecules* **2005**, *38*, 5729-5736.

(193) Zhang, X. Z.; Xu, X. D.; Cheng, S. X.; Zhuo, R. X. *Soft Matter* **2008**, *4*, 385-391.

(194) Muniz, E. C.; Geuskens, G. *J. Mater. Sci.-Mater. Med.* **2001**, *12*, 879-881.

(195) Inomata, H.; Goto, S.; Saito, S. *Macromolecules* **1990**, *23*, 4887-4888.

(196) Geim, A. K. *Science* **2009**, *324*, 1530-1534.

(197) Brumfiel, G. *Nature* **2009**, *458*, 390-391.

(198) Van Noorden, R. *Nature* **2006**, *442*, 228-229.

(199) Wu, Y.; Xiang, J.; Yang, C.; Lu, W.; Lieber, C. M. *Nature* **2004**, *430*, 704-704.

(200) Iijima, S.; Qin, L. C. *Science* **2002**, *296,*611-611.

(201) Dai, S.; Ravi, P.; Tam, K. C. *Soft Matter* **2008**, *4*, 435-449.

(202) Wu, D. C.; Liu, Y.; He, C. B. *Macromolecules* **2008**, *41*, 18-20.

(203) Smith, G. L.; McCormick, C. L. *Macromolecules* **2001**, *34*, 5579-5586.

(204) Yan, N.; Zhang, J. G.; Yuan, Y.; Chen, G. T.; Dyson, P. J.; Li, Z. C.; Kou, Y. *Chem. Commun.* **2010**, *46*, 1631-1633.

(205) Li, W.; Zhang, A.; Schluter, A. D. *Chem. Commun.* **2008**, 43, 5523-5525.

(206) Iwasaki, Y.; Wachiralarpphaithoon, C.; Akiyoshi, K. *Macromolecules* **2007**, *40*, 8136-8138.

(207) Crespy, D.; Rossi, R. N. *Polym. Int.* **2007**, *56*, 1461-1468.

(208) Rackaitis, M.; Manias, E. *Materials and Devices for Smart Systems* **2004**, *785*, 259-264.

(209) Meng, H.; Hu, J. L. *J. Intelligent Mater. Sys. Struct.* **2010**, *21*, 859-885.

(210) Snyder, E. A.; Tong, T. H. *Micro. Nanosys.-Mater. Devices* **2005**, *872*, 353-358.

(211) Jaycox, G. D. *J. Polym. Sci. A-Polym. Chem.* **2006**, *44*, 207-218.

(212) Lustig, S. R.; Everlof, G. J.; Jaycox, G. D. *Macromolecules* **2001**, *34*, 2364-2372.

(213) Hiorns, R. C.; Cloutet, E.; Ibarboure, E.; Vignau, L.; Lemaitre, N.; Guillerez, S.; Absalon, C.; Cramail, H. *Macromolecules* **2009**, *42*, 3549-3558.

(214) Imahori, H.; Fukuzumi, S. *Adv. Func. Mater.* **2004**, *14*, 525-536.

(215) Guldi, D. M.; Illescas, B. M.; Atienza, C. M.; Wielopolskia, M.; Martin, N. *Chem. Soc. Rev.* **2009**, *38*, 1587-1897.

(216) Cuniberti, G.; Gutierrez, R.; Fagas, G.; Grossmann, F.; Richter, K.; Schmidt, R. *Physica E-Low-Dimensional Systems & Nanostructures* **2002**, *12*, 749-752.

(217) Ghosal, S.; Muruganandam, A. V. *J. Ind. Chem. Soc.* **2008**, *85*, 911-919.

(218) Simon, F.; Peterlik, H.; Pfeiffer, R.; Bernardi, J.; Kuzmany, H. *Chem. Phys. Lett.* **2007**, *445*, 288-292.

(219) Howe, L. A.; Jaycox, G. D. *J. Polym. Sci. A-Polym. Chem.* **1998**, *36*, 2827-2837.

(220) Jaycox, O. D. *Abs. Papers Am. Chem. Soc.* **1998**, *216*, U31-U31.

(221) Volodin, B. L.; Kippelen, B.; Meerholz, K.; Javidi, B.; Peyghambarian, N. *Nature* **1996**, *383*, 58-60.

APPENDIX A

CLAY AS SOLID SURFACTANT FOR CARBON BLACK

A1. Introduction.

Electrically conductive polymer composites (CPCs) have many potential applications that include electromagnetic interference shielding,[1-3] electrostatic dissipation,[4] heat dissipation films,[5] chemical sensors,[6-8] actuators[9-12] and photovoltaic devices.[13-14] Addition of conductive particles to an insulating polymer matrix produces a (semi)conducting composite (i.e, CPC).[15] The mode of electrical transmission in these composites relies on the formation of three-dimensional network structures of the conducting filler in the polymer matrix. The lowest concentration of filler at which these networks can be formed is known as the percolation threshold. Significant research has been focused on reducing the percolation threshold by altering filler microstructure in an attempt to increase the electrical conductivity at low filler concentration.[16-23] Despite significant progress, difficulties associated with dispersion and stabilization of these fillers in the polymer matrices limits their widespread use.

Carbon nanofillers, such as carbon nanotubes,[24] nanofibers[2] and carbon black (CB),[1] are electrically conductive and useful for improving polymer properties. CB filled polymers are widely used in industrial applications due to their cost advantage over other fillers. Typically, polymer matrices require large concentrations of CB to achieve sufficient electrical conductivity for various applications. These high CB concentrations can produce high viscosity during processing and impair mechanical performance.[25] It is

precisely this ease of processing and durability of the final object that makes CPC an attractive alternative for applications traditionally reserved for metals. Therefore, it is important to increase the electrical conductivity of CB filled polymer composites, while preserving beneficial mechanical properties. One way to accomplish this is to increase the electrical conductivity of the composite to a desirable level at low filler concentration. Low conducting filler volume fractions are often required to reduce processing cost and improve ductility and mechanical strength for matrices that have poor matrix-filler adhesion.[26]

There are several methods to lower the percolation threshold in CPCs. For example, the use of polymer blends, instead of single polymers as the matrix, has successfully lowered the percolation threshold for CB filled CPCs.[27-29] Despite its promise, this method is not suitable for many polymers because they do not form compatible blends. For single polymer matrices, lower percolation thresholds have been achieved by annealing the polymer to increase crystalline fraction[30-31] or by using polymer emulsions that generate a seggregated network of conductive filler.[21,32] Although significant effort has been made to lower the percolation threshold in CPCs, few studies have focused on increasing electrical conductivity at a given filler loading.[26,33]

Recently, the use of electrically inert fillers was shown to lower the percolation threshold, increase electrical conductivity and improve mechanical properties of CPCs.[34-40] These inert fillers influenced the distribution of conducting fillers and lead to the formation of robust networks with small conductive filler concentration. For

example, it was found that the addition of 2wt% clay increases electrical conductivity of carbon nanotube/epoxy composites by several orders of magnitude without reducing modulus or glass transition temperature.[39] At this point, no comprehensive studies in this direction are reported for clay and CB in a solution-processed thermoset composite. Thermoset resins are different from thermoplastics in that they are viscous liquids before curing and offer less hindrace for fillers to form networks due to lower viscosity and lack of crystalline domains.[41] Further studies with thermosets (e.g., epoxy) are necessary to understand the influence of an electrically inert filler(e.g clay) on the electrical and mechanical properties of CPCs.

Clay is mechanically strong and known to exhibit good dispersion/load transfer characteristics in polymer composites.[42-44] The combination of CB and clay allows electrical conductivity and mechanical properties to be enhanced simultaeneously. Studies on liquid suspensions were performed to investigate the dispersion state of CB and clay prior to composite formation. Suspensions containing CB and clay showed superior stabilization to those containing only clay or CB alone in acetone (a common solvent used to process epoxies). These results indicate an interaction between CB and clay that influences the dispersion of CB in epoxy. Clay was combined with CB in epoxy, which resulted in improved electrical and mechanical properties. An epoxy composite containing 2.5 wt% CB has an electrical conductivity on the order of 10^{-6} S/cm. With the addition of 0.5 wt% clay, conductivity increased by an order of magnitude, but no significant improvement was observed for storage modulus. Composites containing equal amounts of CB and clay showed significant improvement

in storage modulus as compared to those containing an equivalent amount of only one type of filler. The concept of CB stabilizing clay by surrounding it during processing (i.e. haloing) is proposed to explain these observed improvements in composite behavior. Although not the focus of the present study, clay may impart other properties, such as flame retardancy[45-46] and gas barrier,[47] that will make these composites useful for a wide variety of applications.

A2. Experimental Section

A2.1 Materials

Conductex 7055 Ultra CB (primary particle size 42nm, NSA 55 m^2/g, density 1.7-1.9 g/cm^3) was provided by Columbian Chemicals (Marietta, GA) and was used as received. Closite Na^+ (natural montmorrillonite clay) was provided by Southern Clay Products (Gonzalez, TX). This clay has a cationic exchange capacity of 0.926 meq/g, platelet diameter in the range of 10-1000 nm (most are larger than 200 nm), density of 2.86 g/cm^3, and individual platelet thickness of 1 nm.[48] When incorporated into epoxy, these platelets are stacked, which results in larger particles that may be up to one micron (or more) in size. The epoxy resin D.E.R 354 was provided by Dow Chemical (Midland, MI) and used in combination with ECA 100 epoxy curing agent that was provided by Dixie Chemicals (Pasadena, TX). An amine catalyst (N,N-Dimethylbenzylamine) was purchased from Aldrich (Milwaukee, WI). The density of cured epoxy was measured to be 1.2 g/cm^3.

A2.2 Composite Preparation

CB/clay/epoxy composites were made by suspending the appropriate amount of CB and clay in 50ml acetone with sonication at 50W for 20 minutes using a VirTis (Gardiner, NY) Virsonic 100 Ultrasonic Cell Disrupter. Epoxy resin, curing agent and amine catalyst were then dissolved in 50 ml of acetone and mixed with the CB/clay suspension. This mixture was mechanically stirred for five minutes at 1720 RPM, followed by thirty minutes at 3100 RPM, and then sonicated in a Branson 3510 bath sonicator (Danbury, CT) for one hour. Acetone was removed by rotation evaporation at 60°C in a Heidolph Laborota 4001 (Vernon Hills, IL) and the mixture was cured in a glass mold for one hour at 95°C, followed by three hours at 150°C. The weight ratio of epoxy resin to the curing agent was kept at 5:4, while the amine catalyst was maintained at 1wt% of the total epoxy solids. The same procedure was used to make composites with no clay.

A2.3 Characterization

Dynamic mechanical analysis of composites was done with a Q800 DMA (TA Instruments, Newcastle, DE) using a temperature ramp of 3°C/min, a frequency of 1Hz and a 3-point bending fixture on the specimens of dimension 5.8cm x 1.3cm x 0.25 cm (L x W x T). Scanning electron microscopy was performed with an FEI Quanta 600 FE-SEM on freeze fractured samples of composites coated with a 5nm layer of Pt/Pd. Composite sheet resistance of less than 120,000 ohm/sq was measured using a home-built four-point probe apparatus. An Agilent power supply and Keithley multimeter with

a Signatone probe head (Tungsten Carbide tips, 1.6mm spacing and 0.04 mm curvature) were used in conjunction with LabView software to operate the apparatus. Composites with higher resistance (> 120,000 ohm/sq) were measured with a VOYAGER Surface Resistivity Meter (SRM)-110 (PINION Products Corporation, Los Fresnos, TX). Specimens measuring 5cm x 5cm x 0.25 cm (L x W x T) were used for conductivity measurements. Volume conductivity was calculated by taking the inverse of the product of the sheet resistance and specimen thickness. Suspensions of CB and clay were centrifuged at 2500 RPM for 10 minutes with an accuSpin 400 (Fisher Scientific, Pittsburgh PA). To determine suspension stability, zeta potetial measurements were made with a Zeta Phase Angle Light Scattering (ZETA PALS) (Brookhaven Instruments Corporation, Holtsville,NY) using a quartz cuvette. The test chamber was maintained at a temperature of 25 ^{o}C and zeta potential values were determined following the standard operating procedure of the instrument. Cryo-TEM images were taken with an FEI Tecnai G2 F20 operated at 200 kV equipped with cryogenic accessories. The samples were frozen in liquid ethane using an FEI Vitrobot apparatus. Images were recorded with a Gatan Tridiem GIF-CCD camera attached to the microscope.

A3. Results and Discussion

3.1 Liquid Suspensions of CB and Clay

In an effort to understand the interaction between CB and clay particles, suspensions of CB and clay in acetone were first investigated. These interactions, and

the microstructures they influence, largely control the properties of solid composites. Figures A1(a) and (b) show a suspension of CB and clay in acetone after sonication and centrifugation respectively. It should be noted that acetone was used as a solvent for composite processing. Suspensions were sonicated for 15 minutes prior to centrifugation. It can be seen that the suspension containing both CB and clay (0.05 wt% of each) were stable after sonication with no visible settling of particles. Noticeable sedimentation of particles were observed in suspensions containing only CB (or clay) after standing for 10 minutes. After centrifugation, the suspension containing only CB or clay show significant sedimentation of particles, whereas the supsension containing mixture of CB and clay is stable. This suggests that there is an interaction between CB and clay that serves to keep them dispersed/stabilized in acetone. To better understand this interaction, zeta potentials of the suspensions were measured. The zeta potential of CB and clay in acetone was found to be -110 mV and -5 mV, respectively. High zeta potential values (> +25 or < -25) signify high surface charge on the particles.[49] The high zeta potetial values of the CB suspension suggests greater stability due to particle-particle repulsion. The relatively low zeta potential value for clay indicates an absence of exfoliated platelets and instability of the suspensions.

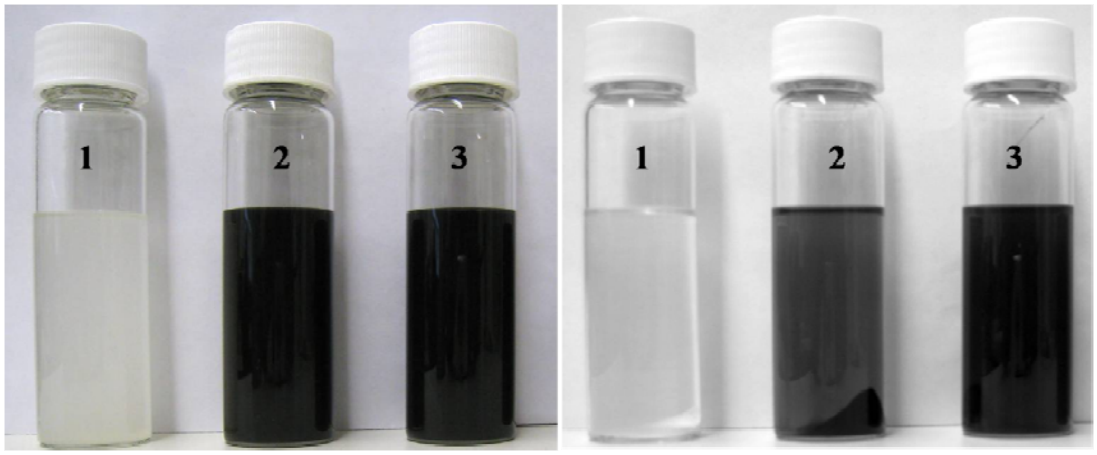

(a) (b)

Figure A1. Suspensions of CB and/or clay in acetone (a) after sonication and (b) after centrifugation. Vial (1) contains 0.1 wt% clay, Vial (2) contains 0.1 wt% CB and Vial (3) contains 0.05 wt% CB and 0.05 wt% clay.

Cryo-TEM was perfomed on one of these suspensions to investigate the dispersion state of CB in acetone in the presence of clay. An image of the acetone suspension, containing 0.05 wt% of both CB and clay, along with a schematic of the observed structure is shown in Figure A2. The clay exists in a non-exfoliated state and is surrounded by CB clusters. The identities of clay and CB was confirmed by energy dispersive analysis that produced Si and C peaks. Recently, the nanoparticle haloing effect (i.e., surrounding of one particle by another) was discovered as a mechanism for stabilization of a mixture of micron and nano-sized particles in solution.[50] One criterion for formation of nanoparticle halos is the presence of high surface charge on the nanoparticles and negligible surface charge on the micron-sized particles. Clay and CB in acetone satisfy these conditions based upon the zeta potential measurements. The presence of CB around clay in Figure A2(a) provides direct evidence of haloing. A similar binary colloidal dispersion was used to sucessfully disperse carbon nanotubes in

water using highly charged zirconia nanoparticles.[51] It is believed that well dispersed nano-sized particles of CB form halos around the micron-sized stacks of clay platelets. It should be pointed out that the results presented in previous studies utilizes spherical and one-dimensional micron-sized particles[40-41] and the generalization of this mechanisim to three-dimensional clay particles is non-trivial and might contribute to the further understanding of this mechanism.

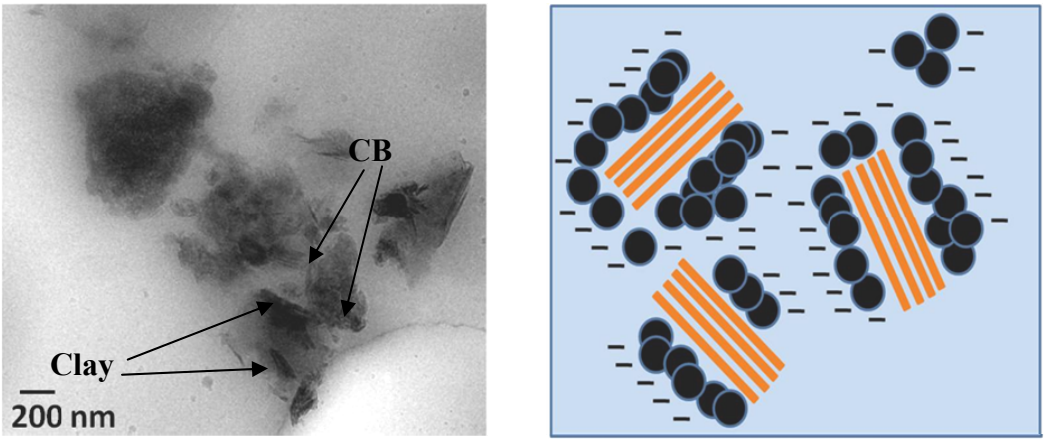

(a) (b)

Figure A2. Cryo-TEM image of (a) 0.5 wt% CB and 0.5 wt% clay in acetone and (b) a schematic of the CB stabilisation of clay in acetone.

3.2 Composite Microstructure

To investigate the influence of clay on the dispersion state of CB in epoxy, scanning electron microscopy was performed on freeze-fractured cross-sections of the composites. SEM micrographs of three epoxy composites, containing 2.5 wt% CB and 0, 2.5 and 5 wt% clay, are shown in Figure A3. It can be seen that CB particles in these composites exists in the form of aggregates. In the case of the composite containing only

CB (Fig. A3(a)), the aggregates are randomly dispersed in the epoxy matrix and are well connected with each other. These well connected aggregates of CB make the insulating epoxy matrix conductive. As shown in Figure A3(b), composites containing equal amounts of CB and clay have a relatively smaller aggregate size and are not well connected with each other. In this scenario, it is unlikely that a percolating network of CB is present and is the reason for the lower electrical conductivity observed in these composites(Section A3.3). Despite reducing composite conductivity, this smaller aggregate size increases the CB surface area interacting with epoxy matrix, which results in enhaced mechanical properties, shown in the next section. Composites containing a 1:2 clay:CB ratio (Fig. A3(c)) show improved connectivity of CB aggregates. Two important aspects to be observed in these micrographs are the differences in the distribution and size of CB aggregates in the composites containing clay. If the effect of clay were to simply increase the excluded volume in the composite, then the CB aggregates in these composites would be of similar size. The presence of different size of CB aggregates suggests an interaction between CB and clay particles, that not only effects their distribution but also their state of aggregation. This synergy between CB and clay has a profound influence on composite electrical and mechanical behavior.

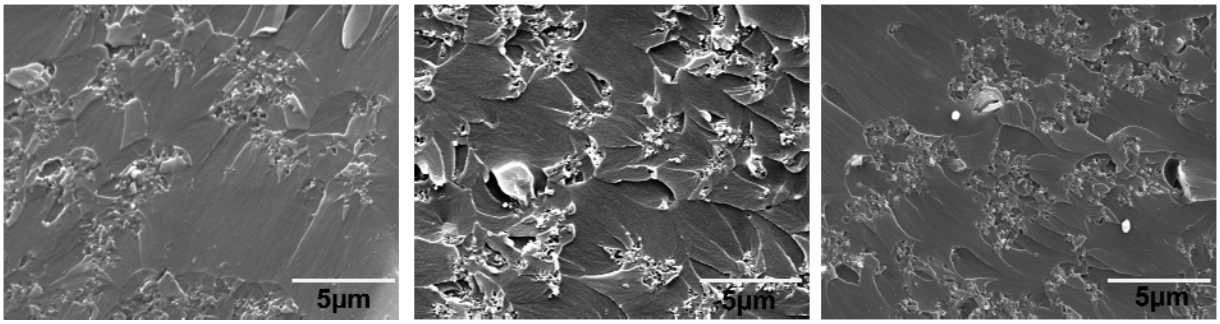

(a) (b) (c)

Figure A3. SEM images of freeze-fractured epoxy containing (a) 2.5 wt% CB, (b) 2.5 wt% CB and 2.5 wt% clay,(c) 2.5 wt% CB and 5 wt% clay.

A3.3 Composite Electrical and Mechanical Behavior

Figure A4(a) shows the electrical conductivity of epoxy composites containing CB and clay. It can be seen that the conductivity of the composites changes with clay concentration. The composite containing 2.5 wt% CB exhibits conductivity on the order of 10^{-6} S/cm, but this increases by an order of magnitude with addition of 0.5 wt% clay. As the clay concentration is further increased, there is a decrease in composite conductivity, with the lowest values achieved (among the ratios studied here) when equal amounts of clay and CB are present. With further increase in clay concentration, the conductivity is again increased. To better understand the influence of clay on electrical conductivity of CB filled epoxy composites, measurements were made on composites containing 5 wt% CB in epoxy. Electrical conductivity of 5 wt% composites follows a similar trend as the 2.5 wt% composites (i.e, at clay concentration of 0.5 wt% conductivity increased by an order of magnitude and the lowest value was observed for composites with a 1:1 clay:CB ratio). It should also be noted that CB-filled epoxy

containing 0.5 wt% clay showed an order of magnitude higher conductivity than composites with no clay at every CB concentration studied, as shown in Figure A4(b). These results suggest that there is an optimum concentration of clay to enhance electrical conductivity. Similar results were observed in nylon/CB/clay composites.[35] Due to problems associated with high suspension viscosity at high filler loadings, no composites were made with clay concentrations greater than 7.5 wt% (see Supporting Information for viscosity as a function of shear rate of several suspensions). A suspension containing 5 wt% carbon black and 5 wt% clay has a viscosity near 10 Pa·s (at a shear rate of 1 s^{-1}), but this value increases beyond 100 Pa·s when the clay concentration is increased to 7.5 wt%. It would likely become a gel with further addition of clay.

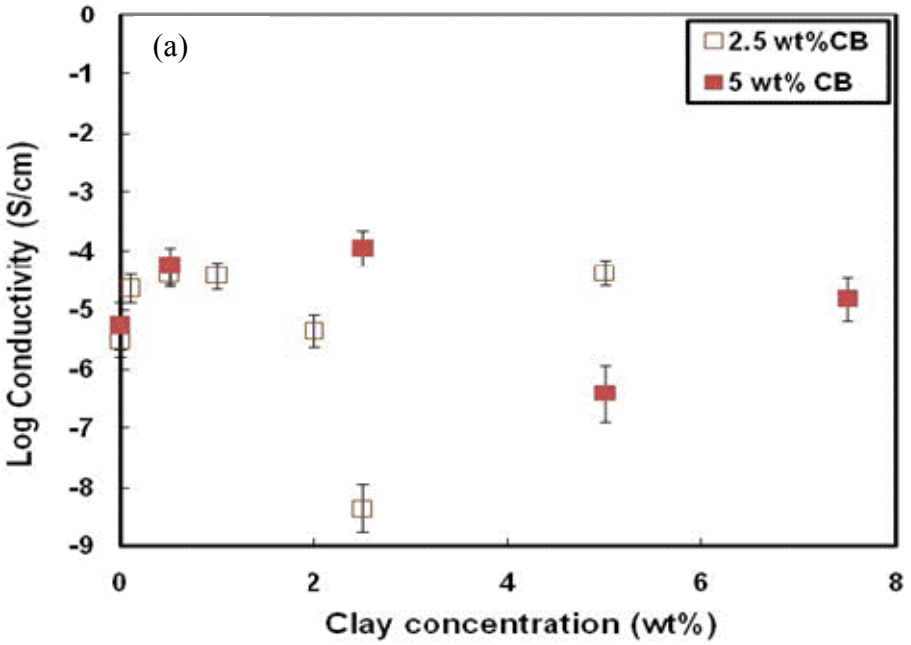

Figure A4. Electrical conductivity as a function of clay concentration for epoxy composites containing (a) 2.5 and 5 wt% CB and (b) as a function of CB concentration for composites with and without 0.5 wt% clay.

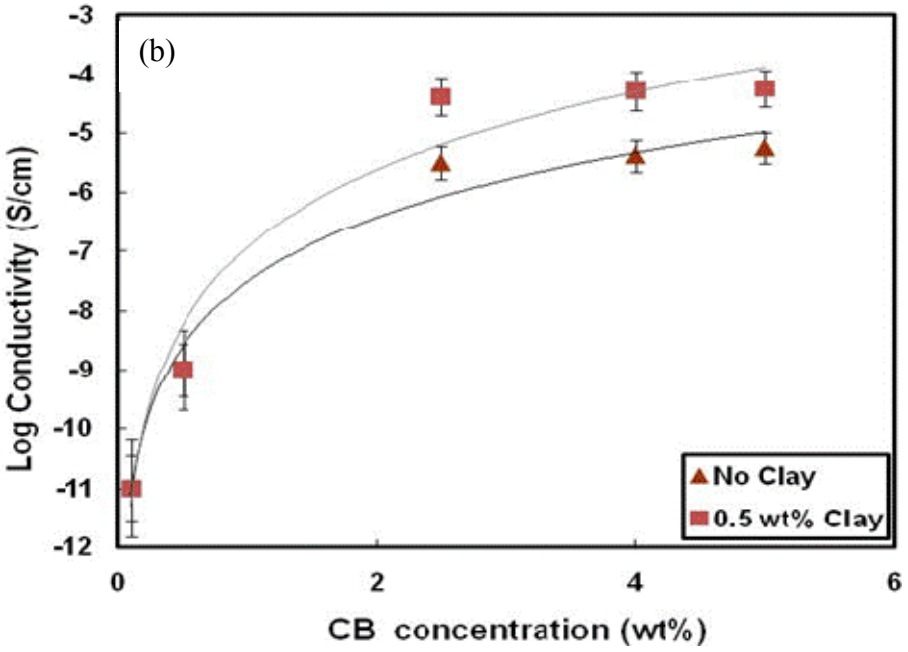

Figure A4. Continued.

Dynamic mechanical analysis was used to evaluate the influence of CB and clay composition on mechanical properties of these epoxy composites. Room temperature (25^{o}C) storage moduli of the composites increased with increasing CB concentration. Composites with 2.5 wt% and 5 wt% CB show 19% and 23% higher modulus than neat epoxy, respectively. For composites containing 0.5 wt% clay, no significant improvement in storage modulus was observed, but equal concentrations of clay and CB increased the modulus by 36% and 40% for 2.5 wt% and 5 wt% CB filled epoxy, respectively. It should be noted that incorporating equal weights of clay and CB results in a doubling of the total filler concentration and the observed increase in storage

modulus could be the result of this. Therefore, it is important to keep the total filler concentration constant to isolate the clay-CB synergy.

Figure A4 shows the storage modulus as a function of temperature for composites containing a constant filler concentration of 5 wt%. Composites with clay:CB ratio of 1:1 exhibited 11% and 15% increases in storage modulus relative to composites containing CB or clay alone, respectively. This synergistic increase in storage modulus further suggests an interaction between clay and CB, which results in better dispersion of CB and clay in the presence of one another. It is known that composites containing more uniformly dispersed filler have improved storage modulus. [52] DMA also provides a measure of glass transition temperature (T_g), which can be taken as the point where storage modulus significantly drops. Composites containing only CB or a mixture of CB and clay show lower T_g than neat epoxy. This may be due to weak interfacial adhesion between unmodified CB and epoxy[53] and/or reduced crosslink density due to interference of filler particles with epoxy during curing.[54-55] It is also observed that composites with constant CB concentration exhibited an increase in T_g with increasing clay concentration. This may be due to greater hindrance to polymer mobility from the high aspect ratio of clay platelets.[56] Table A1 summarizes the electrical conductivity, storage modulus and T_g of each system studied here. The data presented in Table A1 are the average value of 3, 3 and 12 measurements for storage modulus, T_g and electrical conductivity, respectively (the ± value represents one standard deviation.).

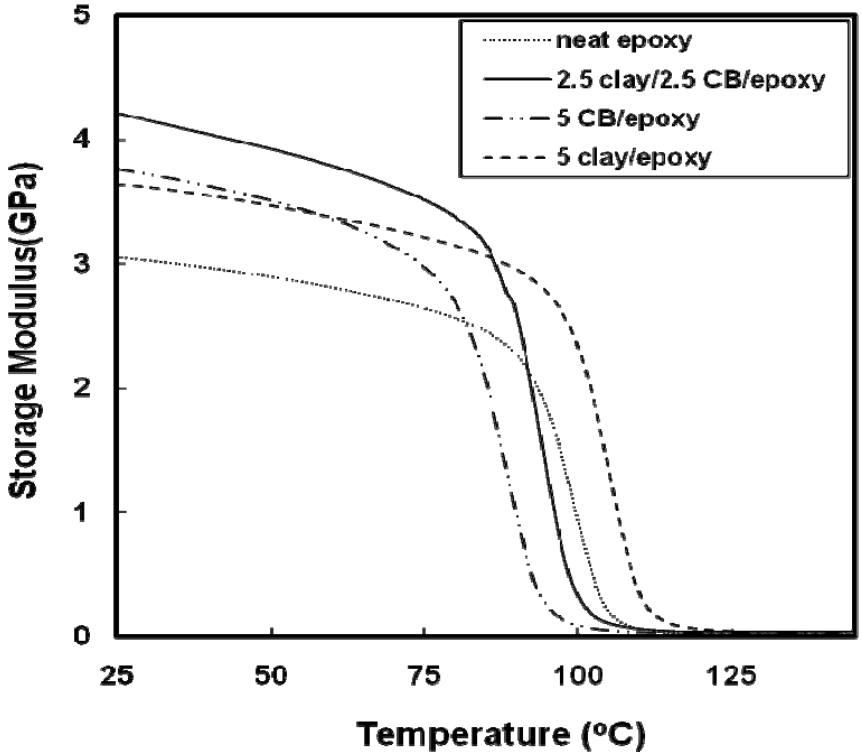

Figure A5. Storage modulus as a function of temperature for epoxy composites containing 5 wt% total filler (CB and/or clay). Neat (unfilled) epoxy is also shown as a reference.

Table A1. Properties of epoxy containing CB and/or clay.

Material	Storage Modulus (GPa) (at 25°C)	T_g (°C)	Log Conductivity (S/cm)
Neat epoxy	3.06±0.02	102±1.0	<-11
2.5 wt%CB (1.7)	3.63±0.10	97±0.6	-5.50±0.35
2.5 wt%CB(1.7)+ 0.5 wt% clay(0.2)	3.69±0.20	94±1.0	-4.39±0.39
2.5 wt% CB (1.7)+2.5 wt% clay(1.1)	4.18±0.07	96±1.0	-8.34±0.42
2.5 wt% CB(1.7) +5 wt% clay(2.2)	4.17±0.08	99±0.4	-4.37±0.19
5 wt% CB (3.4)	3.77±0.10	92.6±1.2	-5.25±0.33
5 wt% CB(3.4) + 0.5 wt% clay(0.2)	3.80±0.20	93.7±1.1	-4.25±0.12

5 wt% CB(3.4) + 2.5 wt% clay(1.1)	**3.87±0.10**	**96.8±1.3**	**-3.94±0.22**
5 wt% CB(3.5) + 5 wt% clay(2.2)	**4.29±0.03**	**99.2±1.0**	**-6.40±0.24**
5 wt% CB(3.5) + 7.5 wt% clay(3.3)	**4.31**	**101**	**-4.80±0.45**
5 wt% clay(2.2)	**3.64±0.13**	**105.3±0.5**	**<-11**

† Values in the parentheses represent volume percent of the fillers.

A3.4 Proposed Mechanism

The preceeding discussion has established that CB dispersion in epoxy is altered by the presence of clay. This altered microstructure is attributed to the interaction between CB and clay in acetone, which results in synergistic stabilization of CB and clay particles that involves a haloing effect(Section A3.1). It is true that acetone, used as a solvent during processing of the epoxy composites, was subsequently removed before curing. Even so, the epoxy resin has a high viscosity and the presence of CB actually acclerates curing,[57] so it is reasonable to assume the liquid state dispersion is preserved to a large extent in the solid composites. Here, a mechanism of microstructural development as a function of clay:CB ratio is speculated based upon the experimental results shown in the preceding sections.

Figure A6 schematically shows network formation with various weight ratios of CB and clay. The CB particles in the composites exist in either the vicinity of clay (due to the haloing effect) or in the vicinity of other CB particles. The former will be referred to as *associated CB* and the latter will be referred to as *free CB* for the following discussion At low clay concentration, the distribution of free CB around the associated CB/clay particles is influenced by steric and/or exclusion effects. The altered distribution

of free CB in the presence of clay leads to the formation of efficient networks because of the formation of *nano-channels*. Nano-channels refer to the network of free carbon black particles that connect the associated CB. The presence of nano-channels leads to an increased number of pathways for electron transport and results in an increase in electrical conductivity. A similar increase in electrical conductivity, at low volume fractions of organically modified clay, was also observed in carbon black-filled polyethylene.[34]

The stabilization of clay by CB haloing requires the availability of free CB that will lead to the formation of associated CB. As the concentration of clay is increased (i.e., more clay particles), more free CB is converted to associated CB. This results in the reduction of free CB that acts as a bridge between associated CB (i.e., the nano-channels are depleted). The observation of low conductivity at equal weight ratio of CB and clay is believed to be the result of the absence of nano-channels in these composites, as shown in Figure A6. At even higher concentrations of clay, it is less likely that associated CB is formed due to increased interaction between clay particles and a dearth of CB particles available for stabilization of clay through halo formation. However, free CB in these composites may lead to the formation networks and results in the observed increase in electrical conductivity.

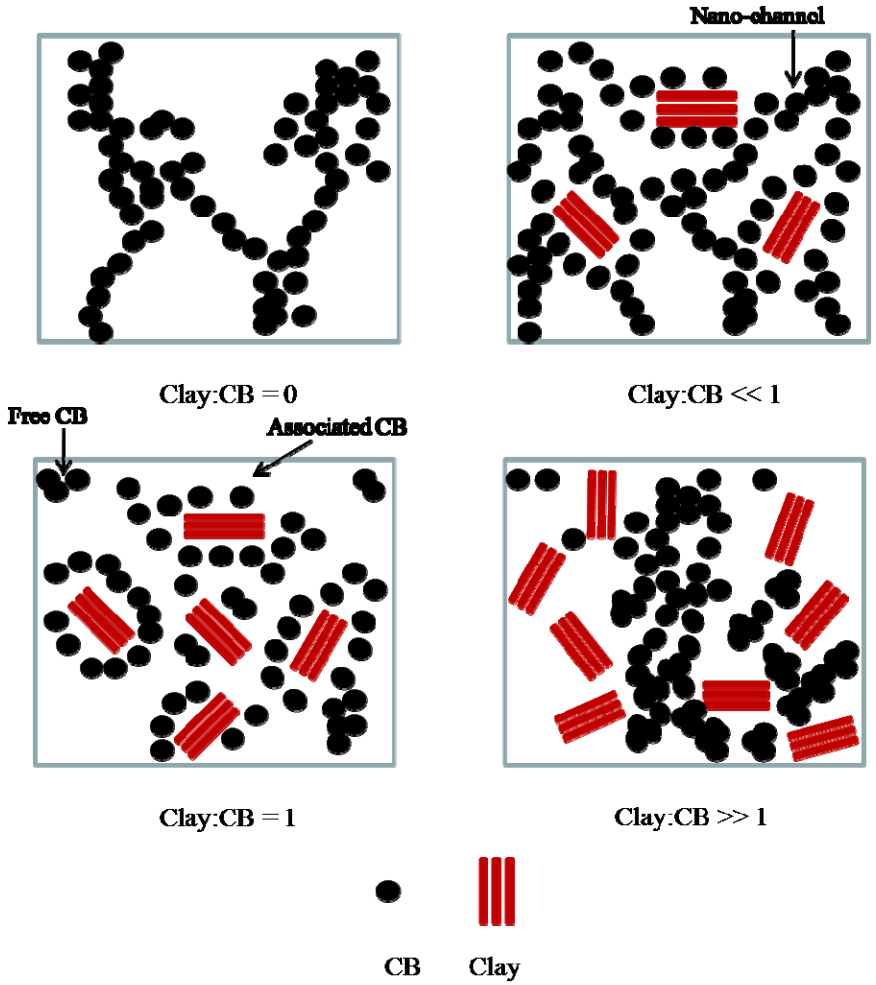

Figure A6. Schematic of microstructural development in epoxy composites containing different weight ratios of CB and clay.

A4. Conclusions

Clay was added to CB filled epoxy in an effort to increase elctrical conductivity without harming mechanical properties. In the concentration range of CB studied (2.5-5.0 wt%), the addition of 0.5 wt% clay increased the electrical conductivity of composites by an order of magnitude. A study on the liquid suspension of CB and clay in acetone revealed superior stabilization of suspensions containing both types of

particles. Cryo-TEM images indicate the formation of CB halos around clay particles. These results suggest an interaction between CB and clay that may be the reason for the improved electrical and mechanical properties of epoxy composites containing both particles. At equal concentrations of CB and clay, the composites exhibited a reduction in electrical conductivity, but an increase in storage modulus at room temperature. Composites containing clay and CB, with a weight ratio of 2:1, exhibited both higher electrical conductivity and storage modulus. These results suggest that an optimum concentration of clay is needed to improve electrical and mechanical properties simultaeneously. Furthermore, composites containing equal amounts of CB and clay showed significant improvement in storage modulus as compared to those containing an equivalent amount of only one type of filler. Further work in this area will focus on better understanding the mechanism of clay particle stabilization in the presence of CB and the effect of organically modified clay on network formation of CB in epoxy. Other useful properties of these composites, such as flame suppression and gas barrier, will also be studied in an effort to expand the utility of this synergistic combination of particles.

REFERENCES

(1) Chung, D. D. L. *Carbon* **2001**, *39*, 279-285.

(2) Yang, Y. L.; Gupta, M. C.; Dudley, K. L.; Lawrence, R. W. *Adv. Mater.* **2005**, *17*, 1999-2003.

(3) Li, N.; Huang, Y.; Du, F.; He, X. B.; Lin, X.; Gao, H. J.; Ma, Y. F.; Li, F. F.; Chen, Y. S.; Eklund, P. C. *Nano Lett.* **2006**, *6*, 1141-1145.

(4) Koul, S.; Chandra, R.; Dhawan, S. K. *Polymer* **2000**, *41*, 9305-9310.

(5) Biercuk, M. J.; Llaguno, M. C.; Radosavljevic, M.; Hyun, J. K.; Johnson, A. T.; Fischer, J. E. *Appl. Phys. Lett.* **2002**, *80*, 2767-2769.

(6) Lonergan, M. C.; Severin, E. J.; Doleman, B. J.; Beaber, S. A.; Grubb, R. H.; Lewis, N. S. *Chem. Mater.* **1996**, *8*, 2298-2312.

(7) Wei, C.; Dai, L. M.; Roy, A.; Tolle, T. B. *J. Am. Chem. Soc.* **2006**, *128*, 1412-1413.

(8) Virji, S.; Fowler, J. D.; Baker, C. O.; Huang, J. X.; Kaner, R. B.; Weiller, B. H. *Small* **2005**, *1*, 624-627.

(9) Landi, B. J.; Raffaelle, R. P.; Heben, M. J.; Alleman, J. L.; VanDerveer, W.; Gennett, T. *Nano Lett.* **2002**, *2*, 1329-1332.

(10) Li, C.; Thostenson, E. T.; Chou, T. W. *Composites Sci. Technol.* **2008**, *68*, 1227-1249.

(11) Bonomo, C.; Fortuna, L.; Giannone, P.; Graziani, S.; Strazzeri, S. *Smart Mater. Struct.* **2007**, *16*, 1-12.

(12) Kim, K. J.; Shahinpoor, M. *Polymer* **2002**, *43*, 797-802.

(13) Kymakis, E.; Amaratunga, G. A. J. *Appl. Phys. Lett.* **2002**, *80*, 112-114.

(14) Baibarac, M.; Gomez-Romero, P. *J. Nanoscience Nanotechnol.* **2006**, *6*, 289-302.

(15) Strumpler, R.; Glatz-Reichenbach, J. *J. Electroceram.* **1999**, *3*, 329-346.

(16) Grunlan, J. C.; Mehrabi, A. R.; Bannon, M. V.; Bahr, J. L. *Adv. Mater.* **2004**, *16*, 150-153.

(17) Song, Y. S.; Youn, J. R. *Carbon* **2005**, *43*, 1378-1385.

(18) Murphy, R.; Nicolosi, V.; Hernandez, Y.; McCarthy, D.; Rickard, D.; Vrbanic, D.; Mrzel, A.; Mihailovic, D.; Blau, W. J.; Coleman, J. N. *Scripta Materialia* **2006**, *54*, 417-420.

(19) Zou, J. F.; Yu, Z. Z.; Pan, Y. X.; Fang, X. P.; Ou, Y. C. *J. Polym. Sci. Part B-Polym. Phys.* **2002**, *40*, 954-963.

(20) Du, F. M.; Scogna, R. C.; Zhou, W.; Brand, S.; Fischer, J. E.; Winey, K. I. *Macromolecules* **2004**, *37*, 9048-9055.

(21) Kim, Y. S.; Wright, J. B.; Grunlan, J. C. *Polymer* **2008**, *49*, 570-578.

(22) Lu, W.; Lin, H. F.; Wu, D. J.; Chen, G. H. *Polymer* **2006**, *47*, 4440-4444.

(23) Wang, L.; Dang, Z. M. *Appl. Phys. Lett.* **2005**, *87,* 042903-1-3.

(24) Ebbesen, T. W.; Lezec, H. J.; Hiura, H.; Bennett, J. W.; Ghaemi, H. F.; Thio, T. *Nature* **1996**, *382*, 54-56.

(25) Zhang, W.; Dehghani-Sanij, A. A.; Blackburn, R. S. *J. Mater.Sci.* **2007**, *42*, 3408-3418.

(26) Chen, P. W.; Chung, D. D. L. *J. Electronic Mater.* **1995**, *24*, 47-51.

(27) Gubbels, F.; Blacher, S.; Vanlathem, E.; Jerome, R.; Deltour, R.; Brouers, F.; Teyssie, P. *Macromolecules* **1995**, *28*, 1559-1566.

(28) Feng, J. Y.; Chan, C. M.; Li, J. X. *Polym. Eng. Sci.* **2003**, *43*, 1058-1063.

(29) Wu, G.; Miura, T.; Asai, S.; Sumita, M. *Polymer* **2001**, *42*, 3271-3279.

(30) Miyasaka, K.; Watanabe, K.; Jojima, E.; Aida, H.; Sumita, M.; Ishikawa, K. *J. Mater. Sci.* **1982**, *17*, 1610-1616.

(31) Zhang, M. Y.; Jia, W. T.; Chen, X. F. *J. Appl. Polym. Sci.* **1996**, *62*, 743-747.

(32) Francis, L. F.; Grunlan, J. C.; Sun, J. K.; Gerberich, W. W. *Colloid. Surfaces a-Physicochemical and Eng. Aspects* **2007**, *311*, 48-54.

(33) Zhang, W.; Blackburn, R. S.; Dehghani-Sanij, A. *Scripta Materialia* **2007**, *57*, 949-952.

(34) Feller, J. F.; Bruzaud, S.; Grohens, Y. *Mater. Lett.* **2004**, *58*, 739-745.

(35) Konishi, Y.; Cakmak, A. *Polymer* **2006**, *47*, 5371-5391.

(36) Bao, H. D.; Guo, Z. X.; Yu, J. *Polymer* **2008**, *49*, 3826-3831.

(37) Kotaki, M.; Wang, K.; Toh, M. L.; Chen, L.; Wong, S. Y.; He, C. B. *Macromolecules* **2006**, *39*, 908-911.

(38) Zhang, W.; Blackburn, R. S.; Dehghani-Sanij, A. A. *Scripta Materialia* **2007**, *56*, 581-584.

(39) Liu, L.; Grunlan, J. C. *Adv. Funct. Mater.* **2007**, *17*, 2343-2348.

(40) Lin, C. G.; Howe, T. A.; Chung, D. D. L. *J. Electronic Mater.***2007**, *36*, 659-668.

(41) Schueler, R.; Petermann, J.; Schulte, K.; Wentzel, H. P. *J. Appl Polym Sci.* **1997**, *63*, 1741-1746.

(42) Wang, K.; Chen, L.; Wu, J. S.; Toh, M. L.; He, C. B.; Yee, A. F. *Macromolecules* **2005**, *38*, 788-800.

(43) Wang, K.; Wang, L.; Wu, J. S.; Chen, L.; He, C. B. *Langmuir* **2005**, *21*, 3613-3618.

(44) Giannelis, E. P. *Adv. Mater.* **1996**, *8*, 29-35.

(45) Dasari, A.; Yu, Z. Z.; Mai, Y. W.; Liu, S. *Nanotechnol.* **2007**, *18,* 445602 (1–10).

(46) Ma, H. Y.; Tong, L. F.; Xu, Z. B.; Fang, Z. P. *Nanotechnol.* **2007**, *18*, 375602 (1-8).

(47) Ebina, T.; Mizukami, F. *Adv. Mater.* **2007**, *19*, 2450-2453.

(48) Ploehn, H. J.; Liu, C. Y. *Ind. Eng. Chem. Res.* **2006**, *45*, 7025-7034.

(49) Tang, F. Q.; Huang, X. X.; Zhang, Y. F.; Guo, J. K. *Ceram. International* **2000**, *26*, 93-97.

(50) Tohver, V.; Smay, J. E.; Braem, A.; Braun, P. V.; Lewis, J. A. *Proc. Nat. Aca. Sci. U.S. A* **2001**, *98*, 8950-54.

(51) Zhu, J.; Yudasaka, M.; Zhang, M. F.; Iijima, S. *J. Phys. Chem.B* **2004**, *108*, 11317-11320.

(52) Tang, H.; Dong, L. S.; Zhang, J.; Ding, M. X.; Feng, Z. L. *J. Appl. Polym.Sci.* **1996**, *60*, 725-730.

(53) Sun, Y. Y.; Zhang, Z. Q.; Moon, K. S.; Wong, C. P. *J. Polym. Sci. Part B-Polym. Phys.* **2004**, *42*, 3849-3858.

(54) Zhao, H.; Gao, J.; Li, Y.; Shen, S. *J. Therm. Analysis Calori.* **2003**, *74*, 227-236.

(55) Wang, S. R.; Liang, Z. Y.; Liu, T.; Wang, B.; Zhang, C. *Nanotechnol.* **2006**, *17*, 1551-1557.

(56) Luo, J. J.; Daniel, I. M. *Composites Sci. Technolo* **2003**, *63*, 1607-1616.

(57) Wu, J. H.; Chung, D. D. L. *Carbon* **2004**, *42*, 3039-3042.

VITA

Krishna Chaitanya Etika was born in Ambala, India, and did his basic schooling in several different schools spread across northern states of India. He graduated from Sri Venkateswara University Tirupati with his B.Tech degree in chemical engineering in June of 1999, securing University Rank 1. He then joined the M.Tech program in materials science and engineering at the Indian Institute of Technology (IIT) Kharagpur and graduated in May of 2005. In his pursuit of doctoral studies, he joined the Ph.D. program in materials science and engineering at Cornell University, Ithaca, NY, in Jan 2006, where he worked on point defects in ceramic materials. He later transferred to Texas A&M University in College Station, TX, to join the research group of Dr. Jaime C. Grunlan in the summer of 2007 and graduated with his Ph.D in December 2010. He has authored 7 journal papers and delivered 12 conference presentations. He is the recipient of Prof. Y. Nayudamma Memorial Medal, given by the Andhra Pradesh Academy of Sciences, and Excellence in Thermoset Polymer Research Award given by the Thermoset Resin Formulators Association. He will be joining Intel Corporation in Hillsboro, OR, in the spring of 2011 as a process technology development engineer. He may be reached at:

Materials Science and Engineering Program,

c/o Dr. Jaime C. Grunlan,

Texas A&M University, College Station, TX 77840.

Email: kcetika@gmail.com